DOI:10.14753/SE.2015.1789

INTERACTION OF NANOPARTICLES WITH NEURAL STEM-AND TISSUE-TYPE CELLS

PhD thesis

Murali Kumarasamy

Neuroscience Doctoral School

Semmelweis University

Supervisor: Dr. Emília Madarász PhD., D.Sc

Official reviewers:
Dr. Jedlovszky-Hajdú Angéla, Ph.D
Dr. Szabó Bálint, Ph.D
Dr. Hegedűs Tamás, Ph.D (Reserve member)

Head of the Final Examination Committee:
Dr. Benyó Zoltán, D.Sc

Members of the Final Examination Committee:
Dr. Czirják Gábor, Ph.D
Dr. Eyre Mark, David, Ph.D

Budapest, 2015

DOI:10.14753/SE.2015.1789

“Anyone who doesn’t take truth seriously in small matters cannot be trusted in large ones either.”

- Albert Einstein

DOI:10.14753/SE.2015.1789

Table of Contents

DOI:10.14753/SE.2015.1789

DOI:10.14753/SE.2015.1789

I. List of Abbreviations

CX3CR1, fractalkine receptor1

DCS, Differential centrifugal sedimentation

DLS, dynamic light scattering;

DMEM, Dulbecco's modified Eagle's medium;

FCS, foetal calf serum;

FITC, fluorescein isothiocyanate;

GFAP, anti-glial fibrillary acidic protein;

ITS, insulin-transferrin-selenite;

LAL, *Limulus* amebocyte lysate;

LDH, lactate dehydrogenase;

LPS, Lipopolysacchride

MEM, minimum essential medium

mPMS, 1-methoxy-methylphenazinium methyl sulfate;

MQ, Millipore water;

MTT, 3-(4,5-dimethylthiazol-2-yl)-2,5 diphenyltetrazolium bromide;

NE-4C, continuous mouse embryonic cell line of neuroectodermal origin

NEDA, 3 N-(1-naphthyl)-ethylenediamine;

NMs, nanomaterial

NPs, nanoparticles

NTA, Nanoparticle tracking analysis

OsO_4, Osmium tetroxide

PBS phosphate buffered saline;

PC, Protein corona;

PEG, polyethylene glycol;

PFA, Paraformaldehyde

PS, polystyrene;

RA, Retinoic acid

ROI, Region of interest;

SDS-PAGE, sodium dodecyl sulfate -polyacrylamide gel electrophoresis;

Si, Silica

TEM, transmission electron microscopy;

ZP, Zeta (ζ) Potential;

DOI:10.14753/SE.2015.1789

I. List of figures

DOI:10.14753/SE.2015.1789

II. List of Tables

DOI:10.14753/SE.2015.1789

1. Introduction

1. Basic features of nanomaterials

The prefix “nano” (Greek: nanos = dwarf) refers to nanometer (nm) which is one billionth of a meter (10^{-9} meter). Nanomaterials (NMs) are either nature-born, accidentally self-assembled or engineered structures with at least one dimension that ranges from 1 – 100 nm (Nel et al., 2006). The term “nanomaterials” (NMs) covers all nanosized materials including engineered nanomaterials (ENMs) and nano like objects existing in nature (Table 1., Figure.1). Nanoparticles (NPs) are discrete 3D particles with at least two dimensions in the nm range.

Table 1. Classification of nanoparticles by origin (Nowack and Bucheli, 2007)

Formation				**Examples**
Natural	Organic	Biogenic	Organic colloids	Humic, fulvic acids
			Organisms	Viruses
		Geogenic	Soot	Fullerenes
		Atmospheric	Aerosols	Organic acids
		Pyrogenic	Soot	carbon nanotubes (CNT)
				Fullerenes
				Nanoglobules, onion-shaped nanospheres
	Inorganic	Biogenic	Oxides	Magnetite
		Geogenic	Metals	Ag, Au
			Oxides	Fe-oxides
			Clays	Allophane
		Atmospheric	Aerosols	Sea salt
Anthropogenic (manufactured, engineered)	Organic	By-product	Combustion by-product	carbon nanotubes (CNT)
				Nanoglobules, onion-shaped nanospheres
		Engineered	Soot	Carbon Black
				Fullerenes
				Functionalized CNT, fullerenes
			Polymeric NP	Polyethyleneglycol (PEG) NP
	Inorganic	By-product	Combustion by-product	Platinum group metals
		Engineered	Oxides	TiO_2, SiO_2
			Metals	Ag, iron
			Salts	Metal-phosphates
			Aluminosilicates	Zeolites, clays, ceramics

DOI:10.14753/SE.2015.1789

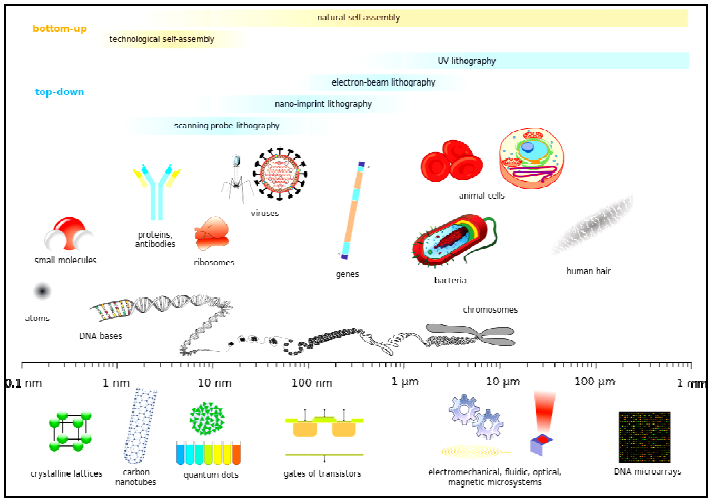

Figure 1.
Place of nanomaterials in the world of small objects, and indicating "top down" and "bottom up" strategies of their productions.

Materials with well-known properties and documented toxicity values can exhibit properly different features when moving from the bulk material to their nano state. The unique characteristics of NPs are the high surface-to-volume ratio, and the size-dependent optical and magnetic properties. As 1 nm corresponds to a row of 3 to 5 metal atoms, many aspects of the altered „behaviour" of nanomaterials are rooted in the large number of surface-exposed atoms, which are different from the atoms of the same element embedded in the bulk material (Roduner, 2006). The surface atoms (with lower coordination number) have fewer neighbours and thus, less cohesive energy. The surface atoms are less stable than the inner ones: they display higher chemical activity, and the melting point of the surface layer is lower than that of the inside material. The relatively large proportion of less coordinated surface atoms results in a distortion of the electron orbits in small particles (Roduner, 2006). The energy-states of electrons are relatively easily modified in these particles, leading to some characteristic semiconductor, magnetic and optical behaviour.

In spherical NPs, all surface atoms have an approximately identical coordination number. In cubic, triangle or rod-shaped NPs, however, the number of bonds of a surface atom will depend on its surface position: at the corners and edges the coordination number will be smaller than on the planar surface areas. As less cohesive energy makes the atoms more reactive, the chemical surface activity of particles will depend on both, their size and shape. Smaller NPs have higher surface to volume ratio, and accordingly more surface-exposed atoms: the smaller a particle is the higher its surface chemical activity will be. Particles with cornered /edged shapes will display higher surface activity than spherical particles at the same size.

DOI:10.14753/SE.2015.1789

2. Modification of nanoparticle features by surface functionalization

The high chemical surface activity of NPs results in steady adsorption of compounds from their environment resulting in molecular layers on particle surfaces with composition depending on the particle characteristics and on the available molecules in the actual surroundings. The interactions of NPs with the environment can be – at least partially – regulated by functionalizing them with specific moieties. NPs can be coated with a large variety of molecules including carboxylic acids, thiols, phosphines, amines, chemically inert polymers and active biomolecules (Roux et al., 2005, Woehrle and Hutchison, 2005, Zayats et al., 2005) using passive adsorption or covalent coupling. In NPs production, functionalisation has been used to protect NPs from aggregations/agglomerations (Grancharov et al., 2005).

With chemical functionalization, however, NPs can be designed for specific applications (Neouze and Schubert, 2008, Schulz-Dobrick et al., 2005). Functionalized nanoparticles (FNPs) can react with specific organic or inorganic compounds, thus offer transport vehicles to targeting defined objects, surfaces, living structures (Panyam and Labhasetwar, 2003). Based on novel results, many NP-carried medicines have already been accepted for clinical use and numerous preparations are under clinical testing (Zhang et al., 2008). Conjugating NPs with biologically inert substances, on the other hand, can prevent invasion of particles into living tissues, thus keeping them in the blood circulation for longer time for improved bio-imaging purposes (Nune et al., 2009). For “passivating” NP surfaces, poly-ethylene glycol (PEG) and Polyvinylpyrrolidone (PVP) are used abundantly.

2.1 Poly-ethyleneglycol **(PEG)** has a general structure of HO-{($CH_2CH_2O)_n$}CH_2CH_2-OH encompassing a chemically inert polyether backbone. The -OH groups of PEG can be used for conjugation of the polymer molecules to a variety of compounds (Roberts et al., 2002) including NP surfaces. The polyether chain can importantly reduce the chemical reactivity of NPs. Therefore PEG coating is regarded as a chemical tool to prevent absorption of NPs by living cells and thus extending the stay of particles in the blood circulation (van Vlerken et al., 2007). PEG is gradually decomposing *in vivo* by enzymolysis and hydrolysis (Guiotto et al., 2004, Kawai, 2002), and in concentrations used for nano-purposes, it is not toxic.

2.2 Polyvinylpyrrolidone **(PVP)** (Figure 2) is a non-ionic, inert polymer which, if adsorbed on NP surfaces, can stabilize monodispersed particle suspensions. PVP is not toxic and depending on the grade of polymerization can be used to prepare large viscosity physiological solutions.

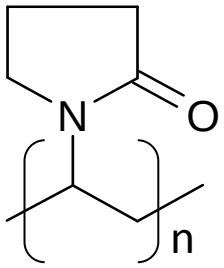

Figure 2. The chemical structure of polyvinylpyrrolidone (PVP).

PVP solutions act as blood plasm supplements and pharmaceutical vehicle material (Kadajji and Betageri, 2011).

3 Environmental and health risks of nanoparticle production and application

Nanotechnology incorporates nanoscale particulates (i.e., 10^{-9} m) into the development of new products and applications. It is a rapidly developing, cross-disciplinary and industrial science. The concept of nanotechnology was first presented by the physicist Richard Feynman at the American Physical Society in 1959 (Feynman 1960). The term “nanotechnology” was used first by Norio Taniguchi at a conference titled on Precision Engineering in 1974, (Taniguchi 1974). Since 2000, nanotechnology has grown from little more than a gleam in the eyes of researchers to a technology which is estimated to produce products between $1 trillion and $2.6 trillion by 2015 (U.S. GAO, 2010). The successful and sustainable use of the new technologies should depend on discovering safety prior to wide application (EEA 2001).

The increased production and industrial use of NPs result in an enhanced environmental nano-pollution and in an enhanced exposure of individuals either through inhalation or skin contact. The health impact of chronic exposure to nanoparticles and the potential accumulation of particles in the body need urgent exploration. Moreover, the increasing application of NPs as food supplement, cosmetic compounds, drug-delivery vehicles or contrast materials for medical

imaging calls for urgent understanding of health risks of different types of NPs, and for a deeper understanding of the interactions of nanomaterials (NMs) with living organisms.

Nanotoxicology, a term coined by Donaldson and his co-workers (Donaldson et al., 2004), refers to the study of the potential toxic impacts of nanoparticles (NPs) on biological and ecological systems (Figure 3).

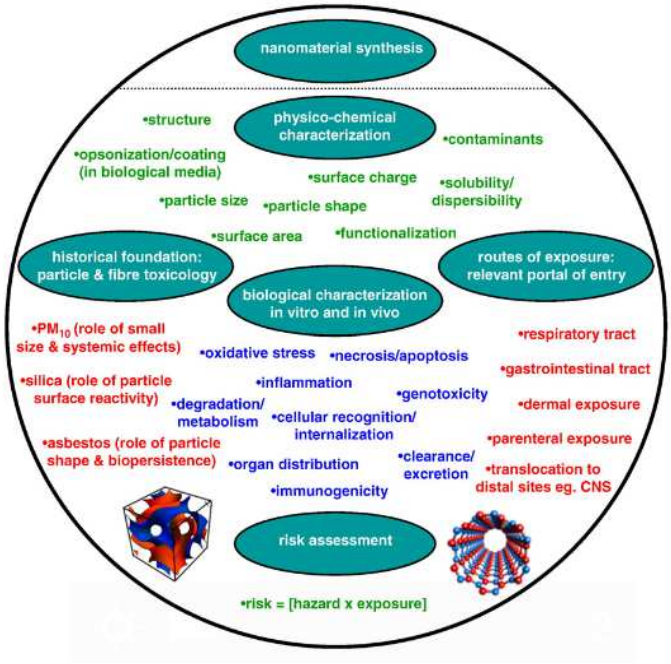

Figure 3. Overview of the interdisciplinary science named nanotoxicology. (Fadeel and Garcia-Bennett, 2010)

Nanotoxicology covers many disciplines like material science, physics, chemistry, biology, ecology and medicine. Besides focusing on physicochemical properties and biological interaction of NPs, research in nanotoxicology focuses on methods to test the safety of particles. Because of the special nano-properties, methods developed for testing toxicity of bulk materials are not suitable to monitor the health risks of NMs. Many important characteristics of NPs including size, shape, surface area, core- and surface chemical composition, solubility of core substances, and aggregation/agglomeration are relevant features for toxicity considerations (Nel et al., 2006)

4 Possible routes of Nanoparticles to entering the human body

Exposures to natural airborne nano-sized particles have been experienced by humans throughout the human history. Nano-sized materials can be generated by natural geological and biological events or from human created processes as NP production,

combustion or even by novel pharmaceutical/medical inventions. Several nanoparticles appear to accumulate in different organs, penetrate individual cells and trigger toxic responses. NPs can enter the body through various routes (Figure 4) including the respiratory system, digestive canal or body fluids. NPs if got into the blood circulation can be transported to various organs including the central nervous system (CNS).

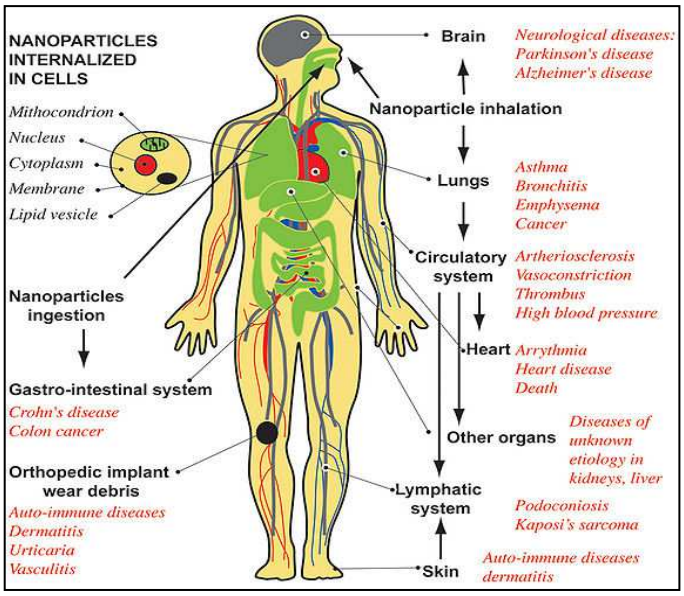

Figure 4. Possible adverse health effects associated with ingestion, inhalation and contact with NPs.

Accumulating evidences show that NPs can reach the CNS also from the nasal cavity through the nasal epithelium (Win-Shwe and Fujimaki, 2011) (Figure 5).

Figure 5.
Potential routes of nanoparticles to the brain and presumed consequences (Adapted from Win-Shwe and Fujimaki, 2011)

.

In the brain, NPs may induce inflammation, oxidative stress and apoptosis of various types of neural tissue cells (Söderstjerna et al., 2014).

5. Interaction of nanoparticles with the central neural tissue

The central nervous system is protected from outside mechanical insults by the solid scaffold of the skull, and by the flexible pressure distributor cerebro-spinal fluid. The chemical/biological protection of the highly controlled intracerebral environment is provided by the blood-brain barrier (BBB). The BBB is a multicellular assembly of endothelial cells, astrocytes and pericytes (Zlokovic, 2008), which escort the entire brain / spinal capillary system (Figure 6).

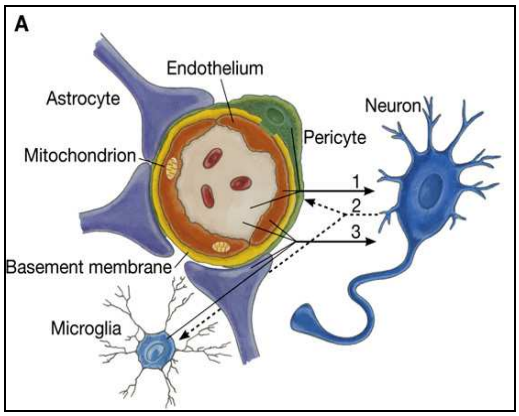

Figure 6. Schematic diagram of the Neurovascular Unit (BBB) (Zlokovic, 2008).

Endothelial cells lining the brain capillaries represent a large part of brain cellular mass and display different functional features than the capillary endothel in the periphery. In the "healthy" brain capillaries, the transepithelial pynocytotic transport is highly reduced and the paracellular solute move is excluded. The material transport is established *via* specified transcellular pathways, controlled by selective transport proteins and specific receptor mediated-transcytoses (Abbott et al., 2006). The specific feature of the brain microvessel endothelium exists only in coupling of endothelial cells with astrocytes and perycytes: the multicellular assembly can provide the controlled physical and chemical border between the circulating blood and the intracerebral extracellular space (Grammas et al., 2011).

Nanoparticles, however, were reported to cross the BBB (Ma et al., 2010). There are three main ways to penetrate NPs from the blood into the brain:

i) small (2-7 nm) metal or metal oxide particles can foul and/or damage the cell membrane, and passively penetrate the endothelial cells (Peters et al., 2006). Using similar mechanisms, they can get to the other side of the barrier, stochastically.

ii) larger (10-70 nm) particles may get through the BBB if molecules from the blood accumulate on NP surfaces and lead them to receptor-specific transcytosis paths. This route is considered for producing specifically functionalized NPs as BBB penetrating vehicles for drug delivery into the brain (Jones and Shusta, 2007)

iii) Large (>80 nm) particles can get through the barrier only if it is severely damaged. Transient damages of the BBB can be evoked by osmotic or local heat shock (Konofagou, 2012, Lindsberg et al., 1996, Wang et al., 2007); these routes are also considered for compound delivery to the brain.

Another route for invasion NPs into the brain is the translocation from the nasal epithelium to the olfactory neuronal pathway along the axons of the primary odor-sensing cells (Elder et al., 2006). While NPs can get directly to the forebrain on this way, the penetration area and therefore the capacity of this gate is much smaller than that of the BBB.

In early embryonic ages the developing brain has no separate barrier systems; the differentiating neural tissue is protected solely by the placenta, the interface between the fetal and maternal environments. Multiple lines (mouse) or syncytia (human) of the trophoblast cells provide the main structural and functional components which bring the fetal and maternal blood systems into close contact. The fetal vascular compartment of the placenta arises from the allantoic mesoderm of the embryo, and the maternal components derive from

the maternal vasculature and uterine decidual cells (Figure 7). Nanoparticles injected into the maternal blood supply, however, may pass through and damage the trophoblast layers and can enter the embryonic circulation.

DOI:10.14753/SE.2015.1789

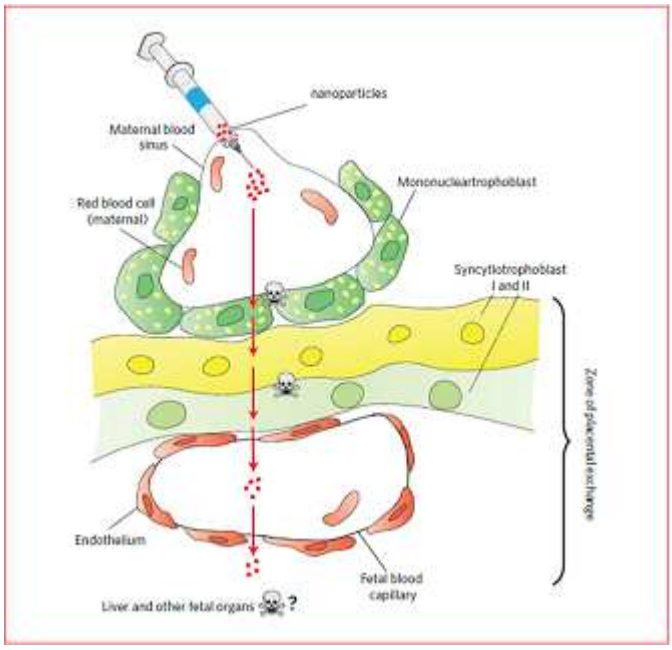

Figure 7. Nanoparticles (shown in red) injected into the maternal blood supply (top) may pass through three layers of trophoblast cells to enter the fetal blood. NPs may damage placental trophoblast layers and enter the embryo. (Yamashita et al., 2011)

Despite of extended studies on the maternal-fetal transfer of nano-scale substances (Alexis et al., 2008) (Peer et al., 2007) and the associated risk of growth and developmental defects in the fetus (Ema et al., 2010); (Bar-Ilan et al., 2009), contradictory data are available on the barrier function of placenta against nano-sized material (Table 2) .

Behind the BBB or placenta, the adult or developing CNS tissue comprises multiple cell types including neurons, astrocytes, oligodendrocytes, microglia, as well as a number of different neural stem/progenitor cells (Madarsz, 2013). According to the fairly different physiological characteristics of these cells, vulnerability and reactions to NPs are expected to show high cell-type dependency. Neurons, the most vulnerable cells, do not display high endocytotic activity, thus will not take up large amount of medium or large-size (>20 nm) particles but might be invaded passively by small NPs. In contrast, astrocytes and especially microglia cells can phagocytose larger particles and give cell-specific responses to internalized foreign bodies. To understand cell-type specific responses, we compared the effects of nanoparticles on in vitro model systems including primary cultures of mouse forebrain neurons (Madarasz et al., 1984), astrocytes (Környei et al., 2005), brain microvessel endothelial cells (Nakagawa et al., 2009) and microglia cells (Saura et al., 2003)., as well as embryonic mouse neural stem cells (Schlett, Madarasz 1997) and their neuron-derivatives.

DOI:10.14753/SE.2015.1789

Table 2. Barrier function of placenta against nano-sized material (Buerki-Thurnherr et al., 2012)

NP type	NP size (nm) /modification	Dose / route of administration	NP application /length of exposure	Model system	Major outcomes
Gold	5 and 30 / radiolabeled	0.02 mg / iv	GD 19 / 24 h	Rat	Transplacental transfer rates of 0.018% for 5 nm and 0.005% for 30 nm NP.
	1.4 and 18 / radiolabeled & TPPTS	N.s. / iv	3rd trimester / 24 h	Rat	Size-dependent uptake in placenta (0.03% of 1.4 nm and 0.0002% of 18 nm NP) and fetus (0.006% of 1.4 nm and 0.00005% of 18 nm NP).
	10 / PEG 15 / PEG 10 and 15 / PEG	9.1*109 NP / ml 9.1*109 NP / ml 3.6*1010 NP / ml	6 h perfusion 6, 24 and 48 h in vitro BeWo	Human	No NP transfer observed, particles accumulate in the trophoblastic cell layer Uptake and retention of NP in BeWo cells
Polystyrene beads (PS)	20, 100, 500/ fluorescent, carboxylic; 200 /fluorescent, amine	from 0.5%w stock: 0.6 µl (PS 20, 100), 8 µl (PS 500), 1.25 µl (PS 200) / injection via extra embryonic tissue.	GD 7.5 / 12 h	Rat	Modification affects transplacental transfer: Amine-PS 200 pass extraembryonic tissue while carboxy PS bigger than 100 nm accumulate in the extraembryonic tissue.
	50, 80, 240, 500 / fluorescent	25 µg/ml	6h perfusion	Human	Size-dependent transplacental transfer (35% of PS 50, 30% of PS 80, 9% of PS 240 and 1% of PS 500)
Silicon nanovectors	519, 834 and 1000	1.2*109 NP/ml/ iv	GD 20 / 4 h	Rat	Transplacental transfer of the particles is size dependent (particles > 800 nm do not cross)
SiO_2 (nSP)	70, 300 and 1000/ nSP70 iv carboxylic or amine	0.8 mg (nSP70 also at 0.4 mg) / iv	GD 16 and 17 / GD 18	Mouse	70 nm SiO2 cause pregnancy complications, and it presents in the placenta, fetal liver and fetal brain
TiO_2	25 70	0.1 mg / sc	GD 3, 7,10 and 14 / P4 and 6 weeks	Mouse	NP cross the placenta and can damage the genital and cranial nervous system.
	21 / modified with Al, Si and Zr and coated with polyalcohols	40 mg/m3; 1h / day / inhalation	GD 8-18 / P2 and P23-24	Mouse	Offspring displays neurobehavioral alterations but unclear if effect is direct or indirect; transplacental transfer of NPs not investigated.
	35	0.8 mg (nSP70 also at 0.4 mg) / iv	GD 16 and 17 / GD 18	Mouse	TiO2 cause pregnancy complications, TiO2 present in the placenta, fetal liver and fetal brain
Quantum- dots	1.7, 2.6 and 3.2 / pristine or coated with MPA, PEG and SiO2	20, 50, 86, 125 µg / iv	GD 20-22 / P0	Mouse	Size-dependent transfer of particles across the placenta; coating of particles reduced the transfer
Fullerenes	Average size < 10	0.3 mg/kg / iv	GD 15 / 24 and 48 h	Rat	Particles cross the placenta and are transmitted to the offspring
Single-walled carbon nanotubes	850 x 2.37 / pristine; 760 x 1.58 / oxidized; 370 x 1.8 / ultra-oxidized	10 ng to 30 µg / injection into retrobulbar plexus 0.1-100 µg/ml	GD 5.5 / 10 d EST (NIH3T3 and mES) / 10 d	Mouse	Low doses of particles affect embryonic development; effects more pronounced for oxidized particles EST predict in vivo data, identifying oxidized particles as the more toxic compound
CoCr	29.5	0.12 mg / iv 0.04 mg/ml	GD 9.5 or 12.5 / 7 d In vitro transwell co-cultures (BeWo + fibroblasts)/ 24 h	Mouse Human	DNA damage of CoCr NPs across bilayered but not monolayered barriers. Indirect DNA damage to fibroblasts without passage of NPs is dependent on thickness of the BeWo barrier

As the characteristics of NPs including size, shape, core- and surface chemical composition, solubility of core substances, and aggregation/agglomeration influence their biological interactions, each sort of particles need separate nanotoxicological / nanosafety considerations. The extension of the thesis does not allow listing the huge amount of data published on reactions of neural cells to various NPs fairly differing in size, surface charge, functionalization and core material. In this project, we used nanoparticles with equal size-range (45-70 nm), but different core materials: polystyrene (PS) silica (Si) and silver (Ag). The overview of the cellular responses to NPs has been restricted to these particles.

6.1. Polystyrene (PS) nanoparticles

PS is a commonly used and well characterised polymer, with many applications in the everyday life. It is an inexpensive hydrophobic polymer which allows physical adsorption of proteins, and can be functionalized with reactive molecule groups which enables covalent binding of various substances. Styrene (Figure 8) oligo- and polymers are present naturally in vegetables, nuts, beverages, and meats (ATSDR 2007) and are widely used in a number of products including fibreglass, automobile parts, plastic pipes, drinking cups, food containers wound dressings, implantable medical devices (Ahmad and Bajahlan, 2007). It can be used also as a hydrophobic encapsulation material in biomedical applications, (Singer et al., 1987).

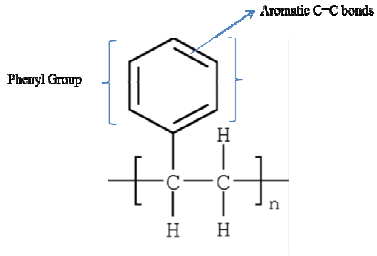

Figure 8. The styrene monomer: the structural unit of polystyrene

The bulk form of PS is non-toxic, not carcinogenic to humans (Snyder 2009). Clinical laboratory reports revealed that the small amount of styrene leaching to food from styrene-based packaging material has low acute toxicity, while its uptake is rapid and the elimintion is slow (t½ 2-4 days) (Cohen et al., 2002). Styrene can be bio-transformed into styrene-7,8-oxide in the liver and 90% of an oral dose is excreted as catabolites. The excretion rate, however, was shown to be species dependent. While polystyrene and even styrene, in their bulk form may be non-toxic, it is imperative for a full toxicological characterization of its nano form before it can

be considered for biological applications. Our choice of nanopolystyrene was influenced by the explicit requirement for investigating the health and environmental risks of PS NPs (OECD 2008).

Polystyrene nanoparticles are commercially available in different sizes, with various surface modifications and fluorescent labels. Such particles are used as immunofluorescent reagents, microinjectable cell tracers as well as calibration standards for microscopy and flow cytometry.

Despite of the non-toxic nature of PS bulk material, recent data indicated mild toxicity of PS NPs. Mahler and co-workers reported that 50 nm polystyrene nanoparticles could interfere with iron adsorption by the gut epithelium (Mahler et al., 2012). Lunov and co-workers showed that PS NPs modulated human macrophage inflammosomes (Lunov et al., 2011). ROS generation by macrophages was detected upon exposure to PS NPs (Xia et al., 2006) with an indication of NP-induced mitochondrial injury leading to oxidative stress. Bexiga and co-workers (Bexiga et al., 2011) demonstrated morphological changes of the mitochondria in a human brain astrocyte cell line resulting in increased ROS production and consequent apoptotic cell death. Size-dependent uptake (Varela et al., 2012) and lysosome-damaging actions of carboxylated polystyrene nanoparticles (Frohlich et al., 2012) were also detected and showed that only small PS NPs (20 nm) induced apoptosis and necrosis in human endothelial cell lines. Frohlich and co-workers (Frohlich et al., 2010) found that while NPs are “attacking” at the first place the endosomes, lysosomes and mitochondria, the drug-metabolizing cytochrome P450 (CYP) enzyme activity is also influenced by small/medium (< 60 nm) PS NPs. Clift and co-workers demonstrated (Clift et al., 2010) that carboxylated PS NPs could cause hemolysis, thrombocyte and granulocyte activation upon in vitro exposure of blood samples to small (< 50 nm) particles. Detailed studies (McGuinnes et al., 2011), however, indicated that platelet aggregation was induced by aminated or carboxylated PS NPs; therefore the cytotoxicity seemed to depend on the surface composition (and not on the PS core material) of the particles. Negatively charged PS NPs induced an up-regulation of adhesion receptors, while positively charged particles caused perturbation of the cell membrane (Liu et al., 2011). In general, cationic (amine group functionalized, positively charged) NPs seem to exert higher cytotoxicity. High cytotoxicity of 60 nm amine-functionalised PS NPs was shown on macrophages and also on epithelial cells (Xia et al., 2008).

In vivo studies revealed large variations in the body distribution of PS NPs depending on the size of the particles and on the route of body penetration (Sarlo et al., 2009) While about 90 % of particles were settled in the lung after minutes of inhalation, the clearance from the lung and the accumulation in other organs were completely different for 20nm, 100 nm and 1000 nm size PS NPS. Small particles were rapidly cleared from the lung and also from the circulation. As particles larger than 10 nm are not excreted by the kidney (Soo Choi et al., 2007), they are cleared from the circulation by penetration into various tissues. Accumulation of PS NPs in the liver had been known for a long time (Moghimi et al., 1991) It is thought that particles can be partially cleared from the body by bile excretion (Cho et al., 2009) The potential penetration of PS-NPs through the bovine nasal epithelia (Sundaram et al., 2009) highlights the importance for studies on their potential toxic effect on neural tissue cells.

6.2. Silica nanoparticles

Silicas are some of the most abundant compounds found naturally in the earth's crust and can be divided into crystalline or non-crystalline (amorphous) silicas, all having the same basic molecular formula (almost 100% SiO_2) (Arts et al., 2007). SiO_2 is widely used in many industrial fields including production and application of glass, microelectronics, insulation material etc. Despite of the large body of studies, the role of SiO_2 as a chemical compound in the mammalian body are far from clear. While SiO_2 is regarded generally as a non-toxic chemical, silica dust (containing micron and nano-sized silica particles) is known to cause silicosis, inflammatory reactions and respiratory system cancers.

In stable cristalline form of silica, 4 oxygen atoms surround a central Si atom providing a tetrahedral coordination and giving a final molecular ratio of SiO_2. Engineered amorphous silica nanoparticles (SiO_2 NPs) are built up by a random packing of $[SiO_4]n$ units with the same general molecular formula SiO_2 (Bergna and Roberts, 2006). The molecular structure at the surfaces, however, May consists of siloxane groups (≡Si-O-Si≡) or silanol groups (≡Si-OH). Different forms of silanols and siloxane are presented in Figure 9.

DOI:10.14753/SE.2015.1789

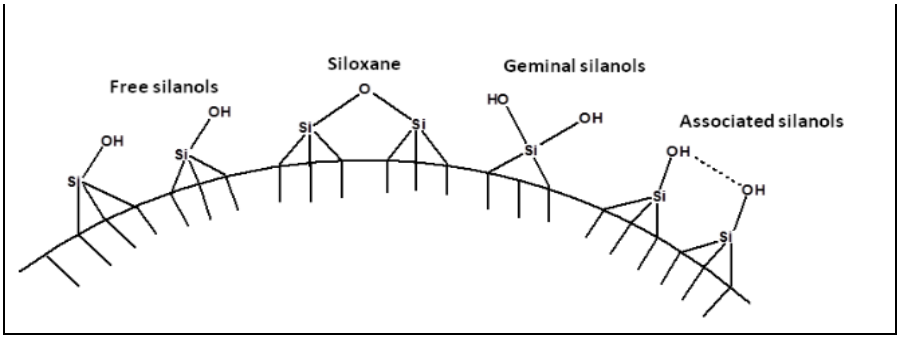

Figure 9. Silica particle with various silanol groups

The surface-exposed oxygen or OH groups result in a net negative charge of the SiO_2 particles and provide reactive sites for spontaneous or intentional chemical modification of particle surfaces.

Silica NPs (SiO_2 NPs) are produced in industrial scale. They are used as additives to cosmetics, drugs, foods and have wide applications in biotechnology and biomedicine as drug delivery systems (Venkatesan et al., 2005), vehicles for anti-cancer therapeutics (Hirsch et al., 2003) or DNA transfecting agents (Bharali et al., 2005). SiO_2 has also found extensive usage as additive in paints and varnishes, anticaking agents in various powders including salt or spices, as coating material in confectionery products and in improved packaging materials, serving as gas barrier to prolong the product shelf life (Chaudhry et al., 2008).

The safety or toxicity of SiO_2 NPs has been studied extensively. Arts et al demonstrated that SiO_2 NP induced respiratory fibrogenesis in Wistar rats (Arts et al. 2007), while other tudies indicated that SiO_2-coated cerium (CeO_2) NPs induced only minimal lung injury and inflammation (Demokritou et al., 2013). Toxic effects of SiO2 NPs with diameters of 10-15 nm were reported in various mouse tissues (Hassankhani et al., 2014).Some in vivo studies reported that silica nanoparticles induced autophagy in endothelial cells and influenced angiogenesis (Duan et al., 2014). Intravenously administrated amorphous silica nanoparticles (SNPs) were found mainly in the macrophages of the liver and spleen in mice (Yu et al., 2013). Silica particles evoked systemic Th2 response and exacerbations of Atopic dermatitis (AD)-like skin lesions by enhanced IL-18 and thymic stromal lymphopoietin (TSLP) production (Hirai et al., 2012).

I*n vitro* studies reported that SiO_2 NPs evoked pro-inflammatory reactions in rat endothelial cells (Peters et al., 2004), showed dose-dependent cytotoxicity on human bronchoalveolar cells (A549), embryonic kidney cells (HEK293) and mouse macrophages (RAW264.7), and could induce oxidative stress and glutathione depletion (Park and Park, 2009, Wang et al., 2009). Napierska et al. demonstrated size-dependent cytotoxic effects of amorphous silica *in vitro* and concluded that the surface area of amorphous silica is an important determinant of cytotoxicity (Napierska et al., 2009). The exposure of Calu-3 cells to 10nm SiO_2-NPs showed time- and concentration-dependent cell death and increased the expression of interleukin (IL)-6, IL-8 and matrix metalloproteinase-9 coding genes, while 150 or 500 nm SiO_2-NP did not exert toxic effect (McCarthy et al., 2012). Studies on 59 nm and 174 nm SiO2-NPs showed clear increase in microtubule (MT) dynamics and reduced cell motility in A549 human lung carcinoma cells (Gonzalez et al., 2014).
50nm silica-coated magnetic nanoparticles were shown to penetrate the blood brain barrier (BBB) (Kim et al., 2006). Wu and co-workers showed that SiO_2-NPs could enter the brain also upon intranasal loading (Wu et al., 2011). Inside the brain, SiO_2 particles were found in the striatum, where they induced oxidative damage and evoked inflammatory responses. (Wu et al., 2011). These data together with the intended medical use of SiO_2 NPs raise important questions concerning the potential neurotoxicity of SiO_2-NPs.

6.3. Silver NPs

Since the earliest times, silver has been used in daily life as well as in medicine. In ancient Italy and Greece silver was used for storage vessels to keep water fresh. Silver has been used in consumer's products for centuries, particularly as jewellery, silverware and photographic material (Wijnhoven et al., 2009). The antibacterial effect of silver, however, was not scientifically described until the late 19th century (Russell and Hugo, 1994). Subsequently, silver has been used in a wide range of medical devices and surgical textiles (Lansdown, 2006). Silver salts have been used to treat a variety of diseases even today to prevent infections (Lansdown, 2006). Silver can be absorbed orally, by inhalation and through damaged skin (Drake and Hazelwood, 2005). Soluble silver compounds are more readily absorbed than metallic or insoluble silver and are thus more likely to cause adverse health effects (Drake and Hazelwood, 2005). The most common adverse health effect associated

with prolonged exposure to silver compounds is the development of a characteristic, irreversible pigmentation of the skin (argyria) and/or the eyes (argyrosis) (ATSDR (1990)) in the ophthalmic mucosal membranes (Jonas et al., 2007).

Silver nanoparticles (Ag NPs) are synthesized using various techniques resulting in different shapes and sizes for use in numerous applications. The most common technique involves the dissolution of silver salt into a solvent and the subsequent addition of a reducing agent supplemented with stabilizing agents to prevent agglomeration of NPs. Some of the most commonly used stabilizing agents are sodium citrate and polyvinylpyrrolidone (PVP) which yield particles with a negative surface charge at physiological pH. The solvents and reducing agents used in the synthesis process affect the physical and morphological characteristics of the resulting Ag NPs.

In contact with living material and/or physiological solutions, Ag+ ions dissolve from Ag NPs. Moreover, the particles serve as a store for Ag+ ions resulting in a prolonged, long-term Ag+ release. Therefore, argyria easily develops in response to direct oral or skin exposure to suspensions of Ag NPs (Kim et al., 2009), or through inhalation of AgNP from room disinfectant spray. Regardless of whether exposure is dermal, oral or respiratory, rodent studies show that silver ions (Ag^+) released from AgNPs enter the systemic circulation and accumulate in a number of tissues, including the brain (Johnston et al., 2010). Silver nanoparticles invade the rat brain after subcutaneous injection (Tang et al., 2008), and maternal exposure to Ag NPs induce oxidative stress and apoptosis in the developing brain (Fatemi et al., 2013). (Lee et al., 2013) reported that silver content in brain and testes were not cleared even after 4 months.

A study on global gene expression analysis (Kyoto Encyclopedia of Genes and Genomes (KEGG) demonstrated that a total of 279 mouse genes were up-regulated and 389 genes were down-regulated in response to silver-NP suspension, while only 3 genes were up-regulated and 41 genes were down-regulated due to silver ion exposure. A pathway analysis on different cells (KEGG) showed that 23 signal transduction pathway-elements were affected after exposure to Ag NP suspension, not silver ion (Ag+) alone.

Several *in vitro* studies have been focused on revealing the cellular mechanisms of Ag+ / AgNP toxicity. On primary rat brain microvessel endothelial cells Ag NPs were shown to increase the membrane permeability mainly by activating

proinflammatory mediators (Trickler et al., 2010). By inducing interleukin-6 (IL-6) mRNA expression, 20 nm Ag NPs were found to activate rat lung epithelial (RLE) and rat aortic endothelial (RAEC) cells (Shannahan et al., 2014). Most significant report indicates that the inflammatory signal pathways were induced by exposure to Ag NPs but not to solutions of Ag+ ions (Xu et al., 2014).

Clathrin mediated endocytotic uptake and cytoplasmic and nuclear accumulation of Ag NPs were revealed in human glioblastoma cells (U251) (Asharani et al., 2009). Also, a concentration-dependent accumulation of Ag NPs was demonstrated in primary astrocytes (Luther et al., 2011). Silver NPs of 20 and 80 nm sizes affected the growth of human embryonic neural precursor cells (Soderstjerna et al., 2013). Recent studies on the same 20 and 80 nm Ag NPs showed that all neuronal layers of the retina took up particles and displayed neural tissue damages (Soderstjerna et al., 2014). Ag NPs of 20nm size were shown to affect the neurite outgrowth and to reduce the viability of premature neurons and glial cells (Xu et al., 2013)

Despite of the large body of literature data, the nano-size caused effects of silver are far from clear.

7. Objectives

The main objective of the studies was to explore the reactions of different neural tissue cells to defined types of nanoparticles. The study focused on

- *the roles of chemical surface composition of otherwise identical nanoparticles*. To avoid variations by size and dissolution of biologically active compounds, particles with uniform size and non-toxic, (polystyrene, silica) core material but with different surface groups were probed in vitro on neural stem cells, stem cell-derived and primary neurons, astrocytes, microglia and brain microvessel endothelial cells.
- *the barrier function of the placenta against the invasion of differently functionalized NPs*. The distribution of negatively charged and PEG-passivated PS NPs in the placenta and embryonic brain was investigated 5 minutes and 4 days after a single intravenous injection of particles.
- *the roles of aging of nanoparticles in biological interactions*. The cellular uptake and viability effects of fresh and aged (shelf-life > 6 months) NPs were compared and were related to the physico-chemical changes of NPs during ageing.
- *the roles of shape of Ag NPs in neurotoxicity.* Ag NPs with different (sperical, cubic triangle, rod) shapes were synthezised, characterized and probed on neural stem cells.

DOI:10.14753/SE.2015.1789

2. Materials and Methods

1. Synthesis of nanoparticles

In the studies, 40-70nm PS NPs, 50 nm silica NPs and silver nanoparticles of different geometries with at least one dimension about 50 nm were used.

1.1. PS NPs of 45-70 nm diameter, core-labelled with NileRed, Yellow or FITC fluorochrome, and with carboxylated or PEGylated surfaces were purchased from Spherotech, Inc. (Lake Forest, IL, USA, IL) and from Kisker Biotechnology Gmbh (Steinfurt, Germany). The PEG chains on the NP surfaces were 600 Da or 2 kDa.

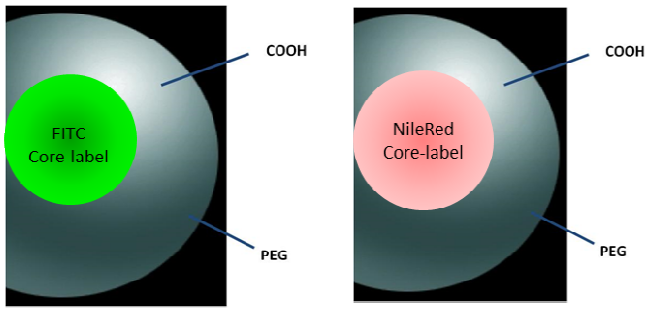

Figure 10. PS NPs with different surfaces and fluorochrome labelling

1.2. Preparation of silica nanoparticles

The silica particles were synthesized, functionalized and characterized by Emilia Izak-Nau at Bayer (Izak-Nau et all, 2014). Technological services, GmBH, Germany. Spherical core-shell 50 nm SiO2 NPs encapsulating fluorescein-isothiocyanate (FITC, ≥90%, Fluka) were synthesized with modified Stöber method (Stöber et al., 1968). The NPs surface was either coated with polyvinypyrrolidone (PVP K-15, Sigma) or modified to generate amino and mercapto functionalities by addition of 3-aminopropyltriethoxysilane (APTES, 98 %, Alfa Aesar) and 3-mercapto-propyl-trimethoxysilane (MPTMS, Sigma-Aldrich) organosilanes, respectively (Cassidy and Yager, 1971).

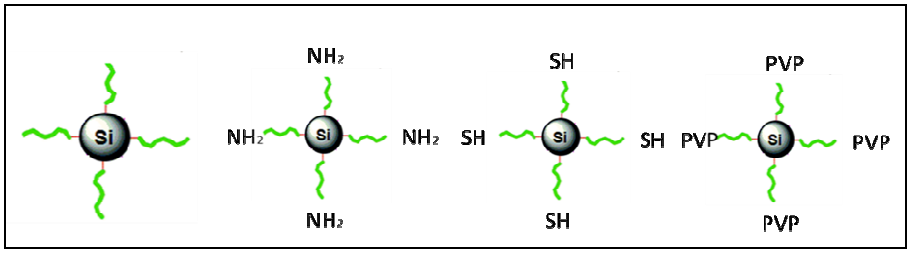

Figure 11. Differently functionalized FITC labelled silica nanoparticles

1.3. Preparation of Silver (Ag) NPs

1.3.1. 50nm bare and PVP-coated AgNPs were synthesized by Murali Kumarasamy, at ICN Barcelona according to Bastús and co-workers (Bastús et al., 2014).

1ml of 0.5M sodium citrate and 1ml of 25mM tannic acid were mixed with 97mL H_2O in a three-neck round bottom flask. The mixture was heated to boiling under vigorous stirring followed by a fast injection of 1ml 50mM $AgNO_3$. The growth of nanoparticles was achieved by consecutive additions of 50mM $AgNO_3$ (1 ml per addition). After 1ml of 50mM $AgNO_3$ each injection, the solution was kept under reflux to complete the reaction for 30 mins. 50nm spherical Ag NPs were obtained at the 10^{th} injection. The as-prepared nanoparticles were centrifuged at 8000g for 15mins prior to conjugation with PVP

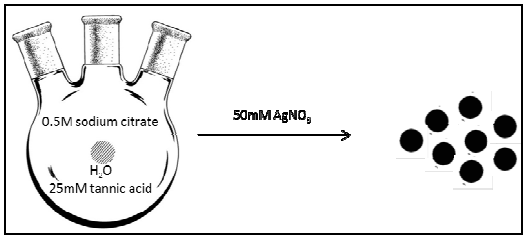

Figure 12. Preparation of spherical Ag NPs

Conjugation of Silver Nanoparticles with Polyvinylpyrrolidone.

Synthesized Ag NPs (~50 nm, 7.5 × 1011 NPs/mL) was redispersed in a fresh solution of 5 mM polyvinylpyrrolidone (PVP, MW = 55,000 kDa) and left during 72 h under vigorous stirring. Then, the Ag NPs were washed again in order to eliminate the excess of PVP.

1.3.2. Synthesis of Ag nanocubes (Zhang et al., 2010)

Ethylene glycol (5 ml; EG) was heated with magnetic stirring in a 100 ml round bottom flask in oil bath preset to 150° C. Sodium hydrosulfide (NaSH; 0.06 ml; 3 mM in EG) was quickly injected into the solution after its temperature reached 150° C. After 2 min incubation, 0.5 ml aliquot of 3 mM HCl in EG, then 1.25 ml PVP (20 mg/ml in EG, MW 360,000) were injected into the reaction solution. After another 2 min incubation, silver trifluoroacetate (CF_3COOAg; 0.4 ml, 282 mM in EG) was added into the mixture. During the entire process, the flask was capped with a glass stopper except the addition of reagents. After addition of CF_3COOAg, the transparent

solution took a whitish color and became slightly yellow in 1 min, indicating the formation of the Ag seeds and then nanocubes.

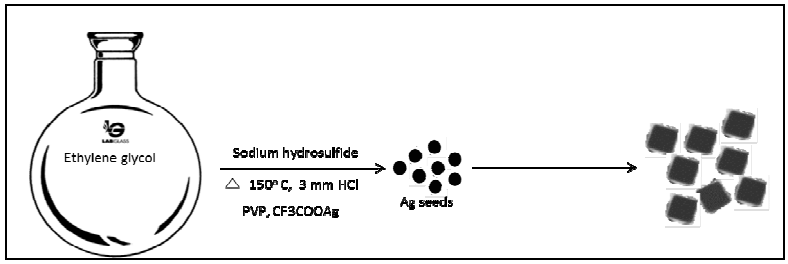

Figure 13. Preparation of silver cubic nanoparticles

1.3.3. Synthesis of PVP coated Ag nanotriangles (Zhang et al., 2011)

A 24.04 mL aqueous solution containing $AgNO_3$ (0.05 M, 50μL), trisodium citrate (75 mM, 0.5 mL), PVP (40K, 17.5mM, 0.1mL) and hydrogen peroxide (H_2O_2) 30 wt %, 60μL) was vigorously stirred at room temperature in air. Sodium borohydride ($NaBH_4$, 100 mM, 250μL) was rapidly injected into this mixture to initiate the reduction. The solution gradually turned from light yellow to dark blue in color within 60 mins.

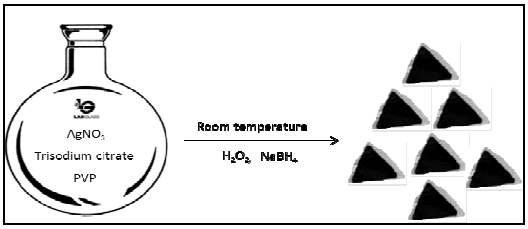

Figure 14. Preparation of silver nanotriangles

1.3.4. Synthesis of Ag Nanorods

0.5 ml of $FeCl_3$ solution (0.6 mM, in EG) was added to 6 ml EG in a round-bottom flask and was heated to 150±4 °C, then 6 ml EG solution containing 0.052 M $AgNO_3$ and 0.067 M PVP (average molecular weight 360 kDa) was added. The reaction mixture was kept at 150±2 °C with stirring at 250 rpm, until $AgNO_3$ was completely reduced (about 70-90 minutes).

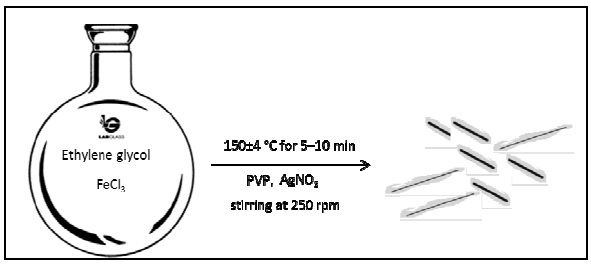

Figure 15. Preparation of silver nanorods

In order to examine the yield and morphology of Ag nanorods, 1 ml of the resulted suspension was diluted with 8 ml acetone and 8 ml of ethanol, and centrifuged at 2000 rpm for 10 min for two times. At every stage, the supernatant solution was measured with a UV-spectrometer to confirm the relative amount of silver nanoparticles.

All the synthesized Ag NPs were washed several times with water and then Stored at 2-8°C and protected from light. In the specified conditions the colloidal silver is stable for at least one year.

2. Physico-chemical characterization of nanoparticles

PS and Ag NPs were fully characterised by different techniques including Dynamic Light Scattering (DLS), Zeta Potential (Z-Potential), Nanoparticle Tracking Analysis (NTA), Transmission Electron Microscopy (TEM), differential centrifugal sedimentation (DCS) and UV–Visible spectrophotometry.

Si NPs were thoroughly characterized by Emilia Izak-Nau, using also X-ray photoelectron spectroscopy (XPS) and time-of-flight secondary ion mass spectrometry (ToF-SIMS, ION-TOF) (Izak-Nau et al., 2014).

2.1. Transmission electron microscopy (TEM)

TEM images were obtained with a (TEM; JEOL JEM 1010, JEOL Ltd., Tokyo, Japan and Phillips CM20; Philips, Amsterdam, Netherlands) at 200 keV and by using carbon grids (S162, Plano GmbH, Wetzlar, Germany). Carbon grids were dried at Room temperature (RT) and the areas of the grid were observed at different magnifications. TEM pictures were computer-analysed on spot, and the size distribution and average size of particles were determined.

2.2. Dynamic light scattering (DLS) and Z-Potential measurement

Nanoparticles suspended in water, phosphate buffered saline (PBS), 10% fetal calf serum in PBS and culture media were characterised by dynamic light scattering (DLS) and by zeta potential determination (Malvern Zetasizer Nano ZS90; Malvern, UK). Particles were sonicated for approximately 20 seconds before being dispersed in the appropriate dispersants. All DLS measurements were done with a Malvern Zetasizer Nano ZS90 (Malvern, UK) operating at a light source wavelength of 532 nm and a fixed scattering angle of 173^{o}, on 1 ml aliquots of the NP suspensions. Zeta

potential and DLS assays were performed at 25°C and 37°C and are presented as averages and standard deviations of data obtained from 3 to 5 assays in each solution.

2.3. UV–visible spectrophotometry of Ag NPs

UV–Visible spectra of 1ml aliquots of the NP suspensions were assayed with a Shimadzu UV-2400 spectrophotometer, in the 300–800 nm wavelength range. This technique provides characteristic absorbance maximum for metallic NPs (due to their surface plasmon resonance), which changes with the size, morphology and surface alterations of the NPs.

UV-vis extinction spectra were taken at room temperature using a 1cm optical path quartz cuvette by diluting 0.1mL of sample solutions into 1mL.

2.4. Nanoparticle tracking analyses (NTA)

Nanoparticle tracking analyses (NTA) were performed using a Nanosight instrument model LM10 (NanoSight Ltd., Salisbury, UK) equipped with red laser (630 nm) and a CCD camera. The samples were dispersed in milli-Q water and the experiments were performed at 22^0 C. The brownian motion of the particles were analysed on 60-second records by NTA software.

2.5. Differential Centrifugal Sedimentation (DCS)

Differential centrifugal sedimentation experiments were performed with a disc centrifuge (Model DC 24000; CPS Instruments Europe, Oosterhout, The Netherlands). A gradient of 2%–8% sucrose equilibrated with spinning at 22000 rpm for 30 minutes was established and calibrated by running standard polystyrene beads. After establishment of the gradient, 100µl aliquots of particles dispersed in water were injected. Samples were spinned for approximately 2 hours in case of PS NPs and 5-10 minutes for Ag spherical NPs. The position of particles in the gradient was analysed with CPS Instrumental software. The tallest peak (the most frequent size value) was regarded as the ‘base’ peak (100%) and all other particle size peaks were normalized against this base peak (relative size distribution).

DOI:10.14753/SE.2015.1789

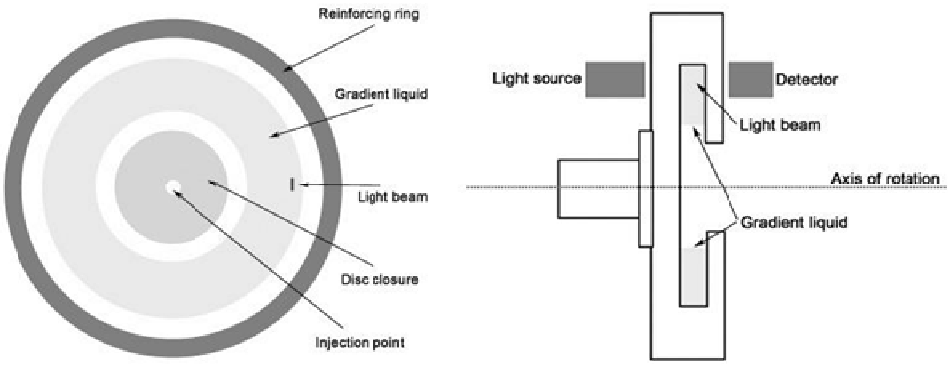

Figure 16. Schematic diagram of DCS Instrument

3. Studies on material adsorption of NPs

3.1. Assays on protein adsorption at NP surfaces

3.1.1. Electrophoretic studies on protein adsorption onto PS NPs

PS NPs were dispersed in MEM supplemented with 10% fetal calf serum (FCS). After 1 h incubation at 37°C, the NPs were centrifuged for 45 min at 20000 x g. Sedimented NPs were washed with PBS to remove non-bound proteins. Washed NPs were resuspended in Laemmli buffer containing 1% (w/v) sodium dodecyl sulfate (SDS), and loaded onto 10% polyacrylamide gel. The protein components of the corona complexes were separated from the NPs and were denatured by boiling at 100ºC for 5 minutes in the loading buffer (62.5 mM Tris-HCl (pH 6.8), 2% (w/v) SDS, 10% glycerol, 0.01% (w/v) bromophenol blue, 40 mM DTT). The denatured corona proteins coated with SDS surfactant (which gives them a negative net charge) were separated by size on 10% polyacrylamide gel (SDS-PAGE). The electrophoresis was run under constant voltage of 130 V for about 45 minutes using a Mini-Protean Tetra electrophoresis system (Bio-Rad). All gels were run in duplicates – one subjected for commassie blue (50% methanol, 10% acetic acid, 2.5% (w/v) brilliant blue) staining for 3 hours and de-stained overnight in 50% methanol, and 10% acetic acid. The other gel was stained with silver staining (Ohsawa and Ebata, 1983) kit (Cosmobio Ltd., Tokyo, Japan) (see below).

3.1.2. Human blood proteins on spherical Ag PVP NPs

In situ protein coronas on spherical Ag PVP NPs were prepared by incubating 0.1 mg/ml NPs in 10%, 80% and 100% human plasma solution (total protein content 34–47 mg/ml) at room temperature for 1 hour.

The human plasma was obtained from Centre for BioNano Interactions (CBNI), School of Chemistry and Chemical Biology, University College Dublin, Dublin, Ireland. The blood donation procedure was approved by the Human Research Ethics committee at University College Dublin. The blood plasma was prepared following the HUPO BBB SOP guidelines (Rai et al., 2005). In brief, after the blood collection, the blood was mixed with the 2 mM EDTA and centrifuged for ten minutes at 1300 g at 4^{o}C. Plasma from each donor were collected into a 50 ml falcon tube and then centrifuged at 2400 g for 15 minutes at 4^{o}C. Supernatant was collected, aliquoted into 1 ml cryo vials and stored at -80^{o}C until use. Following this procedure, the plasma protein concentration was estimated to be 80 g/l. Before the experiments, the plasma sample was thawed at RT and centrifuged for 3 min at 16200 RCF.

After incubation with human plasma, the NP-samples were directly injected into the DCS instrument without spinning down and washing.

3.2. Assays on endotoxin adsorption at NP surfaces

3.2.1. LAL assay

The endotoxin contamination of different NPs was tested by *chromogenic Limulus amoebocyte lysate (LAL) assay* (Lindsay et al., 1989) (Associates of Cape Cod, Inc., East Falmouth, MA, USA) according to the manufacturer's instructions. Two-fold dilution series were prepared with endotoxin-free water (LAL Reagent Water; LRW) from each NP preparation in duplicates, and fresh endotoxin standard was prepared for each test using 0.1, 0.25, 0.5, 1.0 and 2.0 EU/ml LPS. Interference of NPs with the assay readout was investigated.

3.2.2. SDS PAGE

For SDS_PAGE assays on endotoxin adsorption, NPs were dispersed in LRW containing 1 mg/ml endotoxin (LPS from *E.coli* 055:B5; Sigma-Aldrich) and incubated for 1 h at 37°C. After incubation, the particles were collected by centrifugation (12000 g, 45 min) and washed 3x with LRW. Washed particles in LRW and consecutive washing solutions were treated for 5 min at 100°C in Tris-hydrochloride buffer (pH 6.9), 10% w/v SDS, 0.01% bromo phenol blue, and loaded onto SDS-polyacrylamide gel (10 cm by 10 cm by 1 mm) containing 5% and 15% acrylamide in the stacking and separating gels, respectively. Electrophoresis was done at 130 V until the tracking dye had run about 10 cm.

LPS components were visualised by staining the gels with a silver staining kit (Cosmobio Ltd. Tokyo, Japan) according to the method of (Tsai and Frasch, 1982) Briefly, gels were fixed in a 40% ethanol 5% acetic acid solution overnight, then oxidized with 0.7% periodic acid for 20 min. The gels were then washed 3x for 30 min in deionised water, and stained for 15 min with the staining solution of the kit, containing $AgNO_3$, NH_4OH and NaOH. The gels were washed again 3x for 30 min in deionised water, and placed in a developing solution containing citric acid, formaldehyde and sodium thiosulphate until optimal staining had taken place. The gels were rinsed with water and subjected to gel scanning.

3.2.3. Spiking with LPS

‘‘Spiking’’ controls, were made to identify the whether the samples to inhibit/enhance the detection of the endotoxin in the assay, consisted of NP dilutions to which a known amount (0.5 EU/ml) of standard endotoxin was included. Two-fold dilution series were prepared with endotoxin-free water (LAL Reagent Water; LRW) from each NP preparation in duplicates, and fresh endotoxin standard was prepared for each test. NP samples were serially diluted from the stock suspensions with LRW and distributed 50µL/well in endotoxin-free microplates for the endotoxin assay. The traditional chromogenic LAL assay is based on the detection of the endotoxin-stimulated LAL end-product 4-nitroaniline (pNA) at 405 nm but the new chromogenic assay was used in new version, with readout shifted from 405 to 540 nm. Briefly, after sample incubation with enzyme and substrate, the diazo reagents (provided by the kit) were added sequentially: 6mM sodium nitrite in 0.48N HCl (reagent 1), 26.3mM ammonium sulfamate in water (reagent 2) and 3.76mM N-(1-naphthyl)ethylenediamine dihydrochloride in water (reagent 3). The reagents modify pNA to turn from yellow to deep purple, thus allowing detection of the azo dye product at a wavelength of 540 nm.

3.2.4. Studies on interference of NPs with the assay readout

Twofold dilutions of *p*-nitroaniline (pNA, Sigma-Aldrich) were distributed in flat-bottomed 96-well plates in a volume of 50 ml/ well. For each pNA dilution, different concentrations of NPs and corresponding solvents were added in 50 ml aliquots in triplicate wells and mixed. For measuring interference at 405 nm, another 100 µl of water (in place of the substrate) and 100 µl of stop solution (sodium dodecylsulfate

solution) were added to bring the final volume to 300 µl, i.e. the same volume as in the QCL-1000 LAL assay. Optical density was measured with a microplate reader at 405 nm. For measuring interference at 540 nm, diazo reagents were added rapidly into the wells containing pNA and NPs and the optical density was immediately measured with a microplate reader at 540 nm.

3.2.5. Silver staining method

After gel electrophoreses, proteins and LPS components were visualised by staining the gels with a silver staining (Ohsawa and Ebata, 1983) kit (Cosmobio Ltd.) according to the method of Tsai and Frasch. Briefly, gels were fixed in 40% ethanol and 5% acetic acid solution, overnight, and then oxidized with 0.7% periodic acid for 20 min. The gels were then washed 3-times for 30 min in deionised water, and stained for 15 min with the staining solution of the kit, containing AgNO3, NH_4OH and NaOH. The gels were washed again 3-times for 30 min in deionised water, and placed in a developing solution containing citric acid, formaldehyde and sodium thiosulphate until optimal staining occured. The gels were rinsed with water and subjected to gel scanning.

4. Cell cultures

4.1. NE-4C neuroectodermal stem cells

NE-4C neuroectodermal stem cells (ATTC CRL-2925; (Schlett and Madarasz, 1997)) cells were cloned from primary brain cell cultures prepared from the fore- and midbrain vesicles of 9-day-old transgenic mouse embryos lacking functional p53 tumor suppressor protein. NE-4C neuroectodermal stem cells were maintained in poly-L-lysine coated culture dishes, in minimum essential medium (MEM; Sigma-Aldrich, Hungary) supplemented with 4 mM glutamine and 10% fetal calf serum (FCS; Sigma-Aldrich) (MEM-FCS).

NE-4C cells were differentiated into neurons and astrocytes by adding 10^{-6} M *all-trans* retinoic acid (RA; Sigma-Aldrich, Hungary) to confluent cultures for 48 hours ((Schlett and Madarasz, 1997); Varga et al. 2009.; Madarász 2013). After 48-hour treatment with RA, the culture medium was changed to serum-free neural differentiation medium (MEM-ITS: MEM:F12= 1:1 supplemented with 1 % N2 neuronal supplement (Sigma-Aldrich)) containing insulin, transferrin and selenite. In MEM-ITS medium, RA-primed NE-4C cells differentiate into neurons and

astrocytes in a highly reproducible, progressive process, through well-defined stages (Figure 17).

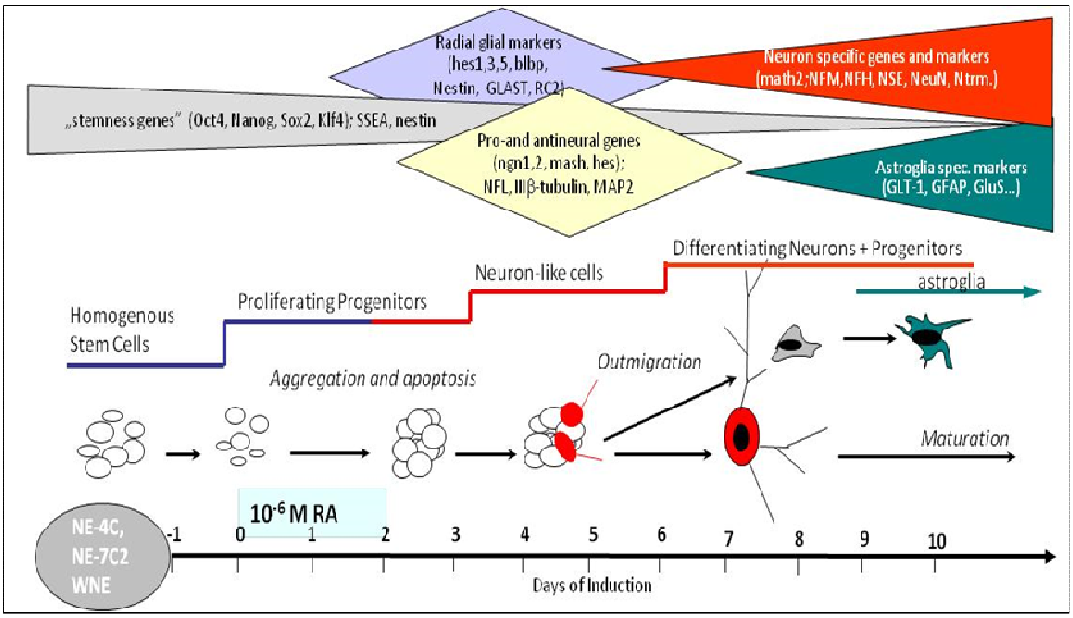

Figure 17. The schematic representation of neural differentiation of neural stem cells using Retinoic acid (RA) (Varga et al., 2009)

4.2. Primary brain cell cultures

Cultures enriched in neurons were prepared from forebrains of 14.5-15 day-old mouse embryos (Madarasz et al., 1984). The meninges were removed from the aseptically dissected forebrains and the brain tissue was mechanically dissociated in MEM-FCS. The cells were plated in MEM-FCS onto poly-L-lysine (PLL) coated dishes ($2.5x10^5$ cells/cm^2). After 3 to 4 days growth at 37°C in humidified 5% CO_2/95% air, the media of embryonic neuronal cultures were changed to serum-free medium (MEM/F-12: 1/1 supplemented with 1% (v/v) insulin-transferrin-selenite (ITS; Sigma-Aldrich) neuronal supplement and were investigated on the 7th to 9th days after plating.

4.3. Astroglial cultures were prepared from late fetal or newborn mouse forebrains. Single cell suspensions were obrained by mechanical dissociation. The cells were plated into PLL coated dishes and were maintained in MEM-FCS at 37°C in humidified 5% CO_2/95% air. Culture media were changed on every second day. The cultures were investigated on the 3rd week after plating (Kornyei et al., 2005).

4.4. Microglial cultures

Microglial cultures were prepared according to (Saura et al., 2003). Briefly, Mixed glial cultures were prepared from forebrains of newborn (1–2 days old) mice. The meninges were carefully removed and the brain tissue was was incubated with 0.05% (w/v) trypsin solution supplemented with 1 mM EDTA. After 5 to 10 min incubation, the tissue was mechanically dissociated. Suspensions of single cells were seeded in DMEM-F12 with 10% FCS and cultured at 37°C in humidified 5% CO_2/95% air. Medium was replaced every 3–4 days. After 10–12 days cultivation, the confluent mixed glial cultures were trypsinized with 0.05% (w/v) trypsin in the presence of 0.2 mM EDTA and 0.5 mM Ca^{2+}. After detachment of astrocytes, the firmly attached microglial cells were further propagated in DMEM-F12 (1:1) supplemented with 10% FCS.

4.5. Mouse brain vascular endothelial cell cultures

Brain vascular endothelial cell cultures were prepared from 8 weeks-old mice according to (Nakagawa et al., 2009). Briefly, animals were deeply anaesthetized and the brains were dissected. The meninges were carefully removed from the forebrains and the brain tissue was minced into approximately $1mm^3$ pieces in ice-cold DMEM. The tissue blocks were suspended in DMEM containing 1 mg/ml collagenase type 2 (Worthington Biochemical Corp., LakeWood NJ, USA), 300 µl DNase (15 µg/ml) (Sigma-Aldrich), gentamycin (50 µg/ml) (Sanofi-Chinoin, Budapest, Hungary) and digested in a shaker for 90 min at 37°C. The cell pellet was separated by centrifugation in 20% bovine serum albumin in DMEM (1000g, 20 min). The microvessels obtained in the pellet were further digested with collagenase-dispase (1 mg/ml; Roche Applied Sciences, Basel, Switzerland) and DNase (0.1 mg/ml) in DMEM for 1 h at 37°C. Microvessel-derived endothelial cells were collected by centrifugation, washed twice in DMEM and plated on 35 mm plastic dishes coated with collagen type IV and fibronectin. The cultures were maintained in DMEM supplemented with 10% FCS, 1.5 ng/ml basic fibroblast growth factor (bFGF; Roche, Applied Sciences), 100 µg/ml heparin and 3 µg/ml puromycin, at 37°C in a humidified atmosphere of 5% CO_2 and 95% air, for 2 days. On the third day, the medium was changed and cells were grown in puromycin-free medium. When cultures reached 80% confluency, the purified endothelial cells were split by a brief treatment with trypsin (0.05%, w/v) EDTA (1 mM) and were used for experiments.

DOI:10.14753/SE.2015.1789

5. Cellular assays

5.1. Exposing the cells to nanoparticles

For viability and toxicity assays, the cells were grown in 96-well plates (10^4 cells/well) and were exposed to different doses of NPs (from 7.8 to 250 µg/ml; see Table 8) in serum-free MEM-F12-ITS medium, for 24 hours.

For uptake experiments, the cells were grown in 24-well plates (10^5cells/well) and were exposed to 50µg NPs (10^{10} NPs/ ml) in MEM-F12-ITS medium for 1 h.

During the exposure to NPs, the cells were kept at 37 ºC in 5% CO_2 and 95% air atmosphere. incubator. The NP dispersions were prepared immediately before use and vortexed before distribution in the culture wells.

5.2. Assays on cell viability (MTT-reduction) and on cell membrane integrity (LDH release)

For assessing MTT reduction, an index of cellular activity, and LDH release, an index of cell membrane damage, we used the redox-reaction of the same compound, the 3-(4,5- dimethylthiazol-2-yl)-2,5-diphenyltetrazolium bromide (MTT). MTT can be reduced to a purple-colored formazan (Mosmann, 1983) and the formazan production can be determined, by photometrical mesuring the absorption of 550-570 nm wavelength light.

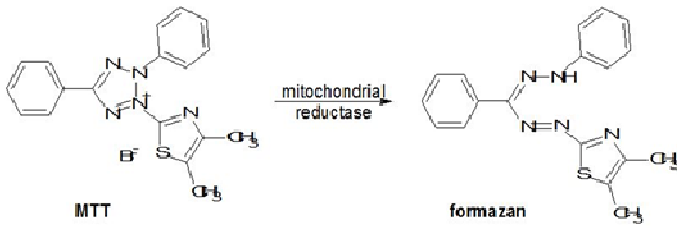

Figure 18. MTT reduction reactions

The metabolic activity of cells was measured by MTT-reduction assay on living cells (Mosmann, 1983). The activity of LDH released by damaged cells were determined from the culture supernatants of the viability-assayed cultures according to Abe *et al.*; 19xx); thus, the metabolic and toxic reactions of the same cell preparations were assayed.

5.2.1. Assays on cell viability (MTT)

Cells grown in 96-well plates (10^4 cells/well) were exposed to NP suspensions (from 7.8 to 250 µg/ml see Table 1.) in 100 µl of MEM-F12-ITS. The cells were incubated for 24 h at 37°C in 95% air and 5% CO_2 atmosphere. Fifty µl aliquots of culture medium were removed from each well for LDH assays (see below), then 10

microliters of MTT stock solution (2.5 mg/ml) were added to the cells into the remaining medium (50 µl) and the cells were incubated for 90 min at 37°C, in the CO_2 incubator. The reaction was stopped by adding 100 µl stop solution containing 50% dimethylformamide and 20% sodium dodecyl sulfate in distilled water (DMF-SDS, pH 4.7). After dissolving the cell material and the formazan product in the stop-solution, the formazan amount was determined by measuring light absorption at dual – 550-570 nm (measuring) and 630-650 nm (reference) – wavelengths using a Bio-Rad 450 (BioRad Hungary Ltd., Budapest, Hungary) or Dynatech MR5000; (Dynatech Industries Inc., McLean, VA, USA). For getting comparable data on different cells and culture-plates, optical density data measured in each well were related to values obtained on control (non-exposed) cells on the same plate (100 %). The data were presented as relative percentages of the control. Averages and standard deviations were calculated from 8-12 identically treated cultures. Significance was calculated by student t tests. Differences were regarded statistically significant if $p<0,05$, and biologically significant, if dose-dependent responses were detected.

5.2.2. Assays on cell death (LDH leakage)

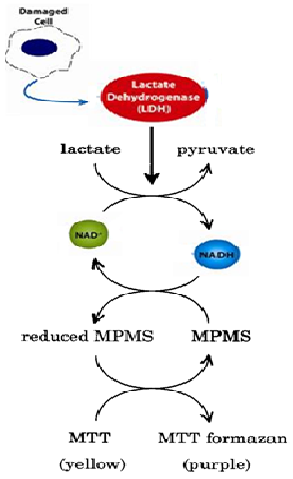

Figure 19. LDH release assay by using MTT reduction

Release of lactate dehydrogenase (LDH) enzyme by damaged cells was assessed by measuring LDH activity in the cell culture media according to Abe *et al.* (Abe and Matsuki, 2000). Briefly, 50 µl culture supernatants were transferred to an empty 96-well plate and 50 µl aliquots of the LDH assay mixture (2.5 mg/ml L-lactate (Sigma-Aldrich), 2.5 mg/ml nicotinamide adenine dinucleotide (NAD; Sigma-Aldrich), 0.25 mg/ml MTT and 0.1 mM 1-methoxy-5-methylphenazinium methylsulfate (MPMS;

Sigma-Aldrich) in 0.2 M Tris–HCl buffer (pH 8.2) were added. The reaction mixtures were incubated for 5 min at 37°C. For calibration, culture supernatants werereplaced with 50 µl MEM-ITS containing known concentrations of LDH enzyme (from 9.3 to 300 µg/ml; corresponding to 0.03 - 1 unit/ml enzyme activity).

The LDH reaction was stopped by adding 100 µl stop solution containing 50% dimethylformamide and 20% sodium dodecyl sulfate in distilled water (DMF-SDS, pH 4.7). The absorbance of the formazan product was measured by a BioRad 450 (BioRad Hungary Ltd., Budapest, Hungary) or Dynatech MR5000; (Dynatech Industries Inc., McLean, VA, USA) at 550 nm test and 650 nm reference wavelengths.

6. Immunocytochemical and uptake studies

For microscopic analyses, cells were grown on poly-L-lysine coated glass coverslips, in 24 well plates (10^5cells/well). The cells were incubated with 500 µl of 50µg (10^{10} NPs ml-1) dispersed in MEM-F12-ITS medium for 1 h at 37 ºC in a CO_2 incubator. Control cells were incubated with MEM-F12-ITS medium without NPs. The treated cells were washed three times with phosphate buffered saline (PBS, pH 7.4) to remove free-floating NPs and fixed for 20 min with paraformaldehyde (4% wt/v, PFA) at room temperature (RT). The cells were occasionally stained with CellMask (Molecular Probes, Invitrogen) according to the manufacturer's instruction or were identified by immunocytochemical staining.

For immunocytochemical identification, fixed cells were permeabilized with 0.1% Triton-X for 10 min at RT. Non-specific antibody binding was blocked by treating with 2% bovine serum albumin (BSA) in PBS for 60 min. Primary antibodies were diluted with 2% BSA, and fixed cells were incubated with the antibodies overnight at 4 ºC. Neurons differentiating from NE-4C stem cells or developing in primary neuronal cultures were stained with mouse monoclonal anti-β-III tubulin antibodies (1:1000, Sigma, Hungary). Astrocytes were stained with rabbit polyclonal anti-glial fibrillary acidic protein (GFAP) antibodies (1:1000, Dako). Microglial cells were stained with Iba-1 goat polyclonal antibodies (Abcam) and brain derived endothelial cells were stained with anti-claudin-5 rabbit polyclonal antibodies (Abcam). After overnight incubation, the cells were washed three times with PBS and incubated for 1 h with alexa-594 or alexa-488 conjugated anti-mouse, anti-rabbit or anti-goat immunglobulin antibodies (1:1000, Molecular probes, Invitrogen). After washing,

the stained preparations were mounted with mowiol (Calbiochem, EMD Chemicals) containing 10 μg/ml bisbenzimide (Hoechst 32558;DAPI; Sigma) and were left to dry in dark for 24 h (Table 3).

Table 3. Primary antibodies used for cell identification

Antibody		Dilution	Identified cell
β-III tubulin	Mouse monoclonal (Sigma)	1/1000	Neurons
Glial Fibrillary Acidic Protein (GFAP)	Rabbit polyclonal (Dako)	1/1000	Astrocytes
Iba	Goat polyclonal (Abcam)	1/500	Microglia
Claudin-5	Rabbit polyclonal (Abcam)	1/1000	Brain endothelial cells

7. Microscopic evaluation

Cell morphology and uptake of NPs were examined using Zeiss Axiovert 200M microscope (Carl Zeiss Jena, Germany) and Olympus FV1000 (Tokyo, Japan) confocal microscope. For fluorescence spectrum analysis (Heider et al., 2010) a Nikon A1R confocal laser scanning microscope (Nikon Instruments Europe B.V., Vienna, Austria) equipped with an enhanced spectral detection unit (SD) was used.

7.1. Fluorescence spectrum analysis

For spectral evaluation a 457 nm argon ion laser was used as excitation source, and the emitted light was detected by the spectral detector unit from 468 nm to 548 nm, with a spectral resolution of 2.5 nm. In order to record continuous spectrum, a 20/80 beam splitter (BS20/80) with continuous transmission was used instead of a paired dichroic mirror arrangement. Regions of interest (ROIs) were delineated and analysed on corresponding fields of NP-treated and non-treated cell preparations. The photocurrent intensities detected at different wavelengths (emission spectra) were plotted and were compared to the autofluorescence spectra of non-treated cells (negative control) and to the spectrum of NPs (positive control).

7.2. TEM analysis of the cellular uptake of Ag NPs with different shape

Neural stem cells were grown on poly-L-lysine coated glass coverslips, in 24 well plates (10^5 cells/well). The cells were incubated with 500µl suspension of 50µg/ml ($2x10^{11}$ NPs/ml) NPs dispersed in MEM-F12-ITS, for 1h at 37^O C in a CO_2 incubator. Control cells were incubated without NPs. The cells were washed three times with phosphate buffered saline (PBS, pH 7.4) to remove free-floating NPs and fixed for 20 min with freshly prepared glutaraldehyde 1% and, 4% PFA solution then post fixed in 2% osmium tetroxide (OsO4) in 0.1M PBS pH 7.4 at 4ºC for 2 hours.

After washing, the preparations were dehydrated in increasing (30%, 60%, 96% v/v) concentrations of ethanol and embedded in LX-112 resin (Ladd, Burlington, Vermont, USA). Sections (60-80nm) were cut by an ultracut (UCT, Leica EM UC7, Wetzlar, Germany), then were contrasted with 1% uranyl-acetate in 50% ethanol and examined with TEM (JEOL JEM 1010, JEOL Ltd., Tokyo, Japan) at 100 keV.

8. In vivo experiments

Animal experiments were conducted with the approval of the Animal Care Committee of the Institute of Experimental Medicine of Hungarian Academy of Sciences and according to the official license (No.: 22.1/353/3/2011; exp. date: 4/7/2016) issued by National Food Chain Safety Office (www.NEBIH.gov.hu), Hungary.

8.1. Injection of PS NPs into mice

Healthy pregnant mice were obtained from Animal Facility (Institute of Experimental Medicine of Hungarian Academy of Sciences, Budapest, Hungary). Four weeks pregnant female mice on the 10th to 15th days post conception were anesthetized with a mixture of ketamine (CP-Pharma mbH, Burgdorf, Germany) and xylazine (CEVA-PHYLAXIA, Budapest, Hungary) 100µg/g and 10µg/g bodyweight, respectively. Nanoparticle stock suspensions (10 mg/ml) were diluted 1:30 in PBS and sonicated before injection. Under proper anesthesia, 7µl/g bodyweight aliquots of PS-COOH and PS PEG NP suspensions were injected into the tail vein. Animals were sacrificed by overdose of anesthetics after 5-minute or 4-day exposure to the single-injection. Placentas and embryos were carefully removed and fixed with paraformaldehyde (8w/v% in PBS; PFA) for 24 hours at 4ºC, then washed with PBS and left in 0.25% glucose for several days. Placentas and embryos were collected from animals not exposed to nanoparticles, and were considered as controls.

8.2. Microscopic evaluation of the tissues

Histological sections (60µm) were made by cryostat section (Leica CM 3050S) of fixed placentas and embryos. Sections were mounted with mowiol (Merk Kft. Budapest, Hungary) containing 10µg/ml bisbenzimide (DAPI; Sigma-Aldrich, Budapest, Hungary), and were left to dry at room temperature in dark. Sections were evaluated by using fluorescence (Zeiss Axiovert 200M; Jena, Germany) and confocal laser microscopes (Olympus FV1000 and Nikon A1R). The Nikon A1R was equipped with a spectral detector unit (Nikon, Shinjuku, Tokio, Japan).

DOI:10.14753/SE.2015.1789

3. Results

1. Characterization of NPs

1.1. Physico-chemical properties of particles with non-toxic core material: Polystyrene (PS) and silica (Si) NPs

1.1.1. Fluorescent silica NPs with core-bound FITC and label-free shell and with different (-NH_2, -SH and -PVP) chemical surface groups were synthesized by Emilia Izak-Nau at Bayer (Germany). The particles were thoroughly characterized by multiple techniques including DLS, SEM, TEM, XRD, XPS and ToF-SIMS analyses. The processes of synthesis and characterization have been presented in two publications (Izak-Nau et al., 2013a, and 2013b) and gave important parts of the PhD thesis of Emilia Izak-Nau. In my thesis, the physico chemical characteristics of Si-NPs will be presented only briefly (Figure 20 and Table 4) in order to show the importance of surface charge of Si-NPs in their biological interactions.

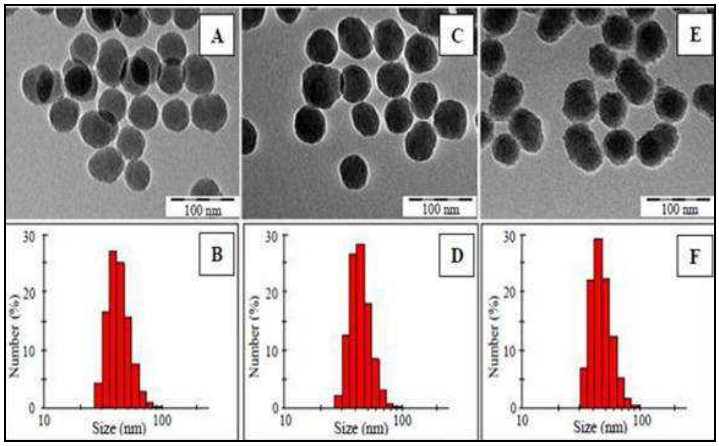

Figure 20. Scanning electron microscopic (SEM) picture (A,C,E) and size distribution determined by DLS (B,D,F) of SiO_2 (A,B), SiO_2-SH (C,D) and SiO_2-PVP nanoparticles.

Table 4. Physicochemical characteristics of core/shell Si NPs (Izak-Nau et al., 2013)

Name	SiO_2	SiO_2_NH_2	SiO_2_SH	SiO_2_PVP
Shape	Spherical	Spherical	Spherical	Spherical
Concentration	2.0 % (wt/wt) 1.5*10^{14} NPs/ml	2.0 % (wt/wt) 1.5*10^{14} NPs/ml	2.0 % (wt/wt) 1.5*10^{14} NPs/ml	2.0 % (wt/wt) 1.5*10^{14} NPs/ml
Specific surface area	8.31*10^{1} m^2/g	-	-	-
Size/size distribution & aggregation/ agglomeration state	DLS: 52.5 nm +/-2.6*; PDI= 0.055 TEM: d_{50}= 50 nm, d_{90}= 55 nm AC: d_{50}= 49 nm, d_{90}= 61 nm	DLS: 56.0 +/- 4.6 nm*; PDI=0.082 TEM: d_{50}= 51 nm, d_{90}= 58 nm	DLS: 49.9 +/- 2.2 nm*; PDI= 0.067 TEM: d_{50}= 49 nm, d_{90}= 57 nm	DLS: 59.5 +/- 2.3 nm*; PDI= 0.079 TEM: d_{50}= 51 nm, d_{90}= 57 nm
Crystal structure	amorphous	amorphous	amorphous	amorphous
Surface chemistry	XPS: Atom % O 62.8, Si 25.6, C 11.6 SIMS: Si_xO_y, $C_6H_{15}O_3Si$	XPS: Atom% O 57.8, Si 24.3, C 16.1, N 1.8 SIMS: Si_xO_y, $(H_2N(CH_2)_3Si(OC_2H_5)_3)$, F	XPS: Atom% O 61.8, Si 25.6, C 12.6, S< 1 SIMS: Si_xO_y, $((CH_3O)_3Si(CH_2)_3SH)$, Cl	XPS: Atom% O 44.5, Si 33.5, C 18.0, N 3.9 SIMS: Si_xO_y, C_6H_9NO, F
Surface charge	- 41.71 mV+/- 0.82 IEP: ~ pH 3.1	+ 42.24 mV+/- 1.49 IEP: ~ pH 6.4	- 47.73 mV+/- 0.91 IEP: ~ pH 1.3	- 40.87 mV+/- 1.31 IEP: ~ pH 4.6

The Si NPs were used in biological experiments as freshly synthesized, monodispersed suspensions and evoked well repoducible cellular responses all over the experiments.

1.1.2. The polystyrene nanoparticles (PS NPs) with –COOH or PEG surface groups were purchased from commercial sources (Spherotec Inc. USA and Kisker Gmbh, Germany). The physico-chemical properties were analysed right after arrival and were compared to characteristics provided by the manufacturers. PS NPs were used either as fresh particles (right after opening the particle container) or as aged particles after long-term (>6 months) storage in order to investigate the role of ageing in the biological effects of NPs.

In fresh preparations of carboxylated (PS-COOH) and PEGylated (PS-PEG) NPs, DLS measurements indicated uniform (45-70 nm corresponding to the manufacturers descriptions) hydrodynamic size in distilled water and good monodispersity (Poly dispersity index, PDI between 0.039-0.072, e.g. below the 20% polydispersity range).

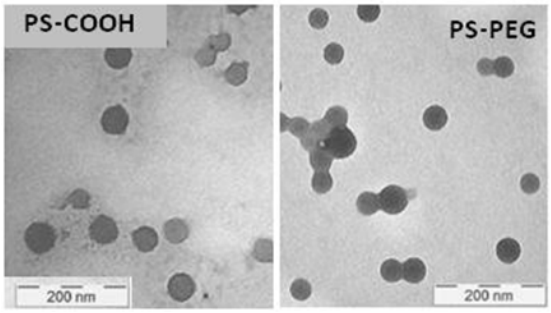

Figure 21. Electronmicroscopic images of fresh PS NPs

Transmission electron microscopic (TEM) images showed spherical shape and a 50±10 nm diameter of the fresh FITC-labelled particles (Figure 21).

Differential centrifugal sedimentation (DCS) data also showed good monodispersity in distilled water for fresh PS NPs without important differences between carboxylated and PEGylated particles (Figure 22).

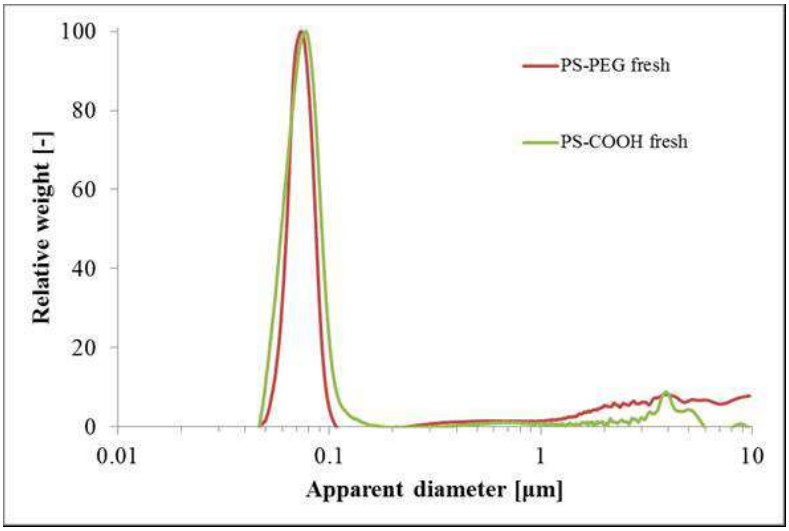

Figure 22 DCS results for fresh PS nanoparticles

Zeta potential measurements, as it was expected, showed that the surface of PS-COOH NPs was more negative (zeta potential -35.4±0.5 mV) than those of PS-PEG particles (-14.8±1.0 mV) (Table 5)

Table 5. Size and surface charge of PS NPs

Nanoparticle	Size [diameter; nm]		Zeta potential [mV]	
	fresh	aged*	fresh	aged*
PS-COOH	65.80 ± 1.12	1329 ± 8	-35.4 ± 0.5	non-evaluable
PS-PEG	65.89 ± 0.98	1203 ± 20,7	-14.8 ± 1.0	

* shelf-life 12 months

The assays demonstrated that with the exception of the surface charge (zeta potential), the main physico-chemical features in distilled water did not change as a consequence of surface functionalization of Si and PS particles. Coating the particle surfaces with PVP or PEG reduced the Zeta potential and was expected to reduce the aggregation and protein adsorption of particles also in physiological solutions.

1.2. Protein adsorption by Si- and PS NPs

The protein adsorption of Si- and PS NPs was investigated by SDS-PAGE and by DLS size determinations (ZetaSizer, Malvern) after incubation with 10% fetal calf serum (FCS; v/v) in PBS. SiO_2, Si-NH_2 and Si-SH NPs adsorbed significant amount of serum proteins (Figure 13) regardless of the positive (Si-SH and Si-NH_2) or negative (SiO_2) surface charge, and showed large-scale aggregation in physiological solutions (Table 6).

DOI:10.14753/SE.2015.1789

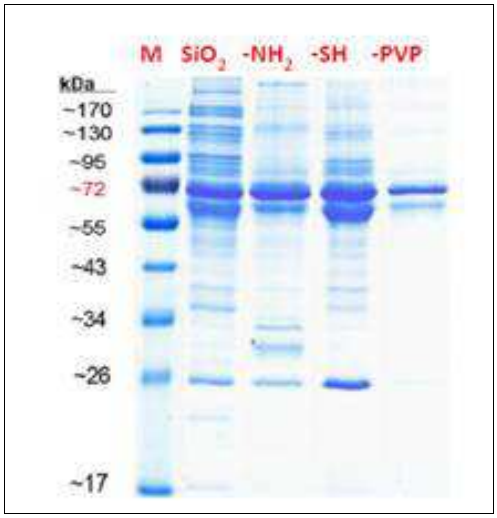

Figure 23. Adsorption of serum proteins by Si NPs after 1-hour incubation in 10% FCS containing PBS . M: molecular weight marker (result of E. Izak-Nau) .

Table 6. The size-distribution of Si NPs after 48-hour incubation in cell culture media supplemented with 10% fetal calf serum

	Size [nm]			
	SiO_2	SiO_2_NH_2	SiO_2_SH	SiO_2_PVP
MEM (48 h; RT; $1x10^{14}$ NPs mL^{-1})	1626 +/- 260	1892 +/- 423	1844 +/- 818	67 +/- 4
MEM-sonication 10 min (48 h; RT; $1x10^{14}$ NPs mL^{-1})	785 +/- 156	873 +/- 199	932 +/- 176	55 +/ 3
MEM-F12-ITS (1 h; 37°C; $5x10^{11}$ NPs mL^{-1})	1119 +/- 62	976 +/- 163	1247 +/- 137	68 +/- 6

The PVP-coat reduced markedly the protein adsorption and completely prevented the aggregation of particles. SDS-PAGE analysis of PS NPs indicated that PS-COOH particles accumulated more proteins than the PS-PEG particles in long-term (24 hours) exposure, while there was no difference after 1-hour incubation (Figure 24)

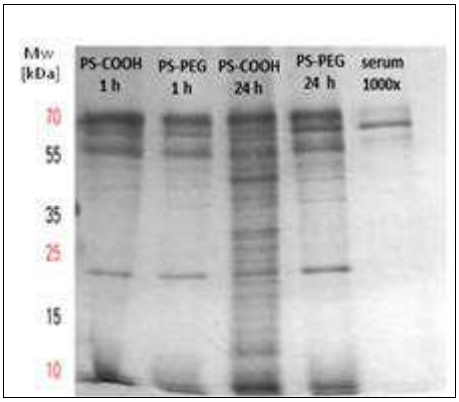

Figure 24. Adsorption of serum proteins by carboxylated and PEGylated PS NPs after 1 and 24 hours incubation in 10 % FCS containing PBS. For comparison, the bands given by a 1 to 1000 diluted FCS sample (last lane) is shown.

DLS size-analyses (Figure 25) showed significant aggregation of both, PS-COOH and PS-PEG particles in PBS (Figure 15). After 48 h in PBS, PS-COOH particles formed larger aggregates than PS-PEG NPs. Aggregates were reduced in the presence of serum indicating that surface-deposited serum components “stabilized” both PS-COOH and PS-PEG particles.

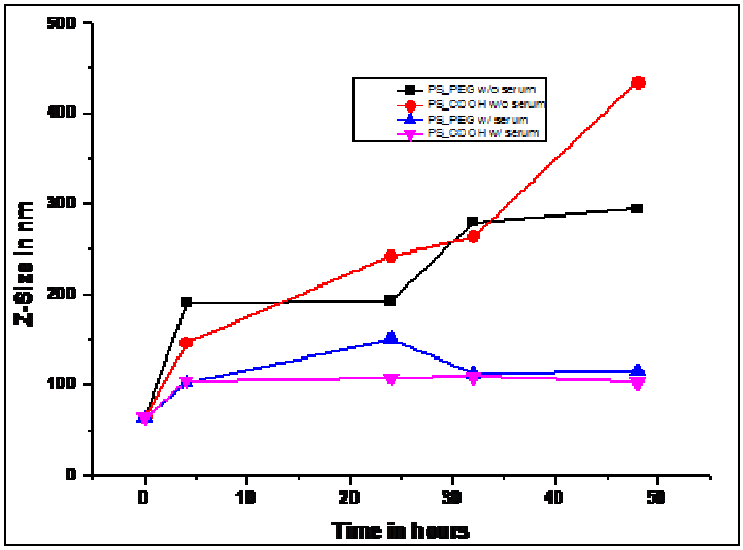

Figure 25. Aggregation of PS-COOH and PS-PEG NPs after 48-hour incubation in PBS with or without 10 % FCS. The size of particles was determined by DLS.

The results demonstrated that while the immediate protein adsorption can not be prevented by coating the particle surfaces with “inert” polymers, the long-term protein corona formation is reduced by both PEG and PVP.

1.2.1. Changes of physico-chemical characteristics of PS NPs after long-term storage

When DLS, Zeta potential, DCS and NTA analyses were repeated on PS NPs stored in distilled water for longer than 6 months after opening the container, completely different physico-chemical characteristics were detected. DLS analyses (Table 7) and transmission electron microscopic images (Figure 26) indicated strong aggregation of „aged” particles regardless of the -COOH or -PEG functionalization. The compact aggregates could not be resolved by heavy sonication. Zeta potential analyses on aged particles gave unreliable results with multiple peaks ranging from -50 to +5 mVs for both PS-COOH and PS-PEG particles. The PDI values for the aged particles varied between 0.924 and 1 indicating high polydispersity.

DOI:10.14753/SE.2015.1789

Table 7. Changes in size and surface charge of PS NPs with ageing

nanoparticle	Size [diameter; nm]		Zeta potential [mV]	
	fresh	aged*	fresh	aged*
PS-COOH	65.80 ± 1.12	1329 ± 8	-35.4 ± 0.5	non-evaluable
PS-PEG	65.89 ± 0.98	1203 ± 20,7	-14.8 ± 1.0	

∗ shelf-life 12 months

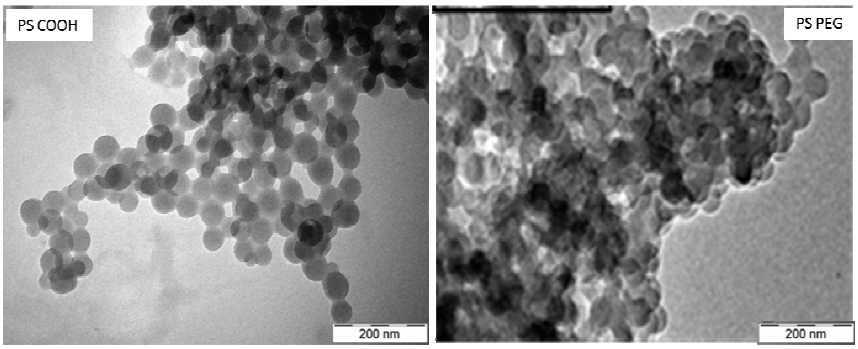

Figure 26 . Electronmicroscopic images of aged (12 months) FITC labelled PS NPs.

DCS analysis indicated the presence of NP aggregates with size >1 μm (Figure 27).

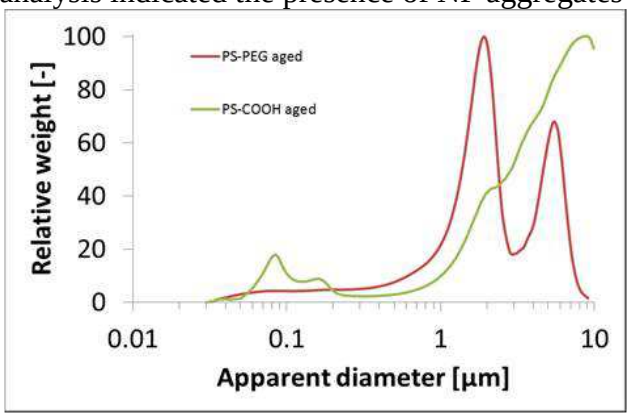

Figure 27.
Size distribution of aged PS NPs according to the differential centrifugal sedimentation analysis

A significant drift in size-distribution of aged PS NPs was further demonstrated by nanoparticle tracking analysis (NTA) (Figure 28) showing a mean size of 111 ± 68 nm for PS-COOH, and 200 ± 82 nm for PS-PEG particles.

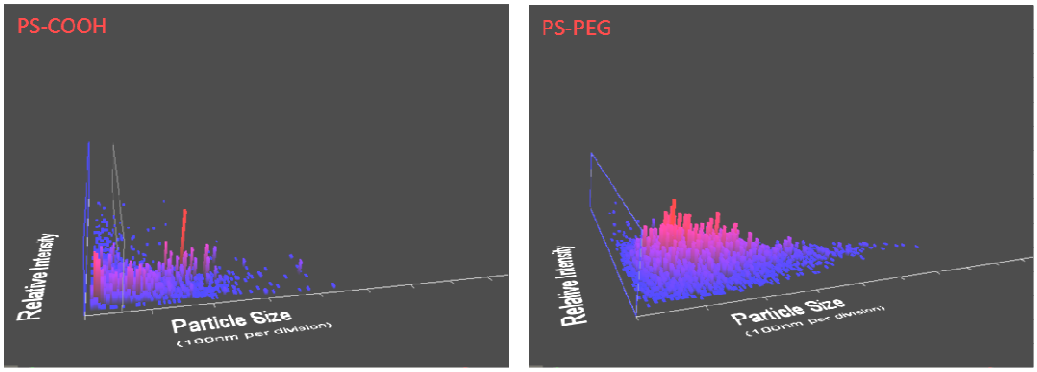

Figure 28. Nanoparticle tracking analysis (NTA) of aged PS-COOH (A) and PS-PEG (B) NPs in water.

1.3. Synthesis and physico-chemical characterization of Ag NPs with different shapes

Silver NPs (Ag-NPs) with cubical, triangular, rod and spherical shapes were synthesized and thoroughly characterized during my quest-research at ICN2, Barcelona. Polyol process (Sun and Xia, 2002, Wiley et al., 2005). was applied using polyvinylpyrrolidone (PVP) as the protecting agent and ethylene glycol (EG) as both reducing agent and solvent. In which the reaction temperatures and times as well as the concentration of protective agent are the key parameters to control the size, geometries of the metal particles. The diameter of silver spheres and the edge-lengths of silver nanocubes, and triangles were in the range of 35-55 nm, while the thickness of triangular platelets was around 5 nm and the length of rods with 40-70 nm cross-section diameter reached several micrometers. Due to theroretical restrictions, the different geometry of Ag NPs was characterized by TEM and UV-Visible light absorption. But the spherical shaped Ag NPs were characterized by different techniques such as UV-visible spectroscopy, NTA, TEM and CPS. UV-visible spectroscopy utilizes the surface plasmon resonance (SPR) of metal nanoparticles which reflects the abundance of edges and sharp points of the particle shapes (Okitsu, 2013).

1.3.1.Spherical shaped Ag NPs were produced in concentrations of 0.1 g/L or $1.5x10^{11}$ NPs/ml. The monodispersity of the suspensions were stabilized by either Na-citrate or by PVP in the solvent. The size distribution was determined by nanoparticle tracking analysis (NTA) (Figure 29 B) and by TEM (Figure 29 C) indicating 47±3 nm and 47±7.8 nm particle sizes, respectively.

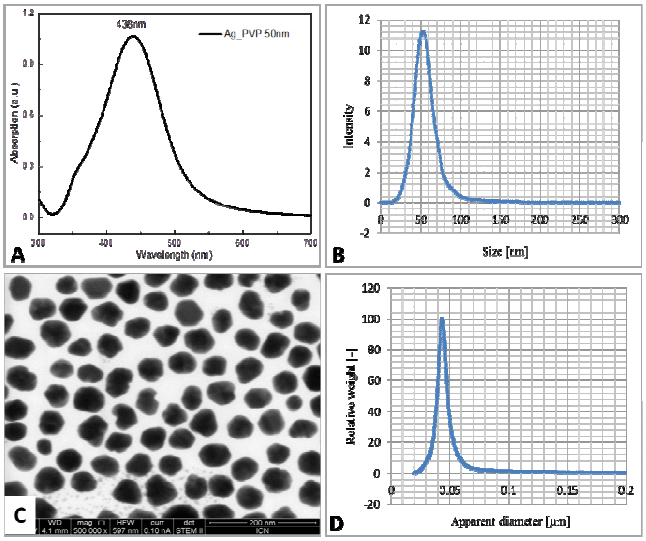

Figure 29. Spherical shape and monodispersity of 50nm spherical Ag NPs are evident in (A) UV-vis, (B) NTA, (C) TEM, (D) CPS

TEM images showed a spherical, more or less isodimensional, edge-free shape and monodispersity of particles (Figure 29C). UV-vis spectrum (Figure 29A) also showed the typical optical characteristics of a colloidal suspension of approximately 50 nm spherical Ag NPs. DLS assays showed a main size range of Ag spheres between 47 and 51 nm. Monodispersity was also proven by DCS measurements (Figure 29D). The Zeta potential measurement of spherical Ag NPs was -20 mV in PVP stabilized suspensions.

1.3.2.Silver nanocubes were synthesized by reducing silver trifluoroacetate with EG in the presence of PVP. After 30 min of the addition of CF_3COOAg, Ag nanocubes with an edge length of 35-40nm were obtained. Depending on the reaction time, the edge lengths of the Ag nanocubes could be increased upto 70nm. As a result, the growth of Ag nanocubes could be monitored and their size tuned in the range between 30-50nm by varying the growth time. We also optimized the synthesis by adjusting the reaction temperature upto 153±5^oC and the molecular weight of PVP (360kD monomeric unit) added into the reaction system as described in the materials and methods section. UV-vis spectrum analysis (Figure 30) showed the characteristic shoulder peak around 350nm indicating the presence of silver nanocubes.

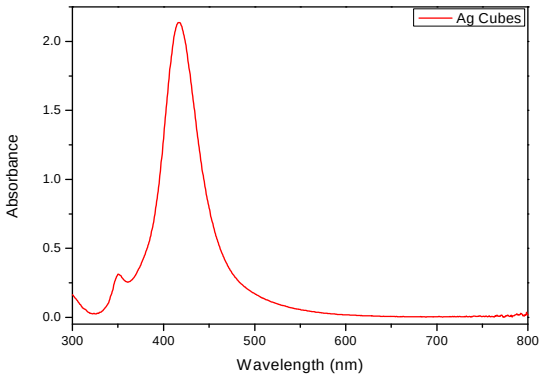

Figure 30. UV/Vis absorption spectrum of the aqueous solutions of silver nanocubes with the edge lengths about 35-45nm.

DOI:10.14753/SE.2015.1789

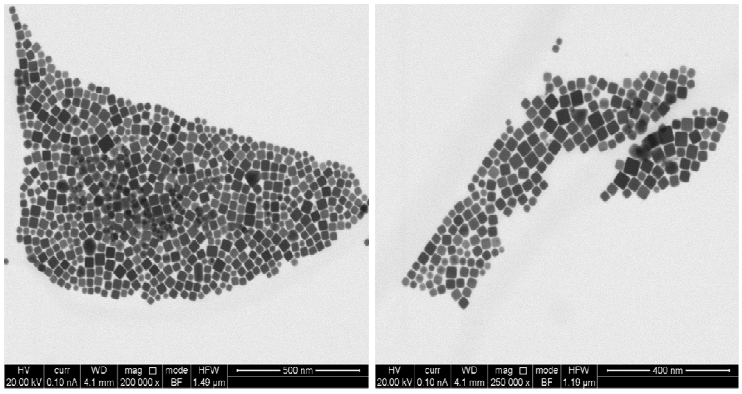

Figure 31.
TEM images of Ag nanocubes obtained by a standard polyol synthesis

1.3.3. Silver nanotriangles were prepared by reducing an aqueous silver nitrate solution with $NaBH_4$ in the presence of trisodium citrate, PVP and hydrogen peroxide (H_2O_2). Here, PVP and H_2O_2 plays an important role in the formation of triangular shape nanoparticles. Especially PVP is used to improve the size distribution of the nanotriangles/plates. The sharp shoulder characteristic peak around 330 nm can be caused by quadrupole resonance of silver nanotriangles. But at the same time another long peak shifting towards longer wavelengths indicates the formation of nanotriangles/plates (Figure 32).

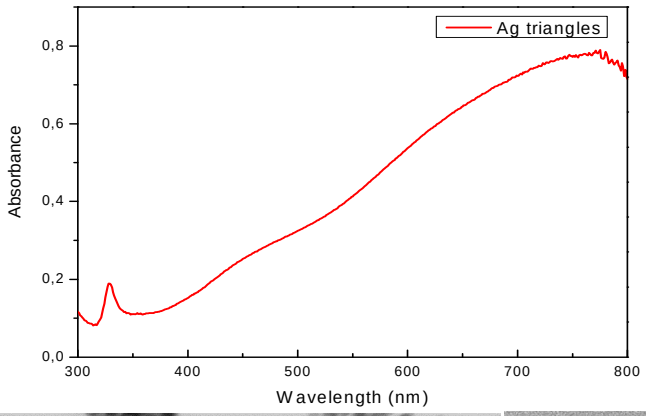

Figure 32.
UV/Vis absorption spectrum of the aqueous solutions of silver nanotriangles/platelets

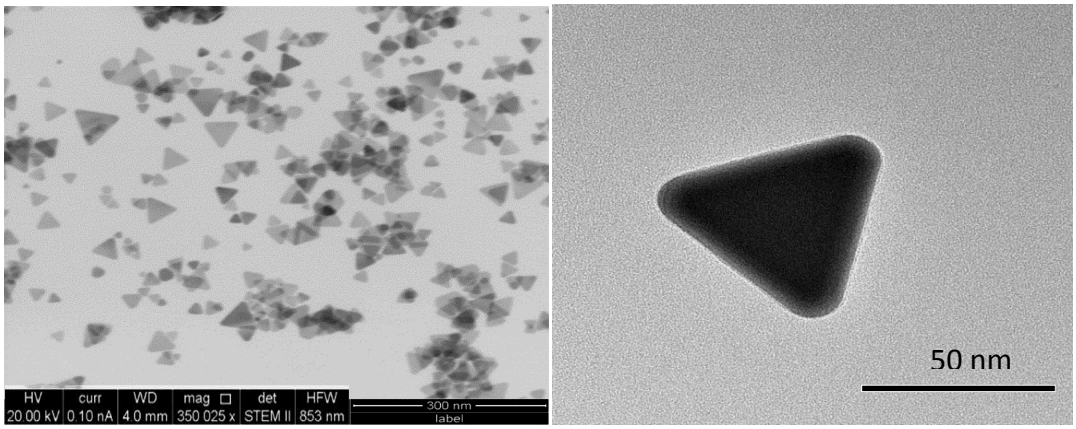

Figure 33. TEM and HR-TEM images of Ag nanotriangles/plates.

On TEM images (Figure 33), the synthesized product was triangular in shape and edge-lengths of 31.5 ± 11 nm and platelet thickness of 4.5 ± 0.9 nm.

1.3.4. Silver nanorods *(Ag nanorods)* were characterized by UV-vis spectrometry which reflects the anisometric geometry of Ag nanorods (Figure 34) showing a sharp absorbance at 350-390 nm, which are the optical finger print of Ag nanorods (Sun et al., 2002a, Sun et al., 2002b).´´The final concentration of freshly prepared Ag nanorod was 3.8 x 10^9 NPs/ml (1.08 g/L by ICP-MS).

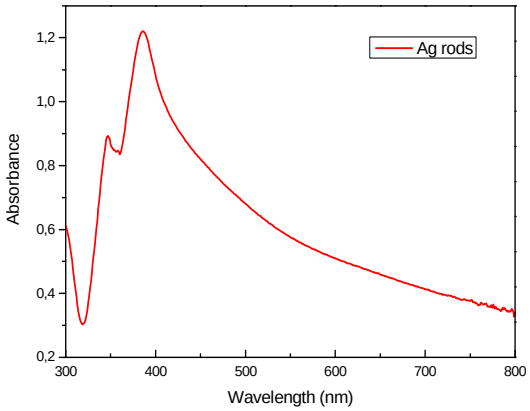

Figure 34. UV/Vis absorption spectrum of the aqueous solutions of silver nanorods

TEM images of Ag nanorods obtained with standard synthesis showed almost uniform 40-50 nm thickness but variable lengths (from a few to several ten µms) of Ag nanorods.

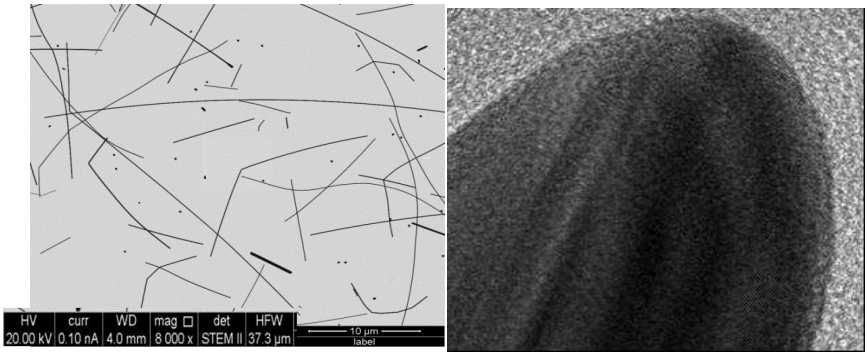

Figure 35. TEM and HR-TEM images of Ag nanorods

1.4. The protein adsorption by Ag NPs

1.4.1. Experiments with human plasma

We studied the dispersion and protein corona formation of Ag NPs *in situ* in 10, 80 and 100 % human plasma solution (v/v in PBS) (Figure 36). The DCS measurements revealed that NP-protein complexes (full corona, FC) were monodispersed in all three concentrations of plasma. As shown in Figure 36, increasing plasma concentration shifted the main size peak to the left. This can be atributed to the

increase in the protein corona thickness. The shift of the peak „to left" upon adsorption of proteins on NP surface is typical for systems where the protein density is smaller than the nanoparticle density. Aggragetion of free plasma proteins at high plasma concentration (from 80%) were sometimes also seen (Figure 36).

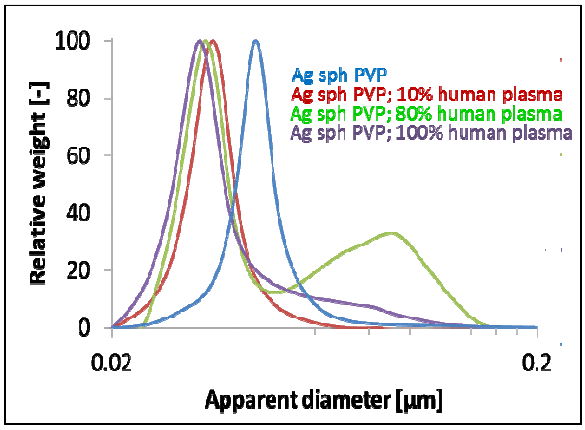

Figure 36. DCS measurements of Ag NP-corona complexes before and after incubation in plasma

The Vroman effect (Vroman et al., 1980), predicts that the adsorption of blood serum proteins to inorganic surfaces is time dependent: serum proteins with the highest mobility (or closest to the surface) arrive to the surface first, and are gradually replaced by less motile proteins that have a higher affinity for the surface; the process may take several hours. We found, that when Ag NPs of different shapes were incubated with non-diluted human blood plasma (100%), besides the time-dependency, the rate of protein adsorption was found to be shape-depedent.

Ag NPs with angels and edges adsorbed more proteins than Ag spherical NPs, in both short and long incubation times (Figure 37).

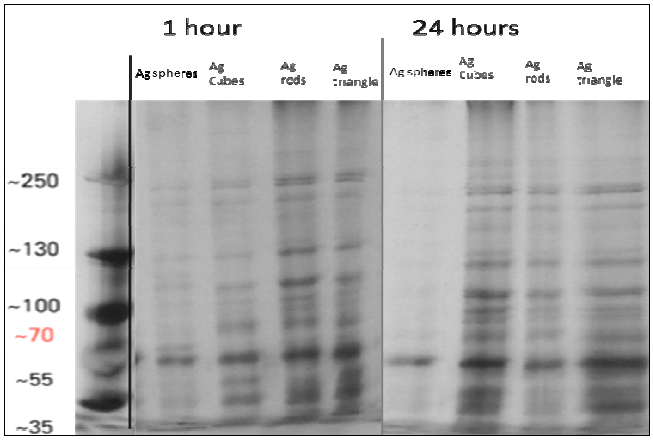

Figure 37. SDS-PAGE of the protein corona of different forms of Ag NPs incubated in 100% human plasma for 1 hr and 24 hrs.

DOI:10.14753/SE.2015.1789

2. Cellular responses to exposure to NPs with non-toxic core material

2.1. The experimental models

2.1.1. The cell models

In vitro effects of PS and Si NPs were investigated on cultures of neurons, astrocytes, brain vascular endothelial cells and microglia cells isolated from mouse forebrains, as well as on cloned neural stem cells and on stem cell-derived neurons.

The *primary cultures of mouse forebrain cells* (Figure 38) (Madarasz et al., 1984) contain astrocytes besides neurons and in small amount also microglia and neural stem cells.

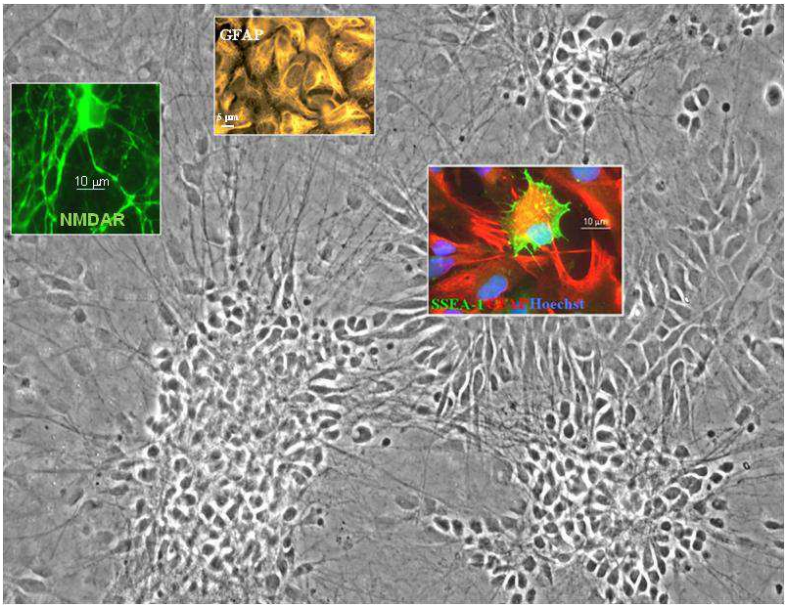

Figure 38. Primary culture of mouse embryonic (E 17) forebrain cells isolated on the 7th day after plating. The cellular constituents have been identified by immunocytochemical staining (see inserts). (Neurons: NMDA receptor, green. Astrocytes: GFAP, yellow on upper insert; red on the right insert. Neural stem cells: green on the right insert)

The primary forebrain cultures were enriched in neurons by using mitotic blockers (as serum-free media and/or cytosine arabinofuranoside) and contained 70-75% neurons (Figure 39A). Astrocytes were prepared from neonate mouse forebrains (Környei et al., 2005), and contained 85-90% glial fibrillary acidic protein (GFAP) positive cells (Figure 39B). Brain microvessel endothelial cells were prepared from the forebrains of 10-day old mouse pups (Nakagawa et al., 2009) and were identified by staining for claudin5 brain endothelial marker (Figure 39C). Microglia cells were prepared from neonate mouse forebrain (Saura et al., 2003) and

identified by staining for Iba macrophage-specific protein (Figure. 39D). Microglial cells were identified also by the presence of lectin-binding proteins (picture not shown) and were prepared from transgenic mice expressing green fluorescent protein (GFP) from the CXC3 fractalkine-receptor gene (Jung et al., 2000b).

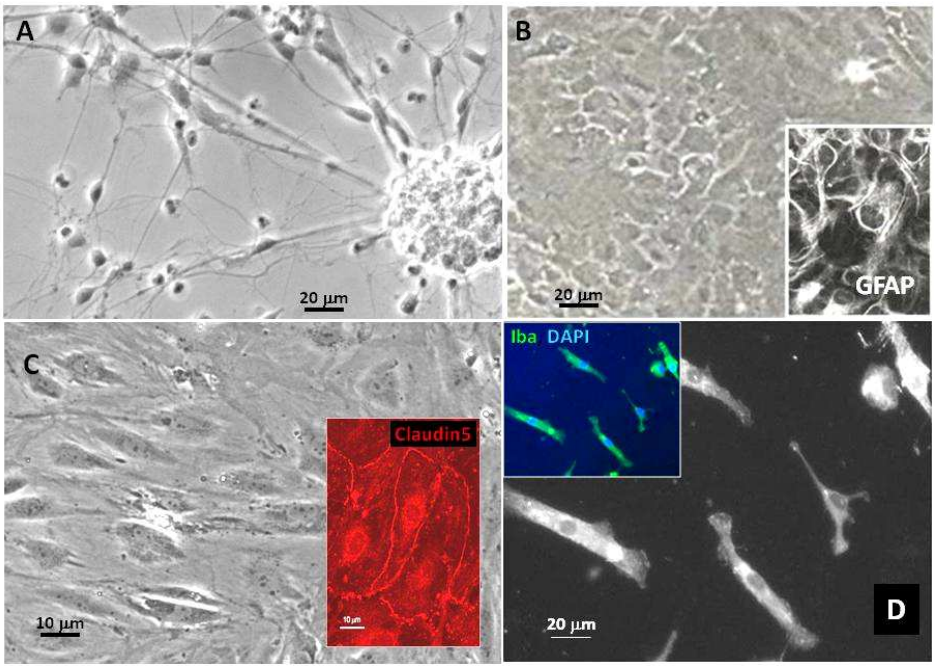

Figure 39. Primary cultures used for studying toxicity and uptake of NPs. **A:** Embryonic (E17) forebrain cultures enriched in neurons on the 10th day after plating. **B:** Neonatal astrocyte culture 14 days after plating. **C:** brain microvessel endothel cells 21 days after plating, **D:** Microglia on the 7th in vitro day after preparation.

For modelling neural stem cell responses and the effects of NPs on neuronal differentiation, studies were conducted on NE-4C embryonic mouse neural stem cells (Schlett, Madarasz 1997; Madarász 2013) and their in vitro differentiating neuron-derivatives. NE-4C cells display epitheloid morphology and proliferate rapidly in non-induced cultures, but give rise to neurons if induced by 10^{-8} – 10^{-6} M all-trans retinoic acid (Figure 40).

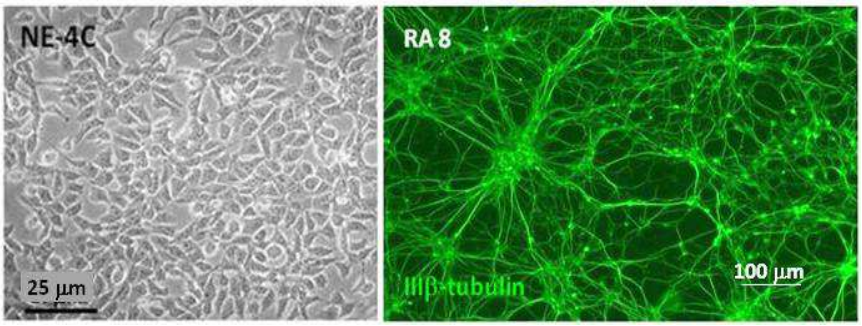

Figure 40. NE-4C embryonic neural stem cells in non-induced stem cell state (left panel) and 8 days after the induction with all-trans retinoic acid (RA); neurons were identified by staining for neuron-specific (IIIβ tubulin; green).

DOI:10.14753/SE.2015.1789

2.1.2. Targeting the cells with nanoparticles

The cells were exposed to freshly sonicated suspensions of NPs containing 10^9 NPs/ml to 10^{13} NPs/ml (corresponding 0.2 µg/ml - 2 mg/ml nanoparticle-mass) Si NPs or 10^{10}-10^{12}NP/ml (3.89 - 250 ug/ml) PS NPs for 4, 24 or 48 hours for MTT reduction metabolic and LDH release toxicity assays. In studies on cellular uptake, particles were added in 10^{11} NP/ml concentration for 1 hour to the cells.

The cell-targeted doses of PS NPs were calculated by using sedimentation velocity data provided by Teeguarden et al., (2007) for PS-NPs in serum-free physiological salt solution (Table 8).

Table 8. Applied doses of PS NPs for viability and toxicity assays

Concentration of NP dispersions added to the cells				Concentration of NPs contacting the cells (24 hours exposure time)#					
Mass [µg/ml]	Number of NPs or NP aggregates [NPs/ml]			NP mass/target area [µg/cm^2]			Number of particuli/target area [NPs/cm^2]		
	fresh NPs	*aged PS-COOH	*aged PS-PEG	fresh NPs	*aged PS-COOH	*aged PS-PEG	fresh NPs	*aged PS-COOH	*aged PS-PEG
250	10^{12}	5 x10^{11}	2.5x10^{11}	0.168	3.36	2.13	167 x10^8	134 x10^8	84x10^8
125	5X10^{11}	2.5 x10^{11}	1.25 x10^{11}	0.084	1.68	1.05	84 x10^8	67 x10^8	42x10^8
62.5	2.5X10^{11}	1.25 x10^{11}	6.1 x10^{10}	0.042	0.84	0.525	42 x10^8	32 x10^8	22 x10^8
31.2	1.2X10^{11}	6.1 x10^{10}	3 x10^{10}	0.021	0.42	0.26	21 x10^8	16 x10^8	10 x10^8
15.6	6X10^{10}	3 x10^{10}	1.5 x10^{10}	0.01	0.21	0.13	10.5 x10^8	8 x10^8	5 x10^8
7.8	3X10^{10}	1.5 x10^{10}	0.75 x10^{10}	0.005	0.1	0.065	5 x10^8	4 x10^8	2.5 x 10^8

The cell-contacting dose of fresh, 50 nm PS particles is composed by particles present in a 50 nm height layer of the NP suspension above the cell surfaces (t_0 load) and by particles arriving to this layer by sedimentation with a velocity of 0.28 µm/hour during the exposure time. In case of aged, aggregated particles, larger particle size (100 nm for PS-COOH and 200 nm for PS-PEG particles in averages, according to the NTA analyses) and consequently, larger sedimentation velocity (1.12 µm/hour for PS-COOH and 4.3 µm/hour for PS-PEG particles) but smaller number of particles were taken into account.

The effects of Si NPs on cell viability and the cellular uptake of Si NPs were measured in large part by a fellow PhD student, Emilia Izak, in our laboratory (Izak-Nau et al., 2014). Accordingly, my thesis covers only those results of the Si NP

studies which were achieved by my active contribution and gave important bases for my further studies on the effects of PS NPs.

2.2. Cell responses

2.2.1. Metabolic responses, cell membrane integrity and uptake reactions of neural cells in response to exposure to Si NPs with different chemical surface composition

The fluorescent core/shell Si NPs were freshly synthesized and thoroughly sonicated before addition to the cells at various (0.2 µg/ml (10^9 NPs/ml) to 2 mg/ml (10^{13} NPs/ml) concentrations. In LDH toxicity assays and MTT cell metabolism tests (Figure 41), incubation with the NPs for 4 or 24 hours did not cause significant cell responses. 48 hours exposure, however, resulted in detectable cellular changes depending on the dose and surface chemistry of the NPs, and also on the type of the cells.

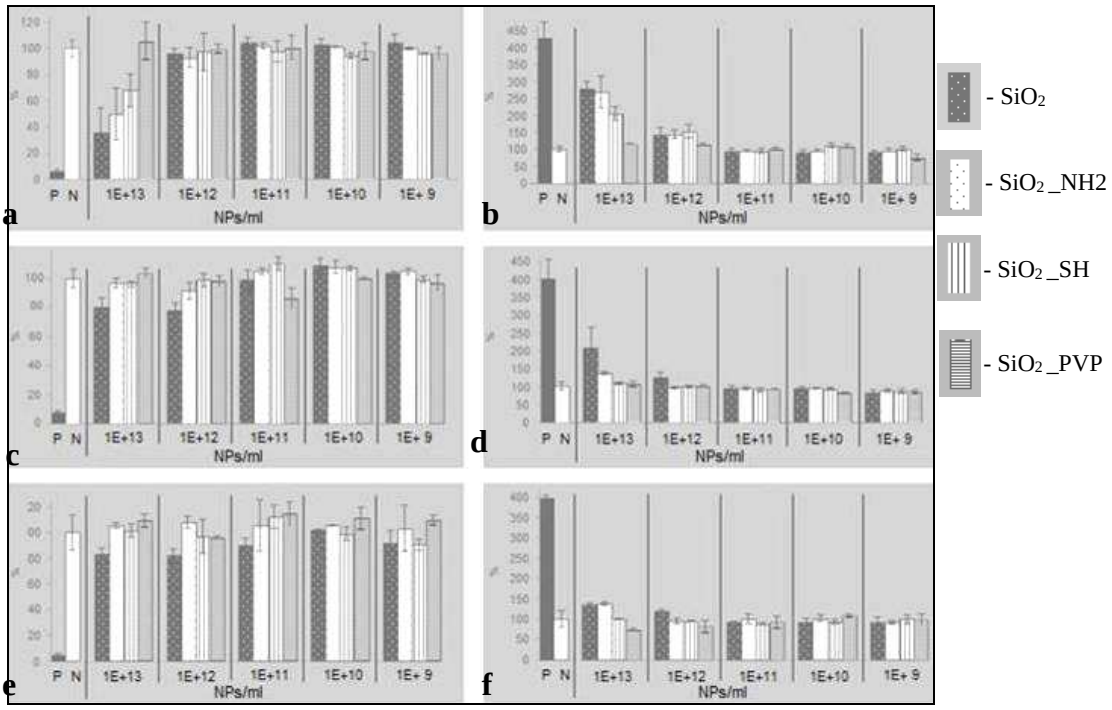

Figure 41. MTT-reduction (a, c, e) and LDH release (b, d, f) of neural tissue-type cells after 48-hour exposure to different concentrations of Si NPs. (a, b) NE-4C stem cells, (c, d), NE-4C derived neurons, (e, f) primary neuron-enriched brain cell cultures. P: "death" control (0.1% Triton X-100 treated cells); N: non-treated cells (Izak-Nau et al., 2014).

Microglia cells were slightly damaged by SiO_2, SiO_2_NH_2, and SiO_2_SH particles, but not by PVP-coated ones. The SiO_2_PVP NPs had no effect even at the highest (2 mg/ml) concentration, while plain and amine-functionalized particles caused an 40% increase in cell death.

DOI:10.14753/SE.2015.1789

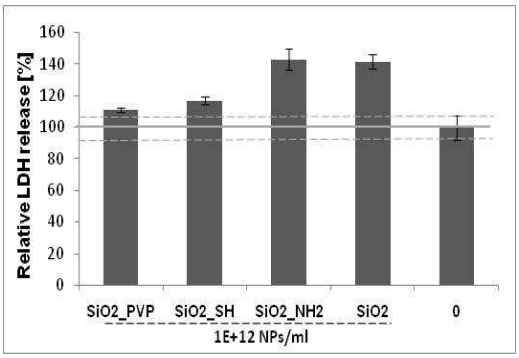

Figure 42. Cell damaging effects of silica core-shell NPs with different surface modifications on primary microglia cells after 1 hour exposure. Averages and standard deviations (n=6) of relative toxicity values are presented as percentages of LDH-activity measured in the media of non-treated (0) cells.

Cellular toxicity (LDH) and metabolic activity (MTT) assays demonstrated that the plain SiO_2 and the amine-functionalized (SiO_2_NH_2) particles exerted cellular toxic effects but only at high particle doses. The SiO_2_PVP particles, on the other hand, did not cause measurable effects in any concentrations and on any of the investigated cells.

2.2.2. Uptake of Si NPs by different neural cells

Uptake of SiO_2 NPs by various neural tissue-type cells were monitored by confocal fluorescence microscopy supplemented with fluorescence spectrum analysis. The spectrum analysis was done by Kata Kenesei who elaborated a method (Kenesei et al., Nanomedicine, 2014. submitted) to distinguish particle-emitted light from background fluoroscence (see Materials and Methods). Z-stack image analysis was used to determine intracellular particle localization.

Incubation with 500 µl of $5x10^{11}$ NPs/ml nanoparticles (dispersed in MEM/F12/ITS medium) did not result in obvious structural damages of any cells compared to untreated controls. In one-hour exposure, the plain SiO_2, SiO_2-NH_2 and SiO_2-SH NPs formed large, light microscopically detectable agglomerates in the fluid environment of the cells. While the aggregates settled on the surfaces of all investigated cells, the particle-fluorescence could be washed out from neuronal cultures (Figure 43) by rinsing with PBS. In contrast, microglial cells were heavily loaded by the plain SiO_2, SiO_2_NH_2, and SiO_2_SH NPs but contained only a few SiO_2_PVP particles. Microscopic spectrum analysis verified that the fluorescence detected in microglia cells was emitted by ingested nanoparticles (Figure 44).

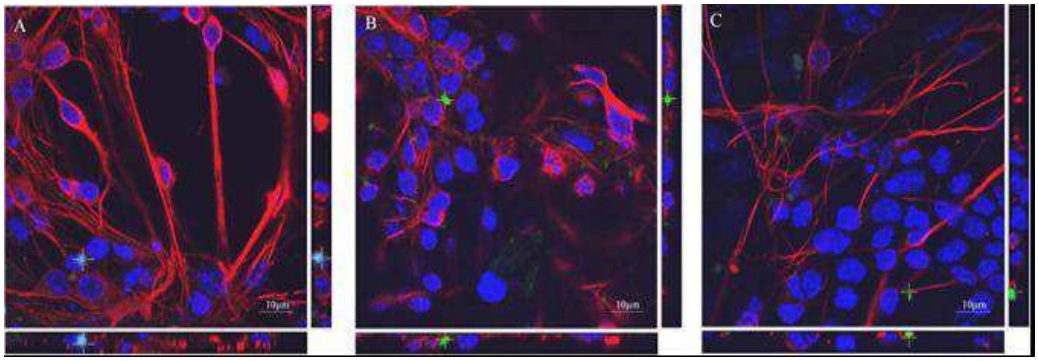

Figure 43. Confocal microscopic images of embryonic mouse forebrain neurons cultured 15 days (A) and treated with SiO_2 (B) or SiO_2_PVP NPs. After 1 hour exposure time and three-time washing, neurons did not retain any of SiO_2 NPs. Red: neurons stained for neuron-specific tubulin; blue: cell nuclei stained with DAPI Hoechst stain; green: fluorescent SiO_2 NPs

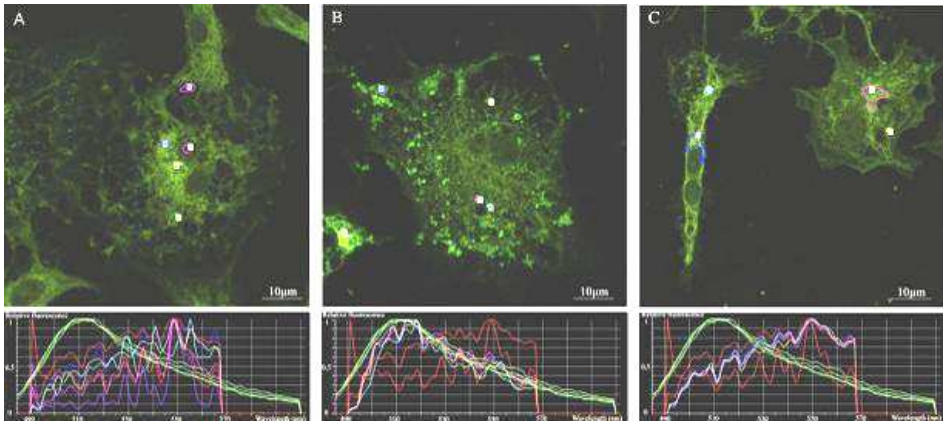

Figure 44. SiO_2 NPs are internalized by microglia cells (B), while SiO2_PVP NPs are rarely found inside the cells. For non-treated microglia cells (A) (Pictures by Kata Kenesei; Izak-Nau et al., 2014)

The microscopic analyses demonstrated that PVP-functionalisation decreased the rate of particle aggregation and importantly reduced the accumulation of particles by phagocytosis.

Data on the cellular effects of core/shell silica NPs clearly showed that the surface chemical composition plays essential roles in the biological activity of otherwise non-toxic particles. Coating the particle surfaces with the chemically inert PVP polymer could significantly reduce the biological interactions of particles. The biological “passivation” might have been due to the reduced aggregation of PVP-coated particles and/or to the masking of ionic groups on the surfaces.

For further studies on the importance of the surface composition of nanoparticles, the cellular actions of polystyrene NPs with negatively charged and PEG-passivated surfaces were investigated.

DOI:10.14753/SE.2015.1789

2.2.3. Cellular responses to exposure to PS NPs

Metabolic responses and cell membrane integrity of neural cells in response to exposure to PS NPs with different surface composition

To exclude size-dependent variations in biological responses, the size of PS NPs were kept constant (in the range of 45-70 nm), while the surfaces contained either –COOH groups or PEG polymer chains. The PS-COOH and PS-PEG NPs carried covalently core-bound fluorochromes, which were either NileRed or FITC (Spherotec Inc.) or Yellow (Kisker Gmbh).

Prior to studies, the potential interference of NPs with the designed assays was investigated in cell free assay systems. The presence of PS-COOH or PS-PEG NPs with different (NileRed, FITC, Yellow) fluorochromes caused ≤10% shifts of the optical density (OD) in cell-free MTT assays (a maximum of 0.020 units shift) in comparison to the OD values measured in cells (normally between 0.130 - 0.400 absorbance units) (Figure 45).

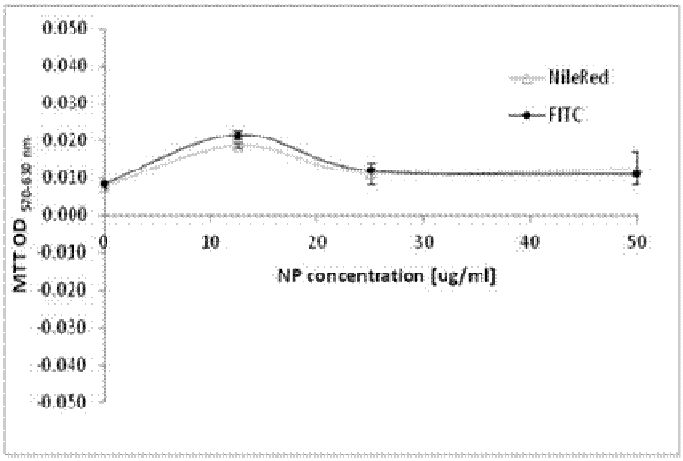

Figure 45. Effect of NileRed and FITC labelled PS-COOH NPs on MTT reduction. Studies with PS-PEG particles gave similar results. Averages and standard deviations are shown (n=4)

The presence of NPs (5-50 µg/ml) did not affect significantly the LDH enzyme activity either, in cell-free assays. The assays were performed by adding increasing concentrations of FITC-labelled PS-COOH or PS-PEG NPs to the assay mixture. The optical density of the formazan product was compared to that measured in the NP-free control.

DOI:10.14753/SE.2015.1789

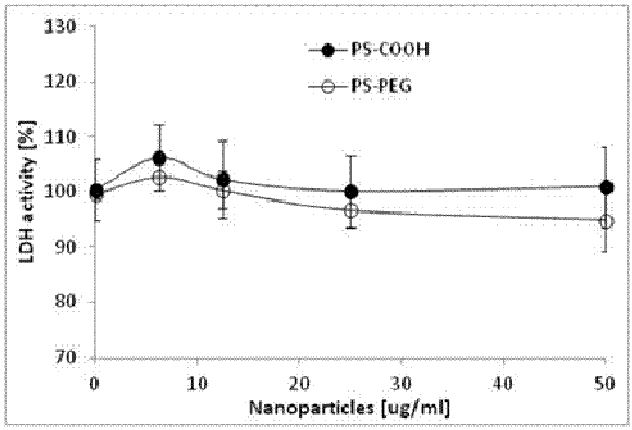

Figure 46. Effect of PS-COOH or PS-PEG NPs on LDH enzyme activity. Optical density of formazan product (OD) was measured in the presence of NPs and related to the OD of NP-free assays (100%). Averages and standard deviations are shown (n=6).

For optimizing the experimental conditions, the cells were exposed to different concentrations (3.89 – 250 ug/ml) of PS NPs, in serum-free tissue culture fluid for 4, 24 and 48 hours. At the end of incubation, the metabolic activity (cell viability) and the cell membrane integrity were measured by MTT-reduction (Mosmann, 1983) and LDH-release test (Abe and Matsuki, 2000) respectively. Initial toxicity (LDH release) studies on primary forebrain cell cultures showed almost no effects in 4-hour exposure, a mild increase in toxicity with increasing NP concentrations during 24-hour incubation, and a significant enhancement of particle toxicity in 48-hour exposure (Figure 47).

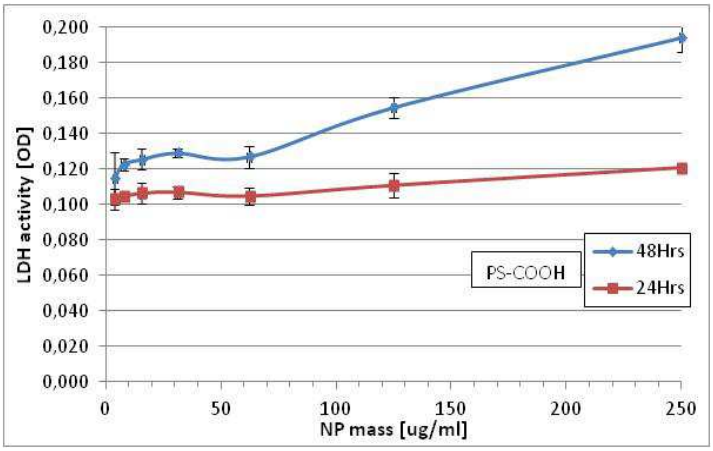

Figure 47. Long-term (48 hours) exposure to PS-COOH NPs resulted in significantly increased LDH release from primary forebrain cells.

As DLS studies showed a high-rate particle aggregation in a 48-hour period in serum-free conditions (with a 8 – 9 times larger size for PS NPs; see page 40), the parameters of cell loading could not be controlled for such long-term exposure periods. As a compromise, 24-hour exposure time was chosen for the experiments.

DOI:10.14753/SE.2015.1789

In metabolic activity and toxicity assays, the cells in 96-well plates (culture surface/well: 0.33 cm^2) were exposed to NP dispersions for 24 hours, in doses shown in Table 1.

Exposure to NPs did not significantly decrease the MTT reduction capacity of the cells, indicating no important effects on cell viability (Figure. 48).

The limited variations (less than 20% *versus* the control) observed in some cases (*e.g.*, at low NP concentrations on neural stem cells, or with PS-COOH NPs on stem cell-derived neurons) were apparently independent from NP concentrations. In brain microvascular endothelial cells, on the other hand, a small but significant increase of MTT reduction was observed with increasing concentrations of NPs up to 10^{11} NPs/ml, regardless of surface functionalization.

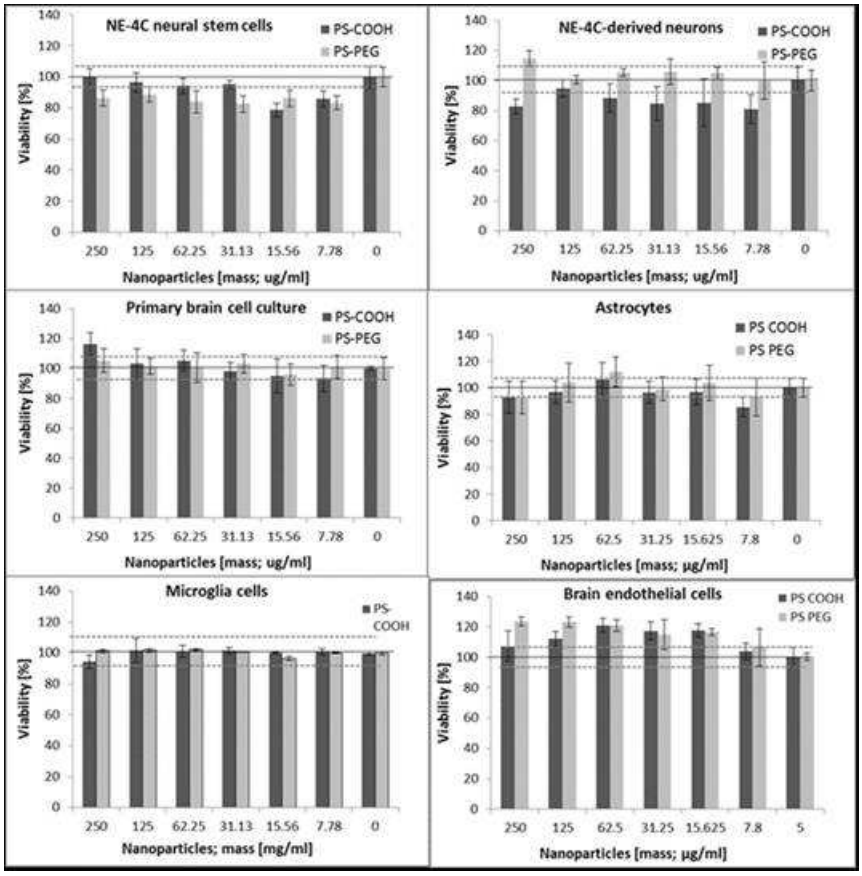

Figure 48. Relative viability (MTT reduction capacity) of cells after 24 hr exposure to carboxylated (PS-COOH) or PEGylated (PS-PEG) poly-styrene nanoparticles did not indicate toxic effects of particles. MTT reduction was measured in 8-12 identically treated cultures of each type of cells (n= 8-12). Each reduction value was related to the average calculated from 8 or 12 non-tretaed (0) sister-cultures (100%). Averages and standard deviations of percentages are presented.

When measuring cell death with the LDH release assay, no significant toxic effects of PS NPs were detected (Figure 49).

Only microglia cells showed a limited increase of LDH release at the highest concentration of PS-COOH NPs, whereas PS-PEG particles did not have such effect. A mild toxicity was observed in primary brain cell cultures containing astrocytes and microglia cells besides neurons. The toxic effects, however, were significant only at the highest concentration of PS-COOH particles (10^{12} NPs/ml). Thus, data obtained with viability and toxicity assays indicated that PS particles were not toxic to neural cells *in vitro*, when used at concentrations between 7.8 and 125 μg/ml.

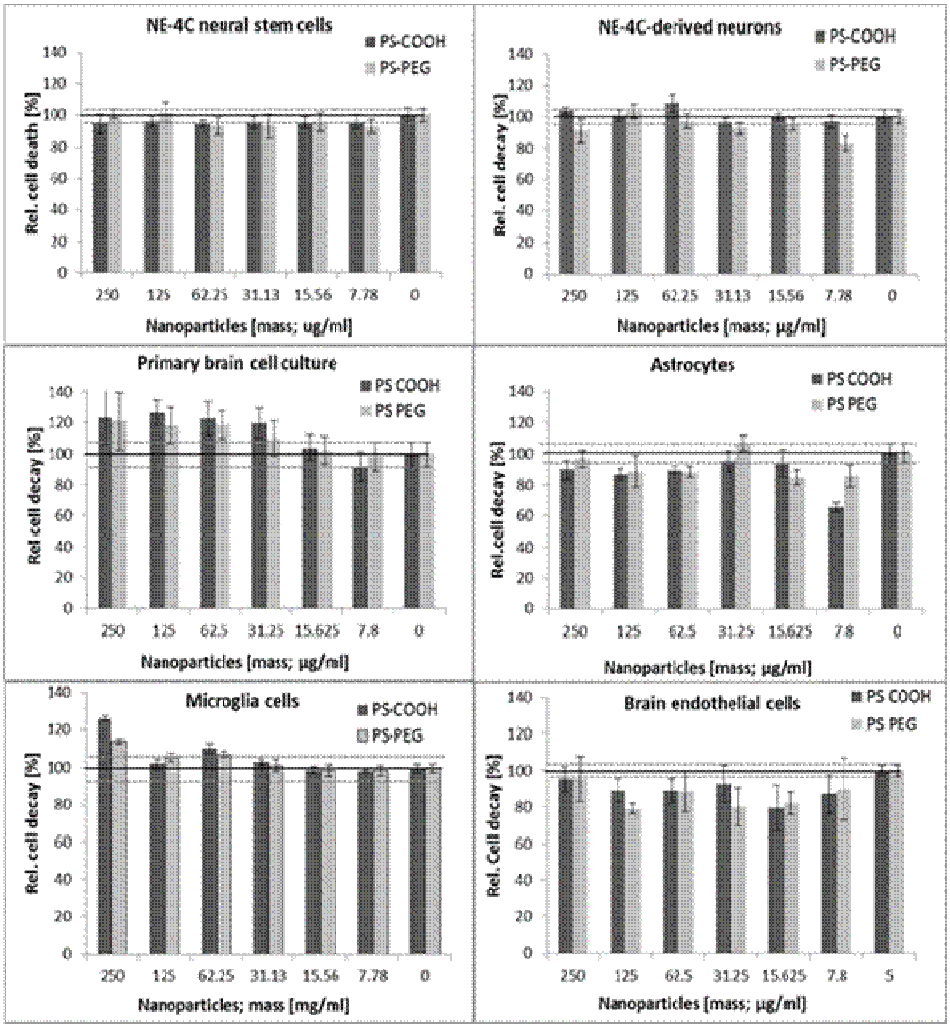

Figure 49. Cell decay (LDH release) responses of different types of neural cells after 24 hour exposure to carboxylated (PS-COOH) or PEGylated (PS-PEG) polystyrene nanoparticles. LDH enzyme activities were determined in the culture media of 8-12 identically treated cultures of each cells and were related to the activity values measured in media of non-treated cells (100%). Averages and standard deviations are shown (n= 8-12).

2.2.4. Morphological effects and cellular uptake of PS NPs

Light microscopic and immunocytochemical studies did not reveal morphologically damaged cells after incubation with PS NPs (10^{11} particles/ml) for 1 hour, regardless of surface functionalization. NE-4C neural stem cells and their neuronal progenies did not take up either PS-COOH or PS-PEG particles in 1 hour incubation (Figures 50 A,B), and the presence of particles did not damage NE-4C derived neurons (Figure. 50C).

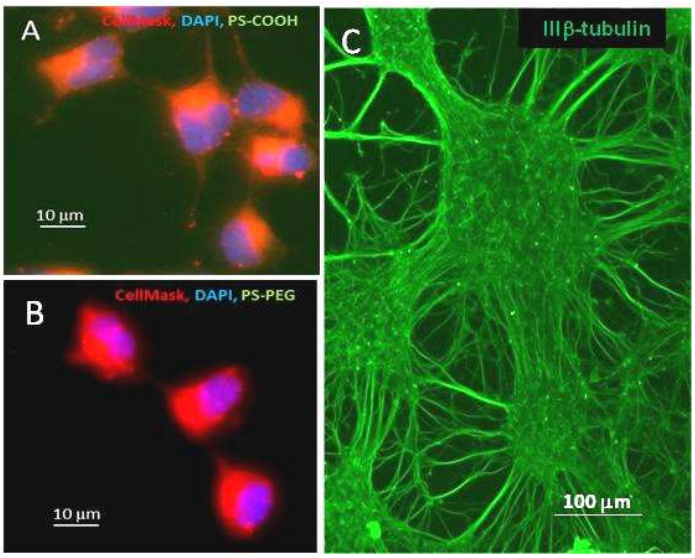

Figure 50. Non-induced NE-4C stem cells (A,B; whole-cell staining with "CellMask";red and nuclear staining with DAPI; blue) and NE-4C-derived neurons did not take up and did not give any morphological reactions to PS-NPs in 1-hour exposure.

In 1-hour exposure, neurons (Figure 51 A). and astrocytes (Figure 51B). did not take up either carboxylated or PEGylated PS-NPs.

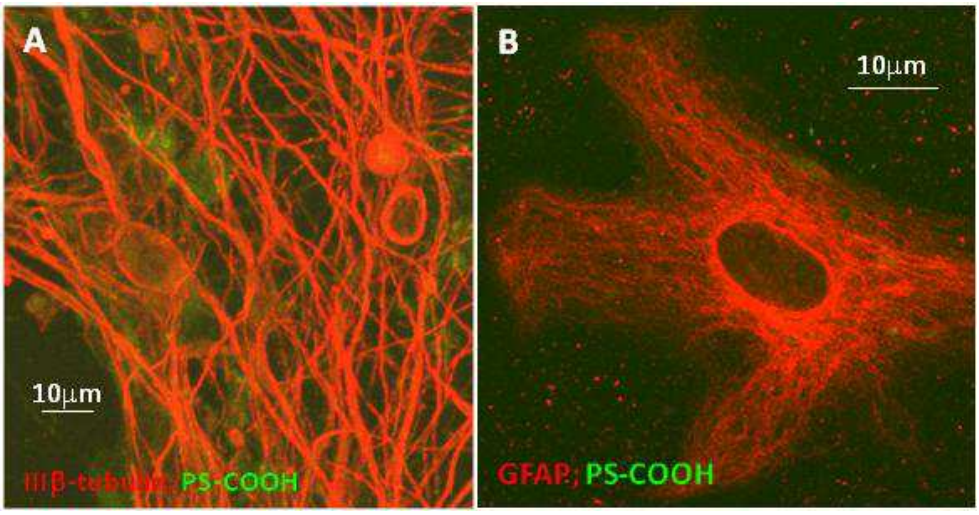

Figure 51. Confocal microscopic picture on primary neurons (A) stained for IIb-tubulin (red) and an astrocyte (B) visualized by anti-GFAP staining (red) after 1-hour incubation with PS-COOH particles (10^{11} NPs/ml).

DOI:10.14753/SE.2015.1789

When primary brain cell cultures containing neurons, astrocytes and also microglia cells were exposed to PS-COOH NPs, only cells with microglial morphology accumulated NPs in sufficient amount for confocal microscopic visualization (Figure 52).

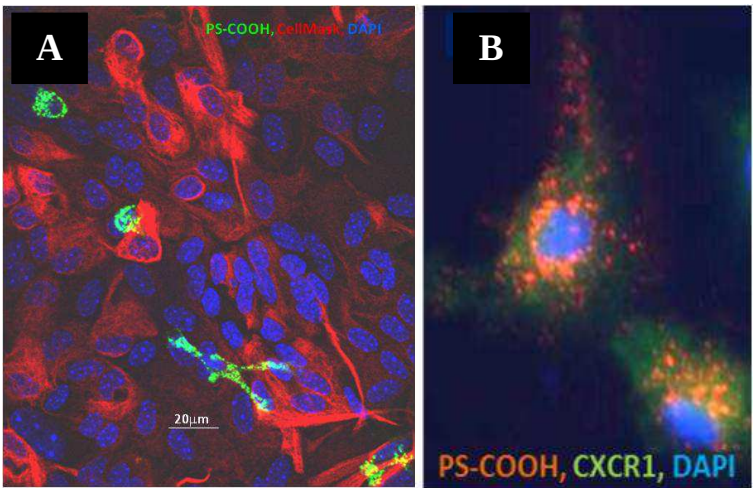

Figure 52. A: In primary brain cell cultures, cells with microglial shape and location, accumulated FITC-labelled PS-COOH particles. Confocal microscopic picture of mouse forebrain cultures prepared from E17 embryos and imagined on 14th day after seeding. B: GFP-labelled (CXCR1; green) microglia cells took up NileRed-labelled (red) PS-COOH NPs. Fluorescence microscopic picture.

The uptake of particles by microglia was further investigated in purified cultures of GFP-labelled microglia cells expressing green fluorescent protein fused to the fractalkine (CX3C) receptor1 (CX3CR1) (Jung et al., 2000a). In a 1-hour exposure, microglia cells accumulated significant amounts of PS-COOH NPs (Figure 53A), while did not take up PS-PEG NPs (Figure 53B).

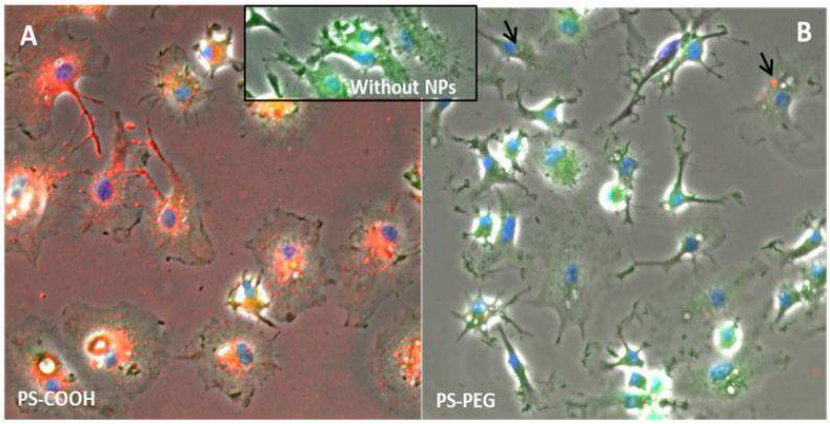

Figure 53. Different uptake of PS-COOH and PS-PEG NPs by primary microglia cells. Microglia cells derived from the forebrain of newborn transgenic mice expressing green fluorescent proteins under the control of the promoter of CX3CR1 (green) were exposed to NileRed-labelled (red) 50 nm PS-COOH (A) or PS-PEG (B) NPs ($2x10^{11}$ NPs/ml), for 1 h. Note the intracelluar accumuations of PS-COOH NPs, and the flattened shape of cells in the presence of PS-COOH NPs (A) in contrast to the ramified form of non-treated cells (insert) or those treated with PS-PEG NPs (B).

In the presence of PS-COOH particles, the ramified “quiescent” shape of microglia cells (Figure 53 insert) changed into a more flattened macrophage-like form (Figure 53A), while the presence of PS-PEG particles induced much less morphological reactions (Figure 53B). As the resolution in fluorescent microscopy does not allow visualising individual 45-70 nm NPs, the observed fluorescence should derive either from spontaneously agglomerated particles, or from particles accumulated into endosomes/lysosomes by active cellular uptake and sorting. To investigate whether particles were internalized through active cellular processes, uptake experiments were run at +4°C and 37°C on microglia.

Confocal microscopic Z-stack analysis showed that microglial cells internalized carboxylated particles at 37 °C (Figure 54 A), while NPs were stuck on the cell surfaces at low temperature (Figure 54 B).

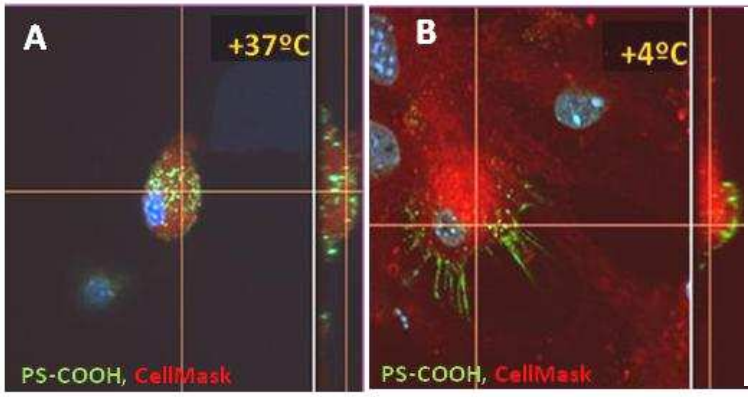

Figure 54. Confocal microscopic pictures and Z-stack images (right margins) of CellMask-stained glial cells incubated with PS-COOH NPs ($2x10^{11}$ NPs/ml) for 1 hour at 37 °C (A) and 4 °C temperature

The results demonstrated that microglia cells take up actively and respond with morphological changes to carboxylated PS NPs, while maintain ramified shape and accumulate much less particles if exposed to PEGylated PS NPs.

Brain microvessel endothelial cells were densely decorated with agglomerates of both PS-COOH and PS-PEG particles (Figure 55). The extreme thinness of these cells, however, made difficult to confirm whether the particle agglomerates were inside the endothelial cells or just on their surfaces.

The results showed that PS NPs, while evoke cell-type dependent responses from different neural tissue cells, are not toxic for these cells, and can cause some mild acute toxicity only at extremely high concentrations. However, when the experiments were repeated with particles stored in distilled water at 4°C for longer than 6 months, surprisingly different results were obtained. The unexpected cellular reactions to “aged” particles led us to analyse the role of particle-ageing in interactions with biological material and living cells.

DOI:10.14753/SE.2015.1789

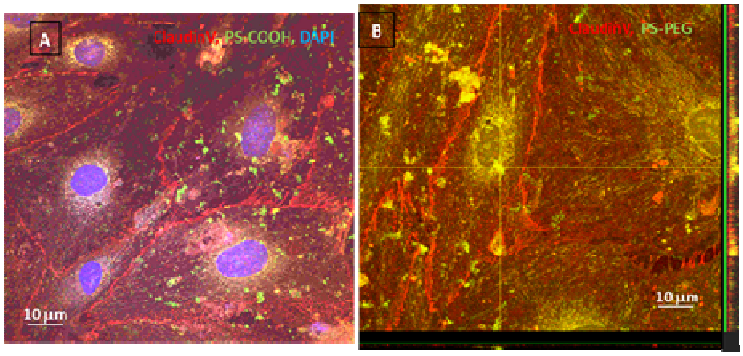

Figure 55. Confocal microscopic pictures of Claudin-5 immonstained brain microvessel endothelial cells incubated with PS-COOH (A) and PS-PEG NPs ($2x10^{11}$ NPs/ml) for 1 hour at 37 °C. Z-stack image (right margin) on PS-PEG-loaded cells shows the extreme thinnes of these cells.

3. Effects of particle aging on interactions of PS NPs with neural cells

3.1. Cellular effects of aged PS NPs

When the MTT and LDH assays were repeated with particles stored in distilled water at 4°C for longer than 6 months, enhanced and dose-dependent toxic effects of PS NPs were detected on NE-4C stem cells (Figure 56).

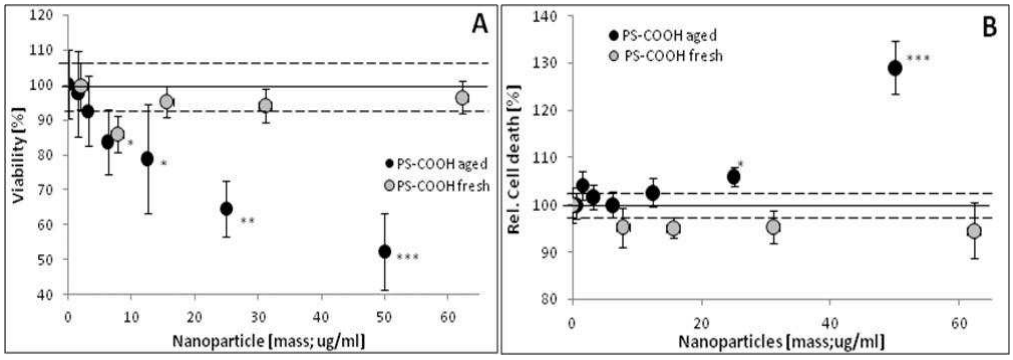

Figure 56. Different responses of NE-4C neural stem cells to fresh and aged PS-COOH NPs. **A**: Formazan production by living cells (Viability) after a 24 h exposure to PS-COOH NPs. **B:** LDH activity in the cell free culture supernatants taken at the end of the 24 h exposure to NPs.The data are the means ± SDs of OD values measured in 8-12 replicate cultures, and are presented as percentages of the average OD of non-treated cultures (100 %; straight line; ± SD: dashed lines) . Significance was determined by t-test *:p<0.05; **:p<0.01; ***:p<0.001

Enhanced toxicity of aged particles was found also in microglia cultures (Figure 57)

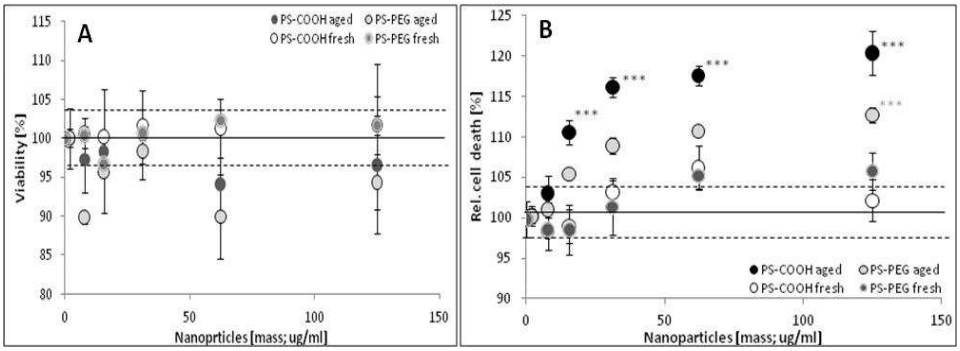

Figure 57. Different responses of microglia cells to fresh and aged PS NPs. MTT reduction by living cells (Viability) (**A)** and LDH activity in the culture supernatants (cell death) **(B)** were determined after 24 h exposure to fresh or aged PS-COOH and PS-PEG NPs. The data are the means ± SDs of ODs (n= 8-12), and are presented as percentages of the control (100 %; straight line; ± SD: dashed lines). Significance was determined by t-test ***:p<0.0001.

In uptake experiments with “aged” particles, large particle-agglomerations were seen on all cell surfaces and could not be removed by repeated washing. In contrast to fresh particles, aged NPs decorated NE-4C stem cells (Figure 58)

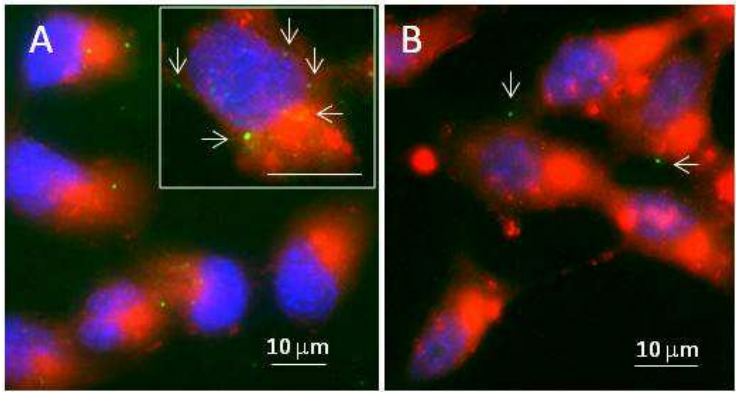

Figure 58. Fluorescence microscopic pictures on NE-4C cells were exposed to FITC-labeled (green; arrows), aged PS-COOH NPs (A) or PS-PEG (B) NPs. The cells were stained with CellMask (red) and nuclei were visualized with DAPI.

In microglial cells, aged PS NPs accumulated in high amounts in the cytoplasm, regardless of the original carboxyl or PEG surface modification (Figure 59). Also, the ramified morphology of non-treated microglia (see Figure on pp 61) changed to a flattened amoeboid shape in response to both, PS-COOH and PS-PEG NPs.

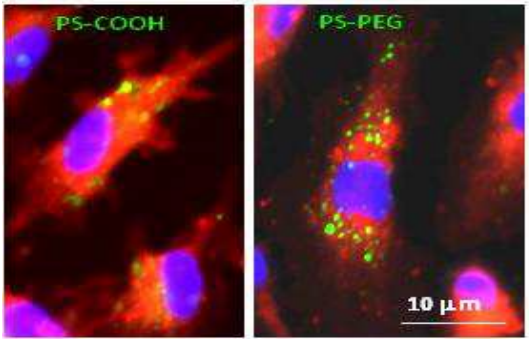

Figure 59. Fluorescence microscopic picture on microglia cells incubated with PS-COOH or PS-PEG NPs (2x 10^{11} NPs/ml). Cells were stained with CellMask (red) and nuclei were visualized with DAPI.

To verify that the enhanced green fluorescence was derived from ingested NPs, confocal microscopic studies supplemented with fluorescence spectrum analysis (Kenesei et al., 2014 submitted) were conducted. With spectral analysis of the emitted light, the fluorescence of NPs could be distinguished from the high auto-fluorescence of cells, intracellular vesicles and cell debris (Figure 60)

Fluorescence spectrum analysis confirmed that the enhanced fluorescence in NP-exposed microglia cells was derived from NPs. The enhanced cellular uptake might be a consequence of particle aggregation during: large aggregates might trigger endocytotic uptake. The formation of large aggregates during prolonged storage was clearly shown by physico-chemical studies on aged particles (see pp 37). The

particle aggregation itself, the reduced significance of the original surface composition and the enhanced cell toxicity, however, suggested that the chemical composition of particle surfaces has changed during prolonged storage.

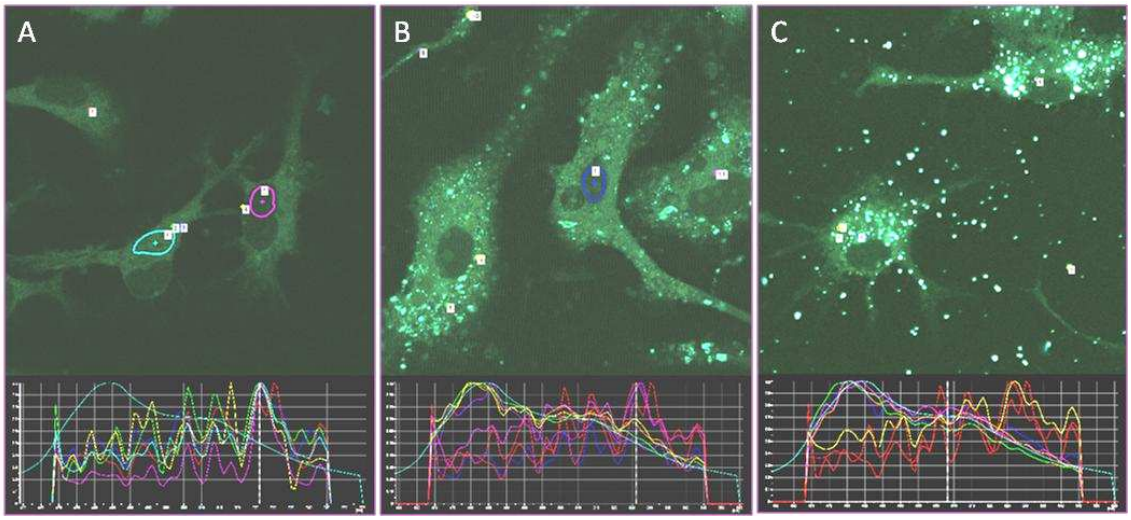

Figure 60. Confocal microscopic images of microglia cells without loading with NPs (A) or exposed to aged (shelf-life >1year) PS-COOH (B) and PS-PEG (C) particles. Lower pannels show the fluorescence spectrum of each spot outlined on the upper pannel. The fluorescence spectrum of naoparticles are shown as a blue-green curve with a maximum light emission at 485 nm. The spectra of individual spots are shown with the same colouring as their outlines on the upper pictures.

3.2. Endotoxin contaminations on PS NP surfaces

As bacterial endotoxins are ubiquitous contaminants of materials, including nanoparticles H. (Vallhov et al., 2006) the potential endotoxin contamination of fresh and aged PS-COOH and PS-PEG particles was measured, by using the chromogenic Limulus amebocyte lysate (LAL) assay.

PS particles with different fluorochromes and from different manufacturers were assayed for the presence of endotoxin with the chromogenic LAL assay. Surprisingly, all particles gave positive LAL-reactions, and PS-PEG NPs turned to be more positive than PS-COOH particles, regardless of ageing (Figure 61).

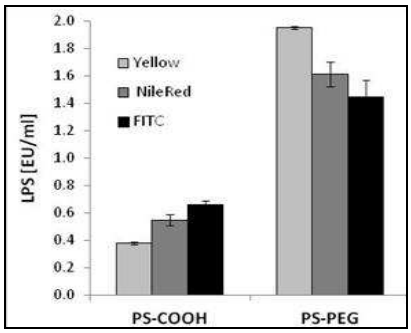

Figure 61. Apparent LPS-contamination of three different batches of „fresh" PS-NPs with different fluorescent labels determined by chromogenic LAL-assay. Averages and standard deviations (n=4) are shown.

The unexpected data suggested some interference of PS-NPs in general, and PS-PEG particles in particular with the LAL-assay. To investigate whether LAL-positivity was due to endotoxin rather than to nonspecific effects of NPs on the LAL assay components, a preliminary test was run on the chromogenic readout of the assay. Different concentrations of p-nitro-aniline (p-NA; the chromophore product of the LAL assay) were brought together with increasing concentrations (from 0 to 250 ug/ml) of NPs (Figure 62).

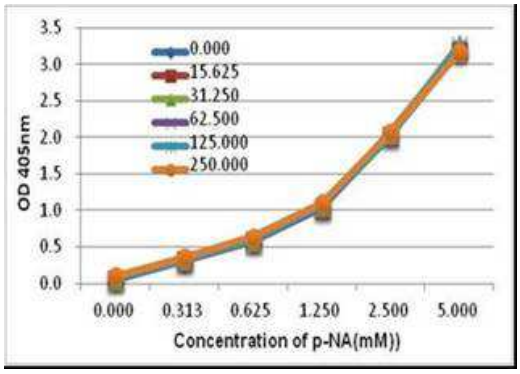

Figure 62. PS-PEG NPs did not interfere with the photometric read-out of p-nitro-aniline (p-NA), the chromophore product of the LAL assay. The colours refer to the different concentrations of PS-PEG NPs added to the p-NA solutions. Data points represent the averages of 3 assays on each NP concentrations (showing no deviations).

The results showed that PS NPs did not interfere with the LAL assay readout, but did not exclude the possibility that PS NPs, and especially PS-PEG particles, might interfere with the enzymatic components – a protein cleavage cascade leading to clotting the hemolymph - of the LAL bioassay. In the lack of unquestionably endotoxin-free PS NP preparations, the endotoxin-concentrations on particle surfaces could not be determined in absolute terms. Next, we investigated whether the relative levels of endotoxin adsorption by NP surfaces could be determined.

PS NPs were incubated with known concentrations of lipopolysaccharide (LPS, endotoxin) dissolved in endotoxin-free distilled water, and the rate of LPS adsorption was studied by LAL-assay and by SDS-PAGE.

After 1 hour incubation with 0.5.EU/ml LPS and repeated rigorous washings, PS NPs showed an increased positivity in the LAL assay (Figure 63).

DOI:10.14753/SE.2015.1789

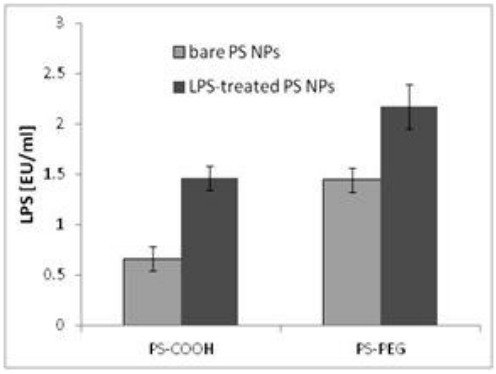

Figure 63.
LAL-assays on bare and LPS-incubated „aged" particles. The particles were incubated with 0.5 EU/ml LPS in water for 1 hour, and were washed three times with rigorous shaking. (Averages and standard deviations; n=4)

SDS-PAGE analyses also indicated firm, non-washable settlement of endotoxins on PS-NP surfaces (Figure 64).

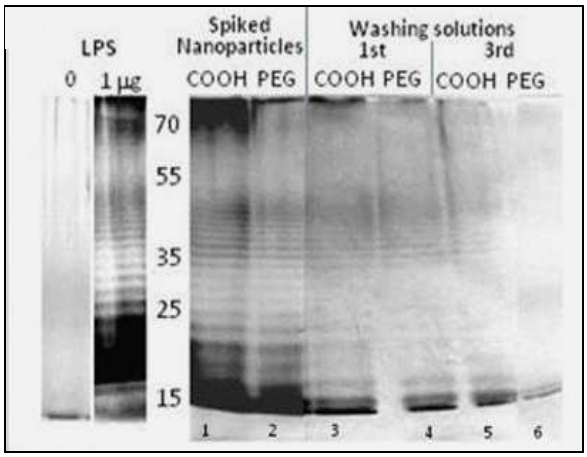

Figure 64. SDS-PAGE of LPS-spiked and washed particles (lanes 1, 2) and the first (lanes 3, 4) and third washing solutions (lanes 5,6). Left two lanes: 0: LPS-free water, 1ug: 1 ug LPS in water.

Knowing that PS NPs can adsorb significant amount of bacterial endotoxins, and that LAL-assays can be used for comparing surface-bound endotoxins in relative terms, we could show that PS-NPs accumulate endotoxins on their surfaces during prolonged storage (Figure 65).

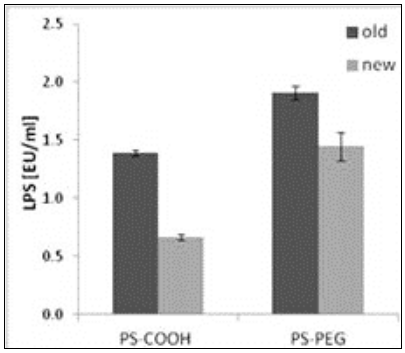

Figure 65.
Apparent LPS -contamination of fresh (new) and aged (old) particles. Averages and standard devietions of 4 LAL-assays.

The most important finding of these studies was that PEG-coating could not prevent the adsorption of endotoxins on the particle surfaces.

DOI:10.14753/SE.2015.1789

3.3. Biological effects of LPS contaminated PS NPs

The direct effect of surface-bound LPS on the microglial uptake of PS-NPs was evidenced by comparing the ingestion of PS-PEG particles with or without spiking with LPS. NileRed-labeled, aged PS-PEG particles were incubated with 0 to 100 ng/ml LPS for 4 hours. After rigorous washing, LPS-spiked and not-spiked particles (62.5 µg/ml) were added to cultures of GFP-expressing microglia, for 1 hour. Confocal microscopic Z-stack analyses showed that pre-incubation of PS-PEG nanoparticles with as less as 10 ng/ml LPS resulted in an increased microglial uptake (Figure 66).

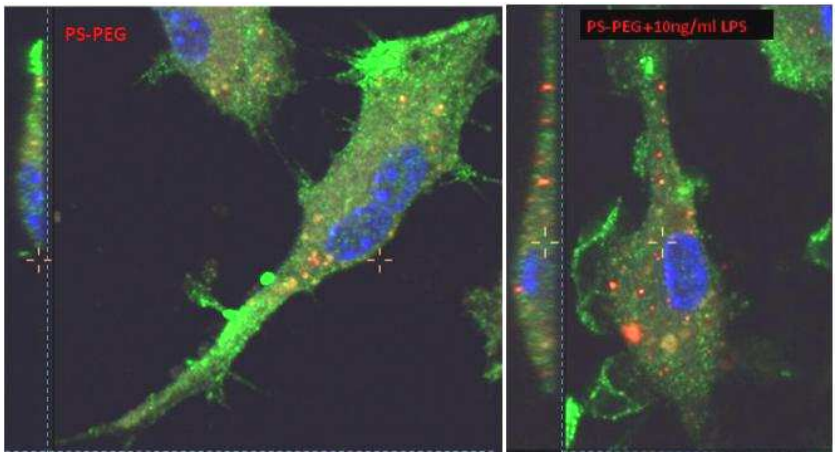

Figure 66. Confocal microscopic and Z-stack analyses on microglial uptake of aged, non-spiked (left) and aged and spiked with 10 ng/ml LPS PS-PEG NPs. Microglial cells displayed the green fluorescence of CXC3R1-GFP construct; cell nuclei were stained with DAPI (blue), and NileRed labeled PS-PEG NPs showed red fluorescence.

The *in vitro* data indicated that even small amount of bio-active compounds adsorbed by NP surfaces can turn the otherwise harmless particles to potential biological-risk agents. The *in vitro* studies, however, should necessarily neglect the powerful protective functions of physiological barriers. The barrier-penetration and *in vivo* body distribution of PS NPs have been thoroughly investigated my fellow PhD student, Kata Kenesei; therefore the data are presented in her thesis work. My work joined to the *in vivo* investigations only in studying the barriers protecting the developing and adult nervous tissue, the placenta and the blood-brain barrier, respectively.

DOI:10.14753/SE.2015.1789

4. Interaction of PS NPs with physiological barriers protecting the central neural tissue.

Short-term (5 min) and long-term (4 days) distribution of PS-COOH and PS_PEG NPs in the embryonic and adult mouse brain and in the placenta of 14 – 17 post-conception pregnant mice were investigated after a single intravenous injection (2.1µg particle mass /g bodyweight) of FITC-labeled PS NPs into the tail vein. After 5-minute and 24-hour exposures the animals were sacrificed, and 30 µm tissue sections were investigated with fluorescence microscopy and with confocal microscopy supplemented with spectrum analysis.

The histological studies (Figure 67 A,C) revealed that 5 minutes after the injection, PS-COOH particles decorated densely the walls of the brain vessels, while PS-PEG NPs were hardly revealed in the brain by the applied methods. Four days after the injection, however, all

particles were cleared from the brain. Similarly, PS-COOH NPs were initially retained by the placenta, while PS-PEG NPs were not seen. In a 4-day period, carboxylated particles were completely cleared from the placenta as well.

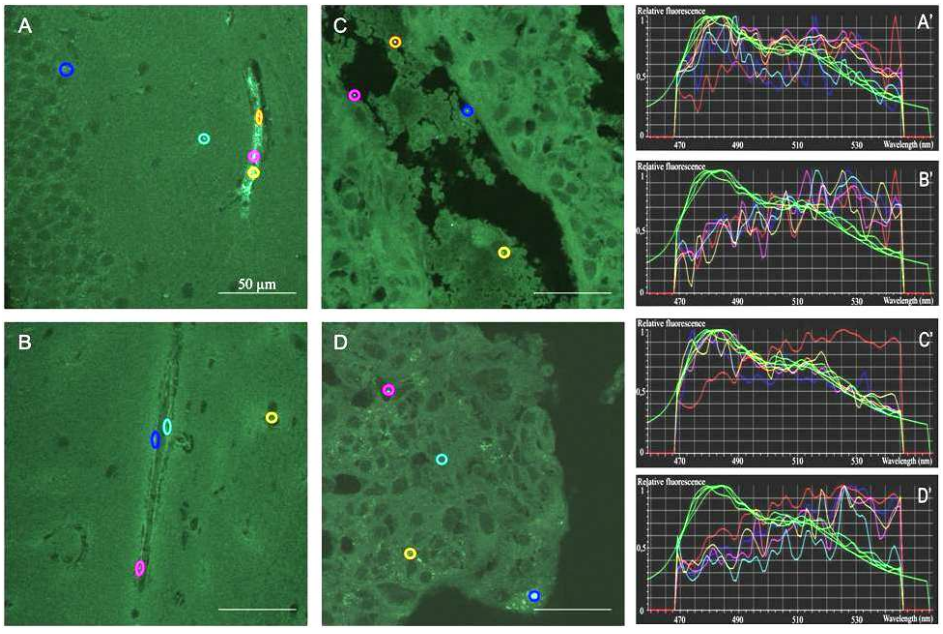

Figure 67. Confocal microscopic pictures and spectral analyses (right panels) of sections made from the adult mouse forebrain (A,B) and the placenta (C,D; 17th day postconception) after **5 min** of injection of PS-COOH (A,C) and PS-PEG NPs (B,D). The fluorescence spectrum of nanoparticles are shown as green curves with a maximum light emission at 485 nm. The spectra of individual spots are shown with the same colouring as their outlines on the upper pictures. Picture and analysis by K.Kenesei (Kenesei et al., Nanomedicine submitted).

DOI:10.14753/SE.2015.1789

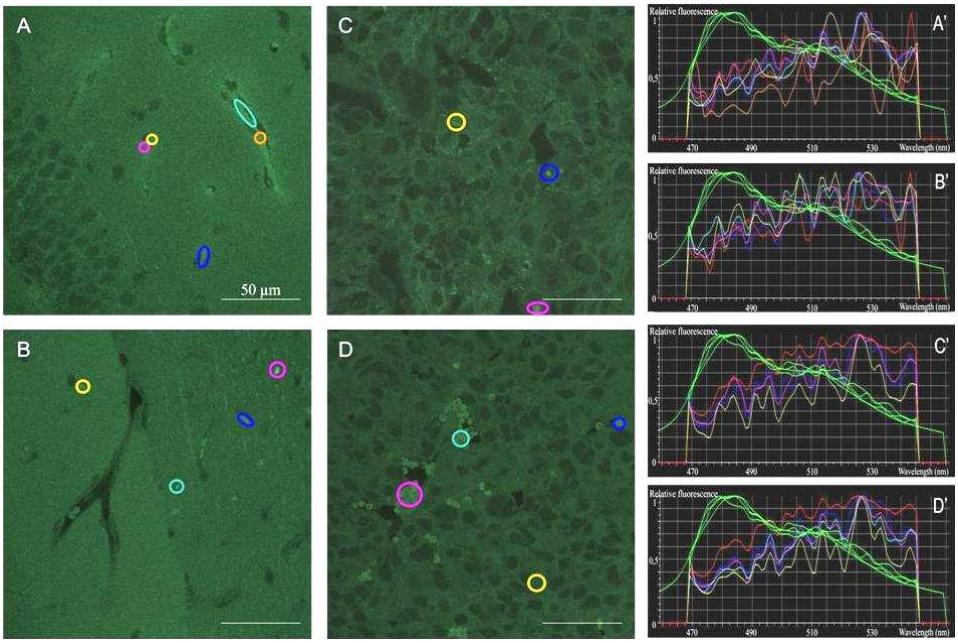

Figure 68. Confocal microscopic pictures and spectral analyses (right panels) of sections made from the adult mouse forebrain (A,B) and the placenta (C,D; 17th day postconception) **4 days** after the injection of PS-COOH (A,C) and PS-PEG NPs (B,D). The fluorescence spectrum of nanoparticles are shown as green curves with a maximum light emission at 485 nm. The spectra of individual spots are shown with the same colouring as their outlines on the upper pictures. Picture and analysis by K.Kenesei (Kenesei et al., Nanomedicine submitted).

In accordance with the data on proper protective functions on the placenta, PS NPs were not revealed in the embryonic brain.

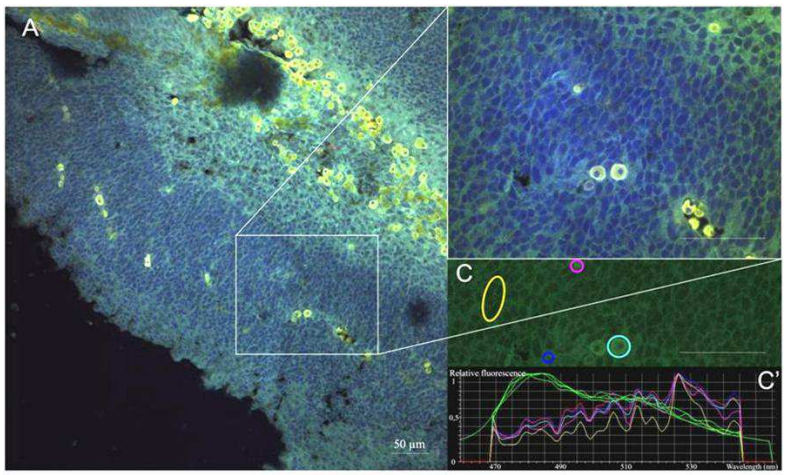

Figure 69. Confocal microscopic pictures (A,C and enlarged part of A on the upper right panel) and fluorescence spectra of encircled regions (right bottom panel) of embryonic (E17) mouse brain cortex

The data demonstrated that in vivo, the cells of the central neural tissue are protected against the invasion of PS NPs of the 50 nm size-range. Targeted studies on the *in vivo* penetration and neurobiological effects of LPS contaminated NPs, however, is considered for the near future.

5. Cellular responses to silver NPs of different shapes

Silver NPs (Ag NPs) are known to be toxic to microbial and tissue cells, mainly due to the release of Ag^+ ions. AgNPs are widely used as anti-infectants because of the higher sensitivity of bacteria than mammalian cells. The aim of this study was to investigate the influence of particle-shape on the mammalian cellular toxicity; therefore Ag NPs with size about 50 nm were synthesized with different – spheroid, cubic, triangle and rod – shapes (see Chapter 1.3.), and their toxicity was measured on NE-4C embryonic neuroectodermal stem cells.

NE-4C neural stem cells were exposed for 24 hours to increasing (1–100 μg/ml) concentrations of silver NPs with different shapes. Cell viability was measured with MTT reduction tests. The metabolic activity (MTT reduction capacity) was reduced below 20% of the control by Ag rods at 1 μg/ml, and by cubes at 50 μg/ml concentrations. Ag triangles showed mild (less than 50%) toxicity at 100 μg/ml concentration, while Ag spheres were not toxic when compared to untreated control. (Figure 70).

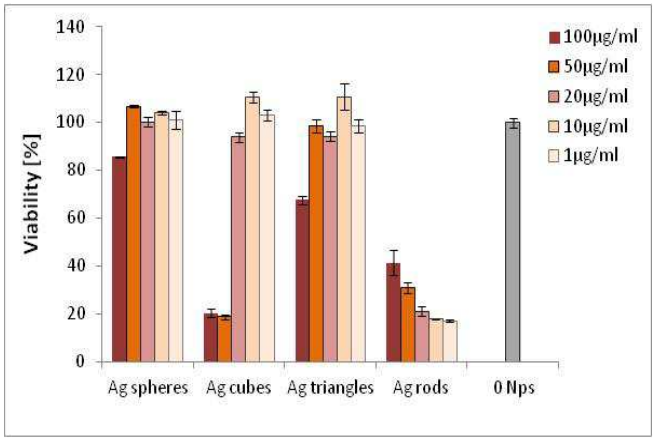

Figure 70. Shape-dependent effects of Ag-NPs on metabolic activity of NE-4C neural stem cells.

The data-indicated a toxicity-rank for the different shapes:

rods > cubes > triangles > spheres

DOI:10.14753/SE.2015.1789

To investigate whether Ag-NP toxicity was caused by the released Ag-ions, NPs were dispersed (100 µg/ml) in cell culture medium, and after 24-hour incubation the particles were removed from the suspensions by centrifugation (30 000g; 15 min). The culture medium of NE-4C cells was replaced with the particle-free incubation solutions and cell viability (MTT reduction capacity) was assayed after 24 hour incubation with particle-free supernatants (Figure 71).

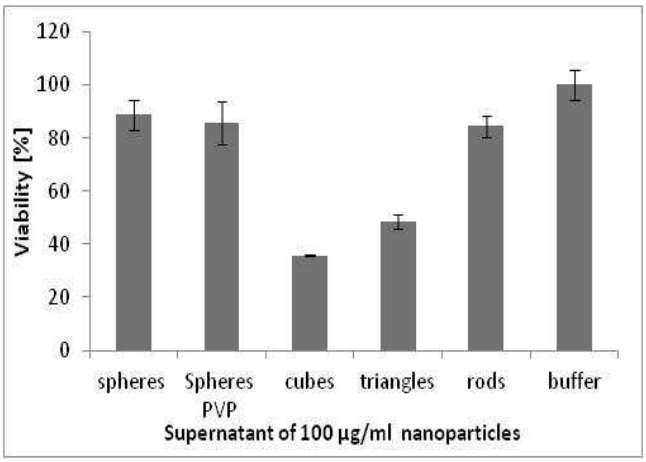

Figure 71. The effects of particle-free supernatants of NP-suspensions on viability (MTT reduction) of NE-4C cells. Spheres PVP: Ag spheres kept in polyvinylpyrrolidon (PVP) containing buffer prior to dispersion in culture medium

The data demonstrated important toxic effects of the particle-free supernatants of Ag cubes and triangles, while, almost no toxic effects of the supernatants of spheres were detected. In the case of rods, the results need further explanation. Ag rods displayed high MTT-reduction capacity in themselves. For the time being, this interference with the assay components is not explored.

The cellular uptake of Ag-NPs was investigated by electron microscopy after exposing the cells for 1 hour to 50 µg/ml doses of NPs. The heavy cytotoxicity of Ag rods was evident on the electron microscopic pictures (Figure 72).

DOI:10.14753/SE.2015.1789

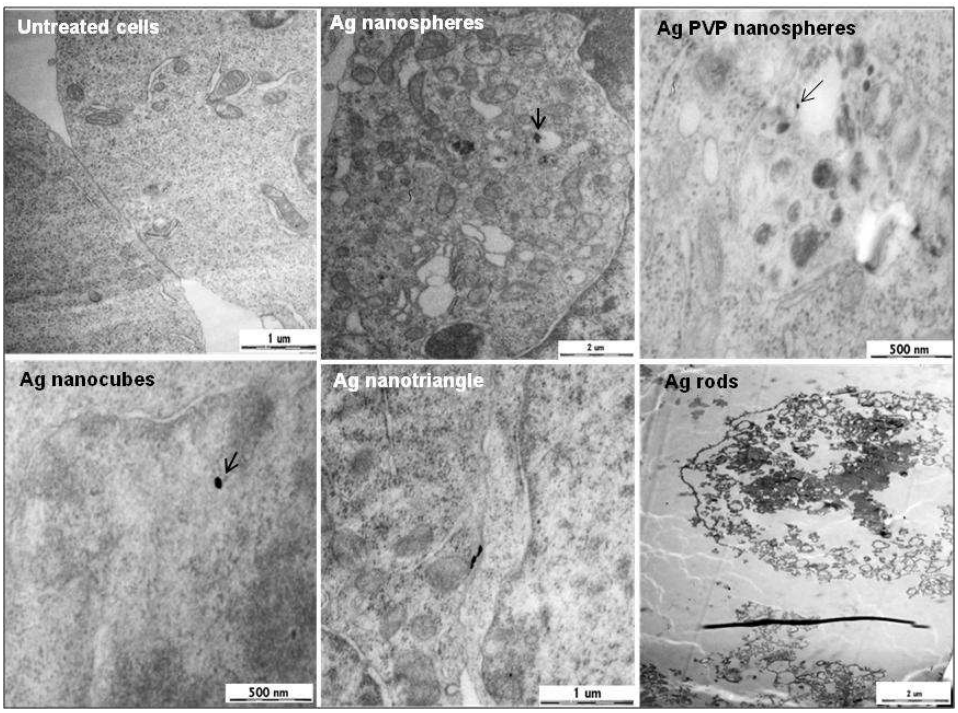

Figure 72. Ag-NPs with spherical, cubical or triangle shape did not cause severe structural damages of NE-4C cells during a 1-hour exposure. In contrast, NE-4C cells were disrupted in the presence of Ag nanorods.

The extreme toxicity of Ag rods was presumably due to the mechanical damage caused by this shape.

Electron microscopic studies failed to demonstrate accumulation of Ag-NPs in intracellular vesicles, and revealed only a very few particles inside the cells. It might be due either to the low cellular penetration, or the rapid dissolution of particles outside and inside of the cells.

DOI:10.14753/SE.2015.1789

4. Discussion

1. The main findings of the work

- NPs with non-toxic (polystyrene or silica) core material and with a size of 45-70 nm, did not exert acute toxic effects on any of the investigated neural cells.
- The low-level toxicity (found at extremely high particle concentrations) was further decreased if the surface of particles were coated with non-ionic polymer molecules as poly-ethylene glycol (PEG) or polyvivylpirrolidon (PVP).
- The cellular responses to NPs reflected the physiological characteristics of different neural tissue cells:
    - neurons did not react to NP-loading with either metabolic or uptake responses
    - endothelial cells showed metabolic activation without cell damages
    - microglia cells displayed metabolic activation besides a significant uptake of NPs
- Passivation of NP surfaces with PEG or PVP resulted in a marked reduction of cell responses
- Aged PS NPs evoked different cell responses due to particle aggregation and accumulation of bacterial endotoxins on NP surfaces
- Passivation with PEG PS NP surfaces did not prevent endotoxin accumulation
- Silver NPs (35-50 nm) exerted shape-dependent toxic effects on neural cells with a toxicity-rank of spheres<cubes<triangles<rods. Toxicity was due to shape-dependent dissolution of Ag ions and the severe mechanical damages by rod-shaped NPs

2. Cellular responses to NPs with non-toxic core material

The main part of the studies focused on the importance of the chemical composition of NP surfaces in the interactions with neural cells. To avoid variations due to size and to the release of biologically active compounds from particles, NPs with uniform

size and with a non-toxic, non-soluble PS or silica core material (Izak-Nau et al., 2013a; Murali et al., 2015) were used. The surface of PS particles carried carboxyl or PEG groups resulting in particles with different negative surface charges (~ -35 mV and -14 mV, respectively). Si NPs carried -OH, -SH or -NH_2 groups on surfaces or were "passivated with PVP coating. Silica particles (50 nm) (Izak-Nau et al., 2013a), or PS NPs with sizes between 45-70 nm (Murali et al., 2015) did not show important *in vitro* toxicity on the investigated neural cell types, with mild toxicity detected only at extremely high concentrations (10^{12} - 10^{13} particles/ml).

Similarly, the *in vivo* studies did not indicate severe invasion of PS NPs or any physiological damages to the adult or developing brain. The physiological barriers, e.g. the blood-brain barrier in the adults and the placenta in the embryos could prevent the penetration of the polystyrene 50nm particles. The surface functionalization of particles caused differences only in the short-term distribution of PS NPs with higher attachment of PS-COOH NPs to the vascular surfaces in both the adult brain and the placenta. In a 4-day period, PS NPs were completely cleared from the brain and also from the placenta.

The mild *in vitro* cellular effects, however, showed well detectable variations according to the chemical surface composition of particles.

Amine functionalisation of Si NPs increased, while PVP coating reduced markedly the particle toxicity. Similarly, carboxylated PS NPs showed slightly but significantly increased cellular effects in comparison to PEG coated particles. The polyether chain (HO-{(CH_2CH_2O)$_n$} CH_2CH_2-OH) of PEG can importantly reduce the chemical reactivity of NPs. Therefore PEG coating is regarded as a chemical tool to prevent absorption of NPs by living material and left them stay longer in the blood circulation. Coating the PS or Si particle surfaces with PEG or PVP, respectively, reduced also the binding of serum proteins to particle surfaces. Both PEG and PVP reduced the surface charge reinforcing the view (Ahn et al., 2014, He et al., 2010, Pozzi et al., 2014) that charges on particle surfaces play important roles in chemical/biological actions of particles in water-based environment.

As it was expected, PS and Si NPs with different surface functionalization evoked different responses in different neural cells. The metabolic reactions of cells were assayed by photometric MTT reduction tests measuring the formation of formazan from a tetrazolium salt. The redox potential of this reaction is slightly lower than the

transformation of reduced $NADPH^+/NADH^+$ to NADP / NAD coenzymes; therefore the tetrazolium salt is reduced by $NADPH^+/NADH^+$ inside the cells (Mosmann, 1983). $NADPH^+$ and $NADH^+$ are produced by cellular metabolic processes in the cell cytoplasm and in the mitochondria, respectively. Thus, measuring their amounts with MTT reduction can well indicate the rate of ongoing cell metabolism. Because the reduced coenzymes provide the main reductive capacity of cells for synthesizing bio-macromolecules, and because cell cannot survive without continuous biomolecule synthesis, the MTT reduction is regarded also as a viability test. Decrease in metabolic activity, however, does not mean necessarily severe cell damages; restructuring of metabolic processes is an adaptive response of cells to changing conditions. Therefore for assessing toxic effects, we measured also the integrity of the cell membranes which is inevitable for cell life. Lactate dehydrogenases (LDHs) are cytoplasmic enzymes which can get outside of the cells only in case of severe (cytotoxic) membrane damages (Abe and Matsuki, 2000). Measuring the activity of released LDH provided a sensitive toxicity assay which indicated cell damages even in cases where MTT reduction did not show any effects.

Neurons including those differentiated from stem cells *in vitro* and those isolated from the mouse forebrain, as well as neural stem cells did not respond to loading with any NPs with changes in metabolic activity or in the rate of mortality. In microglia containing cultures (purified microglia and primary brain cell cultures), a slight increase in metabolic activity was accompanied with a significant increase in the extracellular LDH activity. The increased amount of LDH releasing cells without any decrease in the total metabolic activity of the culture indicated that the metabolism of surviving cells was enhanced.

Brain microvessel endothelial cells responded to PS NPs with increased metabolic activity without any changes in extracellular LDH activity, regardless of the surface functionalization of NPs. The observation raised the possibility that deposition of NPs or NP agglomerates onto the cell surfaces might trigger mechanosensory reactions in endothelial cells known to possess multiple signal transduction and metabolic pathways for reacting to mechanical surface disturbances (Sharma et al., 2009).

In further studies on interactions of particles with living cells, the uptake of fluorescent particles was investigated by fluorescence microscopic and confocal

microscopic methods. The microscopic techniques applied for assessment of cellular uptake of fluorescent NPs allowed visualising larger (micron-size) assemblies of NPs rather than imaging individual 45-70 nm particles. Outside of the cells, large NP assemblies could be formed by spontaneous particle aggregation. Formation of large intracellular particle assemblies, however, presumed active cellular processes, which could collect particles into endocytotic vesicles, lysosomes or autophagosomes by energy-dependent endocytotic or intracellular sorting mechanisms. To get data on intracellular accumulation of NPs, confocal microscopic methods were combined with fluorescence spectrum analysis. To exclude the accumulation of individual particles by time-consuming cellular sorting mechanisms, short-term (1 hour) uptake periods were chosen. The applied methods allowed focusing on the active endocytotic/phagocytotic uptake of particles.

Resolution of particle-aggregates by traditional fluorescence microscopy was further hindered by the high cellular autofluorescence, especially that of lysosomes . Therefore, NP fluorescence had to be distinguished from the autofluorescent tissue background. For reliable detection of particle fluorescence, the spectrum profile of particles was determined and detection settings were optimized for studying particles on tissue sections. It was found, that the highest signal to noise ratio was reached if the specimens were excited at 457 nm wavelength, and the emitted light was detected in a wavelength range from 468 nm to 548 nm, with a spectral resolution of 2.5 nm (Kenesei et al., Nanomedicine. 2015 submitted).

After determining the optimum instrument settings, the fluorescence spectrum of particles was measured in PBS, in protein containing solutions, in contact with the mounting material (mowiol), or in interaction with tissue slices. The fluorescence spectra of Si or PS NPs did not change with surface modifications or in different environments. In spectrum analysis, the autofluorescence of non-treated treated cells was used as negative control, and the fluorescence of NPs seeded on control cells served as positive controls. With the applied spectral analysis, the presence of accumulated NP assemblies could be determined inside the cells.

The microscopic results demonstrated that fresh Si and PS NPs were taken up actively only by microglia cells. The uptake was, however, markedly influenced by the chemical composition of the particle surfaces: PVP-coated Si NPs and PEG-coated PS NPs were not or only sporadically internalized.

3. Effects of ageing on characteristics and biological interactions of PS NPs

Ageing of nanoparticles lead to a number of physico-chemical changes, which could affect dramatically the biological activity of particles (Mudunkotuwa et al., 2012). In preparations of PS NPs stored for longer than 6 months large aggregates were formed, as it was shown by DLS, NTA, TEM and CPS analysis. The aggregates could not be dispersed by heavy sonication. While aggregation of fresh particles was reduced by the presence of serum components, the heavy aggregation of aged PS NPs could not be reversed by dispersing them in serum-containing medium. The surface potential of such "particles" could not be determined.

Large aggregates have higher sedimentation velocities (Teeguarden et al., 2007), thus settle at a higher rate and in an increased amount on cellular surfaces: aggregation results in enhanced cellular load in comparison to exposure to equal mass of monodispersed particles. The increased cell-targeted dose of aged particles could enhance the endocytotic uptake, in itself. Particle-aggregates settled onto the surfaces of endothelial cells or microglia could not be removed with rigorous washing.

Aged particles displayed enhanced toxicity and increased intracellular accumulation, regardless of the original surface functionalization. Settlement of micron-size aggregates, in itself, could cause membrane damages and might trigger endocytotic uptake. The loss of action of original surface functionalization and the cell-selective increase in toxicity with particle ageing, however, raised the possibility that particle surfaces were also chemically changed.

The chemically active NP surfaces can concentrate bio-active molecules present in their microenvironment (Vallhov et al., 2006). Looking for potential contaminants, bacterial lipopolysaccharides (e.g. endotoxins), and the ubiquitous and bio-active pollutants were suspected.

4. Adsorption of bacterial endotoxins by PS NPs

Bacterial endotoxins are present in the outer membrane of Gram-negative bacteria (Luderitz et al., 1981) and are released to the environment by both dividing and dying bacteria. Endotoxins are everywhere, even in sterile tissue culture laboratories and medical cabinets, and can get into any system through air, water, chemicals or equipments.

To determine the potential LPS contamination on particle surfaces, the *Limulus* Ameobocyte Lysate (LAL) assay was used. The LAL assay with highly sensitive chromogenic development-system can detect as low as 0.001 EU/ml LPS which corresponds to 1 pg/ml LPS. To our surprise, all PS NP preparations gave positive LAL reactions, with higher positivity for PEGylated than carboxylated particles.

The LAL assay, however, is a bio-assay, which utilizes the hemolymph-agglutination enzyme cascade of the *Limulus* crab (Armstrong et al., 2013, Ding and Ho, 2010, Armstrong and Conrad, 2008, Roth and Levin, 1992). The enzyme cascade can be modified by a number of compounds including various polysaccharides, proteolytic enzymes, Ca^{2+}-chelators or pH. While we could show that NPs did not interfere with the chromogenic development system of the assay, we could not exclude the interference with the enzymatic components. The exact composition of or the presence of LAL-intervening compounds on the highly adsorptive nanosurfaces are difficult to determine. Moreover, the main enzyme components of the assay might be adsorbed or even denatured by NPs.

We could demonstrate, however, that all aged particles were more positive than the corresponding fresh NPs. As endotoxin-free (LAL-negative) PS NPs were not available, the LPS contamination on particle surfaces could not be determined in absolute terms.

Instead, the ready accumulation of LPS by NPs was shown by “spiking” experiments.

Incubating NPs with defined concentrations of LPS resulted in accumulation of bacterial endotoxins on PS NP surfaces. An important finding of the study was that while PEGylation reduced the binding of serum proteins to particle surfaces, it did not prevent the adsorption of endotoxins.

Incubating NPs with as low as 10 ng/ml concentrations of LPS showed that small amount of surface-adsorbed endotoxin was sufficient to cause enhanced phagocytic responses. The finding that LPS-spiked particles were taken up at a much higher rate by microglia and also by neural stem cells suggested that at least a part of cell responses evoked by aged particles was mediated by contaminating LPS.

Contaminants as endotoxins may lead to erroneous biological conclusions and might lead manufacturers to abandon particle preparations which otherwise, if free of contamination, might provide promising nanomaterials. In the normal environment,

endotoxin concentration is low (and the physiological barriers of the living systems are highly effective), thus its presence does not imply health risks. Our NP preparations, however, were opened under sterile conditions, and were stored in sterile MilliQ water at 4^{o}C. Even under such biologically clean conditions, NPs could accumulate LPS. Despite of recent efforts and wide test-applications, fully reliable assays for LPS determination in NP preparations are not available. We applied a SDS-PAGE method with sensitive silver stain (Tsai and Frasch, 1982) for detecting lipopolysaccharides adsorption on nanoparticle surfaces. The LPS gel-eletrophoretic assay, however, is time-consuming, not highly sensitive (the limit of detection is approximately 0.1µg/ml) and does not provide quantitative data for routine analysis. Conventional bio-assays (as in our case the LAL assay) should be used with caution and with accurate controls if applied on nanoparticles. Elaboration and validation of novel toxin-assessing methods seem to be inevitable for routine nano-safety screening. In agreement with previous work (Vallhov et al., 2006), these data call for introducing potent screening methods for detecting toxic contaminants of nanoparticles, especially those intended for nutritional and biomedical use.

5. Effects of particle shape on Ag NP toxicity.

Silver NPs are known to exert toxic effects to bacteria, fungi and also on mammalian tissue cells. The main reason of their severe toxicity is the dissolution of Ag ions from the particles. In this respect, it was expected that the shape of the more-or less equal sized particles will influence cytotoxicity: the dissolution is expected to be accelerated by geometrical edges. Our dissolution studies clearly showed that cubes and triangles release higher amount of ions than the spheres, and accordingly cause higher toxicity. In case of Ag rods, we find a recently non-explained interference with the MTT-reduction assay. Therefore, we could not reasoned experimentally the very high rod-toxicity with an increased ion-release. The shape, however, can influence also the interaction of particles with the membrane of living cells. Namely, the wraping of particles into the membrane material during endocytosis or phagocytosis is also influenced by edges and lines on particle surfaces (Verma and Stellacci, 2010). Furthermore, many literature precedents reported that, physicochemical properties that shape may be important in understanding the toxic effects of nanomaterials (Oberdorster et al., 2005, Powers et al., 2007).

Based on the electronmicroscopic images, the extreme toxicity of Ag nanorods indicated severe mechanical cell injures, rather than chemical toxicity. While TEM images showed unexpectedly low number of particles inside NE-4C neural stem cells after 1 -hour exposure, the few nanorods seen ont he images seemed to completely disrupt the cells. For proper interpretation, further studies are needed. While Ag particles with all shapes absorbed large amounts of blood plasma proteins, the amount of absorbed proteins also changed with shape: rods and triangles adsorbed equally large amount of proteins. Ag spheres bound the less proteins, indicating that edges and lines largely influence the interactions of NPs also with macromolecules.

As all Ag NPs showed important cytotoxicity, their wide application as anti-bacterial medical and food-packaging additives need sever consideration. The studies on shape-dependency of the cytotoxicity might help to find the right types and doses of Ag particles for optimal use.

DOI:10.14753/SE.2015.1789

5. Conclusions

Particles of 50 nm size and with polystyrene and silica core material are not severely toxic for a series of different neural tissue cells. Coating NP surfaces with PVP or PEG further reduces both the toxic effects and the cellular uptake of NPs.

The physico-chemical characteristics and biological activity of NPs change importantly with ageing resulting in large particle-aggregates and modified surface composition.

Endotoxins are readily adsorbed by PS NPs during storage and the toxin adsorption is not prevented by coating the surfaces with PEG. Endotoxin-adsorption increases toxicity and phagocytotic uptake of particles.

In assessing the health risks and biological actions of nanoparticles, the accumulation of toxins or other bio-active compounds on nanosurfaces should be seriously taken into account. Particles with all shapes absorbed a large amount of blood plasma proteins, but the amount of absorbed proteins changed with shape: rods=triangles>cubes>spheres. Cellular toxicity showed strong shape-dependency: rods were highly toxic even in 1 hour exposure. Cubes (50 mg/ml) and triangles (100 mg/ml) exerted toxic effect at relatively high concentrations, in 24-hour exposure. Rods displayed extreme toxicity presumably due to the mechanical damage this shape can cause and the rapid release of Ag ions.

6. Summary

DOI:10.14753/SE.2015.1789

We investigated the *in vitro* effects of nanoparticles (NPs) on different neural cell types and studied the penetration of particles into the adult and developing central nervous system. Among various physico-chemical properties known to influence the biological effects of nanoparticles, our studies focused on the role of chemical composition of NP surfaces. For this end, particles of the same (45-70 nm) size-range and of non-toxic core-material (silica or polystyrene) were included in the studies. The particles were thoroughly analysed by using several methods. The interaction of 50 nm fluorescent core/shell silica NPs with neural tissue cells depended strongly on both, the surface charge of particles and the type of the interacting cells. "Passivating" the particle surfaces with polyvinyl-pyrrolidone (PVP) reduced the interactions with biological material resulting in reduced protein adsorption by NP surfaces, decreased toxicity and cellular uptake. The cellular effects of 50-70 nm polystyrene (PS) NPs with negatively charged (carboxylated) or PEG-passivated surfaces also showed important surface-dependent differences and cell-type dependent variations. Silica and PS NPs used within 6 months of synthesis proved to be not severely toxic to neural tissue cells: toxicity was detected only at extremely high particle doses. Uptake experiments using confocal spectrum analysis microscopy showed that neurons did not take up any particles, while microglial cells internalized a large amount of negatively charged particles but almost no particles with passivated (PEGylated or PVP coated) surfaces. The *in vivo* tissue penetration of PS NPs was investigated. Significant differences were found in the short-term tissue invasion between carboxylated and PEG-coated PS particles. The distribution of PS-NPs in the adult mouse body is presented in the PhD thesis of Kata Kenesei. From the in vivo effects of NPs, my work concerned only on barriers protecting the developing and adult CNS. Regardless of functionalization, PS NPs were not found in embryonic tissues, and were completely cleared from the placenta in a 4-day after injection period.When experiments on cellular responses were repeated with "aged" NPs (shelf-life longer than 6 months), enhanced toxicity and cellular NP uptake were detected. Endotoxin assays including *Limulus* ameobocyte clotting (LAL) tests and SDS-PAGE showed that both PEGylated and carboxylated PS NPs adsorbed significant amounts of bacterial lipopolysaccharides (LPS). Nanoparticle size analyses proved the formation of large particle-aggregates during prolonged storage. Besides the non-toxic PS and silica NPs, the role of the shape of Ag NPs (35-50 nm) in the interactions with living material was also investigated.

DOI:10.14753/SE.2015.1789

Az egyéb hatások kizárása érdekében, azonos méret-tartományba (45-70 nm) eső, nem mérgező anyagból készített (szilicium és polisztirol) részecskéket vizsgáltunk. A biológiai alkalmazások előtt a részecskéket többféle módszerrel DLS, zéta-potenciál mérés, DCS, NTA, TEM jellemeztük. Az 50 nm méretű mag/héj szilicium NP-ok (Si NP) idegszöveti sejtekkel való kölcsönhatásait jelentősen befolyásolta mind a NP-ok felszíni töltése, mind a reagáló sejtek típusa. A részecskék felszínének bevonással poli-vinilpirrolidonnal csökkentette a biológiai anyaggal való kölcsönhatásokat: a részecskék fehérje adszorpcióját, sejt-toxicitását és a sejtek általi felvételét. Az 50-70 nm méretű polisztirol NP-ok (PS NP) karboxilált (PS-COOH) és poli-etilénglikol (PEG) bevonattal ellátott (PS-PEG) változatainak vizsgálatai is jelentős felület- és sejttípus-függő eltéréseket eredményezetek. A frissen (gyártás után <6 hónap) felhasznált SI NP-k és PS NP-k az idegszöveti sejtekre csak extrém koncentrációban gyakoroltak toxikus hatást. A sejtek általi NP felvételt konfokális mikroszkópos spektrum-analízis módszerével elemeztük. Az eredmények szerint, az idegsejtek nem vettek fel NP-t, míg a mikroglia sejtek nagy mennyiségben internalizálták a negatív felszín-töltésű részecskéket, de nem fagocitáltak PEG-gel vagy PVP-vel „passzivált” partikulumokat. A PS NP-k in vivo szöveti penetrációját 33µg/testsúly kg részecske intravénás beadása után vizsgáltuk a vemhes egéranyákban és embriókban. Jelentős eltérést találtunk a PS-COOH és PS-PEG részecskék test-eloszlása között. A testbeli eloszlás elemzését a munkacsoportban PhD hallgató-társam, Kenesei Kata. A jelen disszertáció keretében csak a részecskék kifejlett vagy fejlődő agyba való bejutását vizsgáltuk. Az adatok azt bizonyították, hogy a placenta komplett barrierként akadályozza a PS NP-k bejutását az embrióba. Amikor a fenti kísérleteket megismételtük „elöregedett” (6 hónapnál tovább tárolt) részecskékkel, megemelkedett toxikus hatást és megnövekedett sejt-felvételt mértünk. Az elöregedett részecskéket, az eredeti felszíni sajátságaiktól függetlenül, igen nagy mennyiségben fagocitálták a mikroglia sejtek, és felvették az idegi őssejtek is. Több-féle LAL és SDS-PAGE) elemzésekkel bizonyítottuk, hogy a PS-COOH és PS-PEG részecskék is jelentős mennyiségű bakteriális LPS képesek a felszínűkön adszorbeálni. A részecskék méret-elemzése megmutatta, hogy a tárolás során a partikulumok nagy mértékben aggregáltak. A nem-mérgező (szilicium, polisztirol) alapanyagú részecskék mellett, vizsgáltuk az azonos mérettartományba (35-50 nm) tartozó, de *különböző geometriájú* – gömb, kocka, gúla és rúd) ezüst nanorészecskék (Ag NP) sejtes kölcsönhatásait.

7. References

ATSDR. 1990. Agency for Toxic Substances and Disease Registry. Toxicological profile for Silver. . *Prepared by Clement international corporation, under Contract.*

ATSDR. 2007. Toxicological profile of styrene., U.S. Department of Health and Human Services: Atlanta, Georgia.

ABBOTT, N. J., RONNBACK, L. & HANSSON, E. 2006. Astrocyte-endothelial interactions at the blood-brain barrier. *Nat Rev Neurosci,* 7**,** 41-53.

ABE, K. & MATSUKI, N. 2000. Measurement of cellular 3-(4,5-dimethylthiazol-2-yl)-2,5-diphenyltetrazolium bromide (MTT) reduction activity and lactate dehydrogenase release using MTT. *Neurosci Res,* 38**,** 325-9.

AHMAD, M. & BAJAHLAN, A. S. 2007. Leaching of styrene and other aromatic compounds in drinking water from PS bottles. *J Environ Sci (China),* 19**,** 421-6.

AHN, J. M., EOM, H. J., YANG, X., MEYER, J. N. & CHOI, J. 2014. Comparative toxicity of silver nanoparticles on oxidative stress and DNA damage in the nematode, Caenorhabditis elegans. *Chemosphere,* 108**,** 343-52.

ALEXIS, F., PRIDGEN, E., MOLNAR, L. K. & FAROKHZAD, O. C. 2008. Factors affecting the clearance and biodistribution of polymeric nanoparticles. *Mol Pharm,* 5**,** 505-15.

ARMSTRONG, M. T., RICKLES, F. R. & ARMSTRONG, P. B. 2013. Capture of lipopolysaccharide (endotoxin) by the blood clot: a comparative study. *PLoS One,* 8**,** e80192.

ARMSTRONG, P. & CONRAD, M. 2008. Blood collection from the American horseshoe crab, Limulus polyphemus. *J Vis Exp*.

ASHARANI, P. V., HANDE, M. P. & VALIYAVEETTIL, S. 2009. Anti-proliferative activity of silver nanoparticles. *BMC Cell Biol,* 10**,** 65.

BAR-ILAN, O., ALBRECHT, R. M., FAKO, V. E. & FURGESON, D. Y. 2009. Toxicity assessments of multisized gold and silver nanoparticles in zebrafish embryos. *Small,* 5**,** 1897-910.

BASTÚS, N. G., MERKOÇI, F., PIELLA, J. & PUNTES, V. 2014. Synthesis of Highly Monodisperse Citrate-Stabilized Silver Nanoparticles of up to 200 nm: Kinetic Control and Catalytic Properties. *Chemistry of Materials,* 26**,** 2836-2846.

BEXIGA, M. G., VARELA, J. A., WANG, F., FENAROLI, F., SALVATI, A., LYNCH, I., SIMPSON, J. C. & DAWSON, K. A. 2011. Cationic nanoparticles induce caspase 3-, 7- and 9-mediated cytotoxicity in a human astrocytoma cell line. *Nanotoxicology,* 5**,** 557-67.

BHARALI, D. J., KLEJBOR, I., STACHOWIAK, E. K., DUTTA, P., ROY, I., KAUR, N., BERGEY, E. J., PRASAD, P. N. & STACHOWIAK, M. K. 2005. Organically modified silica nanoparticles: A nonviral vector for in vivo gene delivery and expression in the brain. *Proceedings of the National Academy of Sciences of the United States of America,* 102**,** 11539-11544.

BUERKI-THURNHERR, T., VON MANDACH, U. & WICK, P. 2012. Knocking at the door of the unborn child: engineered nanoparticles at the human placental barrier. *Swiss Med Wkly,* 142**,** w13559.

CASSIDY, P. E. & YAGER, B. J. 1971. Coupling Agents as Adhesion Promoters. *Journal of Macromolecular Science: Part D - Reviews in Polymer Processing,* 1**,** 1-49.

CHAUDHRY, Q., SCOTTER, M., BLACKBURN, J., ROSS, B., BOXALL, A., CASTLE, L., AITKEN, R. & WATKINS, R. 2008. Applications and implications of nanotechnologies for the food sector. *Food Additives and Contaminants Part a-Chemistry Analysis Control Exposure & Risk Assessment,* 25**,** 241-258.

CHO, M., CHO, W. S., CHOI, M., KIM, S. J., HAN, B. S., KIM, S. H., KIM, H. O., SHEEN, Y. Y. & JEONG, J. 2009. The impact of size on tissue distribution and elimination by single intravenous injection of silica nanoparticles. *Toxicol Lett,* 189**,** 177-83.

CLIFT, M. J., BHATTACHARJEE, S., BROWN, D. M. & STONE, V. 2010. The effects of serum on the toxicity of manufactured nanoparticles. *Toxicol Lett,* 198**,** 358-65.

COHEN, J. T., CARLSON, G., CHARNLEY, G., COGGON, D., DELZELL, E., GRAHAM, J. D., GREIM, H., KREWSKI, D., MEDINSKY, M., MONSON, R., PAUSTENBACH, D., PETERSEN, B., RAPPAPORT, S., RHOMBERG, L., RYAN, P. B. & THOMPSON, K. 2002. A comprehensive evaluation of the potential health risks associated with occupational and environmental exposure to styrene. *J Toxicol Environ Health B Crit Rev,* 5**,** 1-265.

DEMOKRITOU, P., GASS, S., PYRGIOTAKIS, G., COHEN, J. M., GOLDSMITH, W., MCKINNEY, W., FRAZER, D., MA, J., SCHWEGLER-BERRY, D., BRAIN, J. & CASTRANOVA, V. 2013. An in vivo and in vitro toxicological characterisation of realistic nanoscale CeO(2) inhalation exposures. *Nanotoxicology,* 7**,** 1338-50.

DING, J. L. & HO, B. 2010. Endotoxin detection--from limulus amebocyte lysate to recombinant factor C. *Subcell Biochem,* 53**,** 187-208.

DONALDSON, K., STONE, V., TRAN, C. L., KREYLING, W. & BORM, P. J. 2004. Nanotoxicology. *Occup Environ Med,* 61**,** 727-8.

DRAKE, P. L. & HAZELWOOD, K. J. 2005. Exposure-related health effects of silver and silver compounds: A review. *Annals of Occupational Hygiene,* 49**,** 575-585.

DUAN, J., YU, Y., LI, Y., HUANG, P., ZHOU, X., PENG, S. & SUN, Z. 2014. Silica nanoparticles enhance autophagic activity, disturb endothelial cell homeostasis and impair angiogenesis. *Part Fibre Toxicol,* 11**,** 50.

EEA. 2001. Late Lessons from Early Warnings: The Precautionary Principle 1896–2000. Environment Issue Report, no. 22. (Harremoes P, Gee D, MacGarvin M, Stirling A, Keys J, Wynne B, et al., eds). Copenhagen:European Environment Agency.

EMA, M., KOBAYASHI, N., NAYA, M., HANAI, S. & NAKANISHI, J. 2010. Reproductive and developmental toxicity studies of manufactured nanomaterials. *Reprod Toxicol,* 30**,** 343-52.

FADEEL, B. & GARCIA-BENNETT, A. E. 2010. Better safe than sorry: Understanding the toxicological properties of inorganic nanoparticles manufactured for biomedical applications. *Adv Drug Deliv Rev,* 62**,** 362-374.

FATEMI, M., ROODBARI, N. H., GHAEDI, K. & NADERI, G. 2013. The effects of prenatal exposure to silver nanoparticles on the developing brain in neonatal rats. *Journal of Biological Research-Thessaloniki,* 20**,** 233-242.

FEYMANN, RICHARD P. 1960. There's Plenty of Room at the Bottom. Engineering and Science, 23 (5), 22-36.

FROHLICH, E., KUEZNIK, T., SAMBERGER, C., ROBLEGG, E., WRIGHTON, C. & PIEBER, T. R. 2010. Size-dependent effects of nanoparticles on the activity of cytochrome P450 isoenzymes. *Toxicol Appl Pharmacol,* 242**,** 326-32.

FROHLICH, E., MEINDL, C., ROBLEGG, E., EBNER, B., ABSENGER, M. & PIEBER, T. R. 2012. Action of polystyrene nanoparticles of different sizes on lysosomal function and integrity. *Part Fibre Toxicol,* 9**,** 26.

GONZALEZ, L., DE SANTIS PUZZONIA, M., RICCI, R., AURELI, F., GUARGUAGLINI, G., CUBADDA, F., LEYNS, L., CUNDARI, E. & KIRSCH-VOLDERS, M. 2014. Amorphous silica nanoparticles alter microtubule dynamics and cell migration. *Nanotoxicology***,** 1-8.

GRAMMAS, P., MARTINEZ, J. & MILLER, B. 2011. Cerebral microvascular endothelium and the pathogenesis of neurodegenerative diseases. *Expert Rev Mol Med,* 13**,** e19.

GRANCHAROV, S. G., ZENG, H., SUN, S., WANG, S. X., O'BRIEN, S., MURRAY, C. B., KIRTLEY, J. R. & HELD, G. A. 2005. Bio-functionalization of monodisperse magnetic nanoparticles and their use as

biomolecular labels in a magnetic tunnel junction based sensor. *J Phys Chem B,* 109**,** 13030-5.

GUIOTTO, A., CANEVARI, M., POZZOBON, M., MORO, S., ORSOLINI, P. & VERONESE, F. M. 2004. Anchimeric assistance effect on regioselective hydrolysis of branched PEGs: a mechanistic investigation. *Bioorg Med Chem,* 12**,** 5031-7.

HASSANKHANI, R., ESMAEILLOU, M., TEHRANI, A. A., NASIRZADEH, K., KHADIR, F. & MAADI, H. 2014. In vivo toxicity of orally administrated silicon dioxide nanoparticles in healthy adult mice. *Environ Sci Pollut Res Int*.

HE, Q., ZHANG, J., SHI, J., ZHU, Z., ZHANG, L., BU, W., GUO, L. & CHEN, Y. 2010. The effect of PEGylation of mesoporous silica nanoparticles on nonspecific binding of serum proteins and cellular responses. *Biomaterials,* 31**,** 1085-92.

HEIDER, E. C., BARHOUM, M., PETERSON, E. M., SCHAEFER, J. & HARRIS, J. M. 2010. Identification of single fluorescent labels using spectroscopic microscopy. *Appl Spectrosc,* 64**,** 37-45.

HIRAI, T., YOSHIKAWA, T., NABESHI, H., YOSHIDA, T., TOCHIGI, S., ICHIHASHI, K., UJI, M., AKASE, T., NAGANO, K., ABE, Y., KAMADA, H., ITOH, N., TSUNODA, S., YOSHIOKA, Y. & TSUTSUMI, Y. 2012. Amorphous silica nanoparticles size-dependently aggravate atopic dermatitis-like skin lesions following an intradermal injection. *Part Fibre Toxicol,* 9**,** 3.

IZAK-NAU, E., KENESEI, K., MURALI, K., VOETZ, M., EIDEN, S., PUNTES, V. F., DUSCHL, A. & MADARASZ, E. 2013a. Interaction of differently functionalized fluorescent silica nanoparticles with neural stem- and tissue-type cells. *Nanotoxicology*.

IZAK-NAU, E., VOETZ, M., EIDEN, S., DUSCHL, A. & PUNTES, V. F. 2013b. Altered characteristics of silica nanoparticles in bovine and human serum: the importance of nanomaterial characterization prior to its toxicological evaluation. *Part Fibre Toxicol,* 10**,** 56.

JOHNSTON, H. J., HUTCHISON, G., CHRISTENSEN, F. M., PETERS, S., HANKIN, S. & STONE, V. 2010. A review of the in vivo and in vitro toxicity of silver and gold particulates: particle attributes and biological mechanisms responsible for the observed toxicity. *Crit Rev Toxicol,* 40**,** 328-46.

JONAS, L., BLOCH, C., ZIMMERMANN, R., STADIE, V., GROSS, G. E. & SCHAD, S. G. 2007. Detection of silver sulfide deposits in the skin of patients with argyria after long-term use of silver-containing drugs. *Ultrastruct Pathol,* 31**,** 379-84.

JONES, A. R. & SHUSTA, E. V. 2007. Blood-Brain Barrier Transport of Therapeutics via Receptor-Mediation. *Pharmaceutical research,* 24**,** 1759-1771.

JUNG, S., ALIBERTI, J., GRAEMMEL, P., SUNSHINE, M. J., KREUTZBERG, G. W., SHER, A. & LITTMAN, D. R. 2000a. Analysis of Fractalkine Receptor CX(3)CR1 Function by Targeted Deletion and Green Fluorescent Protein Reporter Gene Insertion. *Molecular and Cellular Biology,* 20**,** 4106-4114.

JUNG, S., ALIBERTI, J., GRAEMMEL, P., SUNSHINE, M. J., KREUTZBERG, G. W., SHER, A. & LITTMAN, D. R. 2000b. Analysis of fractalkine receptor CX(3)CR1 function by targeted deletion and green fluorescent protein reporter gene insertion. *Mol Cell Biol,* 20**,** 4106-14.

KADAJJI, V. G. & BETAGERI, G. V. 2011. Water Soluble Polymers for Pharmaceutical Applications. *Polymers,* 3**,** 1972-2009.

KAWAI, F. 2002. Microbial degradation of polyethers. *Appl Microbiol Biotechnol,* 58**,** 30-8.

KIM, J. S., YOON, T. J., YU, K. N., KIM, B. G., PARK, S. J., KIM, H. W., LEE, K. H., PARK, S. B., LEE, J. K. & CHO, M. H. 2006. Toxicity and tissue distribution of magnetic nanoparticles in mice. *Toxicol Sci,* 89**,** 338-47.

KIM, Y., SUH, H. S., CHA, H. J., KIM, S. H., JEONG, K. S. & KIM, D. H. 2009. A case of generalized argyria after ingestion of colloidal silver solution. *Am J Ind Med,* 52**,** 246-50.

KONOFAGOU, E. E. 2012. Optimization of the Ultrasound-Induced Blood-Brain Barrier Opening. *Theranostics,* 2**,** 1223-1237.

KORNYEI, Z., SZLAVIK, V., SZABO, B., GOCZA, E., CZIROK, A. & MADARASZ, E. 2005. Humoral and contact interactions in astroglia/stem cell co-cultures in the course of glia-induced neurogenesis. *Glia,* 49**,** 430-44.

LANSDOWN, A. B. 2006. Silver in health care: antimicrobial effects and safety in use. *Curr Probl Dermatol,* 33**,** 17-34.

LEE, J. H., KIM, Y. S., SONG, K. S., RYU, H. R., SUNG, J. H., PARK, J. D., PARK, H. M., SONG, N. W., SHIN, B. S., MARSHAK, D., AHN, K., LEE, J. E. & YU, I. J. 2013. Biopersistence of silver nanoparticles in tissues from Sprague-Dawley rats. *Part Fibre Toxicol,* 10**,** 36.

LINDSAY, G. K., ROSLANSKY, P. F. & NOVITSKY, T. J. 1989. Single-step, chromogenic Limulus amebocyte lysate assay for endotoxin. *J Clin Microbiol,* 27**,** 947-51.

LINDSBERG, P. J., FRERICHS, K. U., SIREN, A.-L., HALLENBECK, J. M. & NOWAK, T. S. 1996. Heat-Shock Protein and C-fos Expression in Focal Microvascular Brain Damage. *J Cereb Blood Flow Metab,* 16**,** 82-91.

LIU, Y., LI, W., LAO, F., WANG, L., BAI, R., ZHAO, Y. & CHEN, C. 2011. Intracellular dynamics of cationic and anionic polystyrene nanoparticles without direct interaction with mitotic spindle and chromosomes. *Biomaterials,* 32**,** 8291-303.

LUDERITZ, O., GALANOS, C. & RIETSCHEL, E. T. 1981. Endotoxins of Gram-negative bacteria. *Pharmacol Ther,* 15**,** 383-402.

LUNOV, O., SYROVETS, T., LOOS, C., NIENHAUS, G. U., MAILANDER, V., LANDFESTER, K., ROUIS, M. & SIMMET, T. 2011. Amino-functionalized polystyrene nanoparticles activate the NLRP3 inflammasome in human macrophages. *ACS Nano,* 5**,** 9648-57.

LUTHER, E. M., KOEHLER, Y., DIENDORF, J., EPPLE, M. & DRINGEN, R. 2011. Accumulation of silver nanoparticles by cultured primary brain astrocytes. *Nanotechnology,* 22**,** 375101.

MA, L., LIU, J., LI, N., WANG, J., DUAN, Y., YAN, J., LIU, H., WANG, H. & HONG, F. 2010. Oxidative stress in the brain of mice caused by translocated nanoparticulate TiO2 delivered to the abdominal cavity. *Biomaterials,* 31**,** 99-105.

MADARASZ, E., KISS, J. & BARTOK, I. 1984. Cell production and morphological pattern formation in primary brain cell cultures. I. Pattern formation within the basal layer(s). *Brain Res,* 304**,** 339-49.

MADARSZ, E. 2013. Diversity of Neural Stem/Progenitor Populations: Varieties by Age, Regional Origin and Environment.

MAHLER, G. J., ESCH, M. B., TAKO, E., SOUTHARD, T. L., ARCHER, S. D., GLAHN, R. P. & SHULER, M. L. 2012. Oral exposure to polystyrene nanoparticles affects iron absorption. *Nat Nanotechnol,* 7**,** 264-71.

MCCARTHY, J., INKIELEWICZ-STEPNIAK, I., CORBALAN, J. J. & RADOMSKI, M. W. 2012. Mechanisms of Toxicity of Amorphous Silica Nanoparticles on Human Lung Submucosal Cells in Vitro: Protective Effects of Fisetin. *Chem Res Toxicol,* 25**,** 2227-2235.

MCGUINNES, C., DUFFIN, R., BROWN, S., N, L. M., MEGSON, I. L., MACNEE, W., JOHNSTON, S., LU, S. L., TRAN, L., LI, R., WANG, X., NEWBY, D. E. & DONALDSON, K. 2011. Surface derivatization state of polystyrene latex nanoparticles determines both their potency and their mechanism of causing human platelet aggregation in vitro. *Toxicol Sci,* 119**,** 359-68.

MEDINA, C., SANTOS-MARTINEZ, M. J., RADOMSKI, A., CORRIGAN, O. I. & RADOMSKI, M. W. 2007. Nanoparticles: pharmacological and toxicological significance. *Br J Pharmacol,* 150**,** 552-8.

MOGHIMI, S. M., PORTER, C. J., MUIR, I. S., ILLUM, L. & DAVIS, S. S. 1991. Non-phagocytic uptake of intravenously injected microspheres in rat spleen: influence of particle size and hydrophilic coating. *Biochem Biophys Res Commun,* 177**,** 861-6.

MOSMANN, T. 1983. Rapid colorimetric assay for cellular growth and survival: application to proliferation and cytotoxicity assays. *J Immunol Methods,* 65**,** 55-63.

MUDUNKOTUWA, I. A., PETTIBONE, J. M. & GRASSIAN, V. H. 2012. Environmental implications of nanoparticle aging in the processing and fate of copper-based nanomaterials. *Environ Sci Technol,* 46**,** 7001-10.

NAKAGAWA, S., DELI, M. A., KAWAGUCHI, H., SHIMIZUDANI, T., SHIMONO, T., KITTEL, A., TANAKA, K. & NIWA, M. 2009. A new blood-brain barrier model using primary rat brain endothelial cells, pericytes and astrocytes. *Neurochem Int,* 54**,** 253-63.

NAPIERSKA, D., THOMASSEN, L. C. J., RABOLLI, V., LISON, D., GONZALEZ, L., KIRSCH-VOLDERS, M., MARTENS, J. A. & HOET, P. H. 2009. Size-Dependent Cytotoxicity of Monodisperse Silica Nanoparticles in Human Endothelial Cells. *Small,* 5**,** 846-853.

NEL, A., XIA, T., MADLER, L. & LI, N. 2006. Toxic potential of materials at the nanolevel. *Science,* 311**,** 622-7.

NEOUZE, M.-A. & SCHUBERT, U. 2008. Surface Modification and Functionalization of Metal and Metal Oxide Nanoparticles by Organic Ligands. *Monatshefte für Chemie - Chemical Monthly,* 139**,** 183-195.

NOWACK, B. & BUCHELI, T. D. 2007. Occurrence, behavior and effects of nanoparticles in the environment. *Environ Pollut,* 150**,** 5-22.

NUNE, S. K., GUNDA, P., THALLAPALLY, P. K., LIN, Y.-Y., FORREST, M. L. & BERKLAND, C. J. 2009. Nanoparticles for biomedical imaging. *Expert opinion on drug delivery,* 6**,** 1175-1194.

OBERDORSTER, G., MAYNARD, A., DONALDSON, K., CASTRANOVA, V., FITZPATRICK, J., AUSMAN, K., CARTER, J., KARN, B., KREYLING, W., LAI, D., OLIN, S., MONTEIRO-RIVIERE, N., WARHEIT, D., YANG, H. & GROUP, I. R. F. R. S. I. N. T. S. W. 2005. Principles for characterizing the potential human health effects from exposure to nanomaterials: elements of a screening strategy. *Part Fibre Toxicol,* 2**,** 8.

OECD 2008. Current developments/activities on the safety of manufactured nanomaterials. Paris, France: OECD.

OHSAWA, K. & EBATA, N. 1983. Silver stain for detecting 10-femtogram quantities of protein after polyacrylamide gel electrophoresis. *Anal Biochem,* 135**,** 409-15.

OKITSU, K. 2013. UV-Vis Spectroscopy for Characterization of Metal Nanoparticles Formed from Reduction of Metal Ions During Ultrasonic Irradiation. *In:* KUMAR, C. (ed.) *UV-VIS and Photoluminescence Spectroscopy for Nanomaterials Characterization.* Springer Berlin Heidelberg.

PANYAM, J. & LABHASETWAR, V. 2003. Biodegradable nanoparticles for drug and gene delivery to cells and tissue. *Adv Drug Deliv Rev,* 55**,** 329-47.

PARK, E. J. & PARK, K. 2009. Oxidative stress and pro-inflammatory responses induced by silica nanoparticles in vivo and in vitro. *Toxicol Lett,* 184**,** 18-25.

PEER, D., KARP, J. M., HONG, S., FAROKHZAD, O. C., MARGALIT, R. & LANGER, R. 2007. Nanocarriers as an emerging platform for cancer therapy. *Nat Nanotechnol,* 2**,** 751-60.

PETERS, A., VERONESI, B., CALDERON-GARCIDUENAS, L., GEHR, P., CHEN, L. C., GEISER, M., REED, W., ROTHEN-RUTISHAUSER, B., SCHURCH, S. & SCHULZ, H. 2006. Translocation and potential neurological effects of fine and ultrafine particles a critical update. *Part Fibre Toxicol,* 3**,** 13.

PETERS, K., UNGER, R. E., KIRKPATRICK, C. J., GATTI, A. M. & MONARI, E. 2004. Effects of nano-scaled particles on endothelial cell function in vitro: Studies on viability, proliferation and inflammation. *Journal of Materials Science-Materials in Medicine,* 15**,** 321-325.

POWERS, K. W., PALAZUELOS, M., MOUDGIL, B. M. & ROBERTS, S. M. 2007. Characterization of the size, shape, and state of dispersion of nanoparticles for toxicological studies. *Nanotoxicology,* 1**,** 42-51.

POZZI, D., COLAPICCHIONI, V., CARACCIOLO, G., PIOVESANA, S., CAPRIOTTI, A. L., PALCHETTI, S., DE GROSSI, S., RICCIOLI, A., AMENITSCH, H. & LAGANA, A. 2014. Effect of polyethyleneglycol (PEG) chain length on the bio-nano-interactions between PEGylated lipid nanoparticles and biological fluids: from nanostructure to uptake in cancer cells. *Nanoscale,* 6**,** 2782-92.

RAI, A. J., GELFAND, C. A., HAYWOOD, B. C., WARUNEK, D. J., YI, J., SCHUCHARD, M. D., MEHIGH, R. J., COCKRILL, S. L., SCOTT, G. B., TAMMEN, H., SCHULZ-KNAPPE, P., SPEICHER, D. W., VITZTHUM, F., HAAB, B. B., SIEST, G. & CHAN, D. W. 2005. HUPO Plasma Proteome Project specimen collection and handling: towards the standardization of parameters for plasma proteome samples. *Proteomics,* 5**,** 3262-77.

ROBERTS, M. J., BENTLEY, M. D. & HARRIS, J. M. 2002. Chemistry for peptide and protein PEGylation. *Advanced drug delivery reviews,* 54**,** 459-76.

RODUNER, E. 2006. Size matters: why nanomaterials are different. *Chem Soc Rev,* 35**,** 583-92.

ROTH, R. I. & LEVIN, J. 1992. Purification of Limulus polyphemus proclotting enzyme. *J Biol Chem,* 267**,** 24097-102.

ROUX, S., GARCIA, B., BRIDOT, J. L., SALOME, M., MARQUETTE, C., LEMELLE, L., GILLET, P., BLUM, L., PERRIAT, P. & TILLEMENT, O. 2005. Synthesis, characterization of dihydrolipoic acid capped gold nanoparticles, and functionalization by the electroluminescent luminol. *Langmuir,* 21**,** 2526-36.

RUSSELL, A. D. & HUGO, W. B. 1994. Antimicrobial activity and action of silver. *Prog Med Chem,* 31**,** 351-70.

SARLO, K., BLACKBURN, K. L., CLARK, E. D., GROTHAUS, J., CHANEY, J., NEU, S., FLOOD, J., ABBOTT, D., BOHNE, C., CASEY, K., FRYER, C. & KUHN, M. 2009. Tissue distribution of 20 nm, 100 nm and 1000 nm fluorescent polystyrene latex nanospheres following acute systemic or acute and repeat airway exposure in the rat. *Toxicology,* 263**,** 117-126.

SAURA, J., TUSELL, J. M. & SERRATOSA, J. 2003. High-yield isolation of murine microglia by mild trypsinization. *Glia,* 44**,** 183-9.

SCHLETT, K. & MADARASZ, E. 1997. Retinoic acid induced neural differentiation in a neuroectodermal cell line immortalized by p53 deficiency. *J Neurosci Res,* 47**,** 405-15.

SCHULZ-DOBRICK, M., SARATHY, K. V. & JANSEN, M. 2005. Surfactant-free synthesis and functionalization of gold nanoparticles. *J Am Chem Soc,* 127**,** 12816-7.

SHANNAHAN, J. H., PODILA, R., ALDOSSARI, A. A., EMERSON, H., POWELL, B. A., KE, P. C., RAO, A. M. & BROWN, J. M. 2014. Formation of a Protein Corona on Silver Nanoparticles Mediates Cellular Toxicity via Scavenger Receptors. *Toxicol Sci*.

SHARMA, H. S., ALI, S. F., HUSSAIN, S. M., SCHLAGER, J. J. & SHARMA, A. 2009. Influence of engineered nanoparticles from metals on the blood-brain barrier permeability, cerebral blood flow, brain edema and neurotoxicity. An experimental study in the rat and mice using biochemical and morphological approaches. *J Nanosci Nanotechnol,* 9**,** 5055-72.

SNYDER, J., Styrene Not a Human Carcinogen, Does Not Contain BPA. 2009, Styrene Information and Research Center (SIRC),: Arlington, Va. .

SODERSTJERNA, E., BAUER, P., CEDERVALL, T., ABDSHILL, H., JOHANSSON, F. & JOHANSSON, U. E. 2014. Silver and gold nanoparticles exposure to in vitro cultured retina--studies on nanoparticle

internalization, apoptosis, oxidative stress, glial- and microglial activity. *PLoS One,* 9**,** e105359.

SÖDERSTJERNA, E., BAUER, P., CEDERVALL, T., ABDSHILL, H., JOHANSSON, F. & JOHANSSON, U. E. 2014. Silver and Gold Nanoparticles Exposure to <italic>In Vitro</italic> Cultured Retina – Studies on Nanoparticle Internalization, Apoptosis, Oxidative Stress, Glial- and Microglial Activity. *PLoS ONE,* 9**,** e105359.

SODERSTJERNA, E., JOHANSSON, F., KLEFBOHM, B. & ENGLUND JOHANSSON, U. 2013. Gold- and silver nanoparticles affect the growth characteristics of human embryonic neural precursor cells. *PLoS One,* 8**,** e58211.

SOO CHOI, H., LIU, W., MISRA, P., TANAKA, E., ZIMMER, J. P., ITTY IPE, B., BAWENDI, M. G. & FRANGIONI, J. V. 2007. Renal clearance of quantum dots. *Nat Biotech,* 25**,** 1165-1170.

STÖBER, W., FINK, A. & BOHN, E. 1968. Controlled growth of monodisperse silica spheres in the micron size range. *Journal of Colloid and Interface Science,* 26**,** 62-69.

SUN, Y., GATES, B., MAYERS, B. & XIA, Y. 2002a. Crystalline Silver Nanowires by Soft Solution Processing. *Nano Letters,* 2**,** 165-168.

SUN, Y. & XIA, Y. 2002. Shape-controlled synthesis of gold and silver nanoparticles. *Science,* 298**,** 2176-9.

SUN, Y., YIN, Y., MAYERS, B. T., HERRICKS, T. & XIA, Y. 2002b. Uniform Silver Nanowires Synthesis by Reducing AgNO3 with Ethylene Glycol in the Presence of Seeds and Poly(Vinyl Pyrrolidone). *Chemistry of Materials,* 14**,** 4736-4745.

SUNDARAM, S., ROY, S. K., AMBATI, B. K. & KOMPELLA, U. B. 2009. Surface-functionalized nanoparticles for targeted gene delivery across nasal respiratory epithelium. *FASEB J,* 23**,** 3752-65.

TANG, J., XIONG, L., WANG, S., WANG, J., LIU, L., LI, J., WAN, Z. & XI, T. 2008. Influence of silver nanoparticles on neurons and blood-brain barrier via subcutaneous injection in rats. *Applied Surface Science,* 255**,** 502-504.

TANIGUCHI, N. 1974. "On the Basic Concept of 'Nano-Technology'," Proc. Intl. Conf. Prod. Eng. Tokyo, Part II, Japan Society of Precision Engineering.

TEEGUARDEN, J. G., HINDERLITER, P. M., ORR, G., THRALL, B. D. & POUNDS, J. G. 2007. Particokinetics in vitro: dosimetry considerations for in vitro nanoparticle toxicity assessments. *Toxicol Sci,* 95**,** 300-12.

TRICKLER, W. J., LANTZ, S. M., MURDOCK, R. C., SCHRAND, A. M., ROBINSON, B. L., NEWPORT, G. D., SCHLAGER, J. J., OLDENBURG, S. J., PAULE, M. G., SLIKKER, W., JR., HUSSAIN, S. M. & ALI, S. F. 2010. Silver nanoparticle induced blood-brain barrier inflammation and increased permeability in primary rat brain microvessel endothelial cells. *Toxicol Sci,* 118**,** 160-70.

TSAI, C. M. & FRASCH, C. E. 1982. A sensitive silver stain for detecting lipopolysaccharides in polyacrylamide gels. *Anal Biochem,* 119**,** 115-9.

U.S. GAO. 2010. Nanotechnology: Nanomaterials Are Widely Used in Commerce, but EPA Faces Challenges in Regulating Risk.

VALLHOV, H., QIN, J., JOHANSSON, S. M., AHLBORG, N., MUHAMMED, M. A., SCHEYNIUS, A. & GABRIELSSON, S. 2006. The importance of an endotoxin-free environment during the production of nanoparticles used in medical applications. *Nano Lett,* 6**,** 1682-6.

VAN VLERKEN, L. E., VYAS, T. K. & AMIJI, M. M. 2007. Poly(ethylene glycol)-modified nanocarriers for tumor-targeted and intracellular delivery. *Pharm Res,* 24**,** 1405-14.

VARELA, J. A., BEXIGA, M. G., ABERG, C., SIMPSON, J. C. & DAWSON, K. A. 2012. Quantifying size-dependent interactions between fluorescently labeled polystyrene nanoparticles and mammalian cells. *J Nanobiotechnology,* 10**,** 39.

VARGA, B., MARKO, K., HADINGER, N., JELITAI, M., DEMETER, K., TIHANYI, K., VAS, A. & MADARASZ, E. 2009. Translocator protein (TSPO 18kDa) is expressed by neural stem and neuronal precursor cells. *Neurosci Lett,* 462**,** 257-62.

VENKATESAN, N., YOSHIMITSU, J., ITO, Y., SHIBATA, N. & TAKADA, K. 2005. Liquid filled nanoparticles as a drug delivery tool for protein therapeutics. *Biomaterials,* 26**,** 7154-7163.

VERMA, A. & STELLACCI, F. 2010. Effect of surface properties on nanoparticle-cell interactions. *Small,* 6**,** 12-21.

VROMAN, L., ADAMS, A. L., FISCHER, G. C. & MUNOZ, P. C. 1980. Interaction of high molecular weight kininogen, factor XII, and fibrinogen in plasma at interfaces. *Blood,* 55**,** 156-9.

WANG, F., GAO, F., LAN, M. B., YUAN, H. H., HUANG, Y. P. & LIU, J. W. 2009. Oxidative stress contributes to silica nanoparticle-induced cytotoxicity in human embryonic kidney cells. *Toxicology in Vitro,* 23**,** 808-815.

WANG, M., ETU, J. & JOSHI, S. 2007. Enhanced disruption of the blood brain barrier by intracarotid mannitol injection during transient cerebral hypoperfusion in rabbits. *J Neurosurg Anesthesiol,* 19**,** 249-56.

WIJNHOVEN, S. W. P., PEIJNENBURG, W. J. G. M., HERBERTS, C. A., HAGENS, W. I., OOMEN, A. G., HEUGENS, E. H. W., ROSZEK, B., BISSCHOPS, J., GOSENS, I., VAN DE MEENT, D., DEKKERS, S., DE JONG, W. H., VAN ZIJVERDEN, M., SIPS, A. J. A. M. & GEERTSMA, R. E. 2009. Nano-silver - a review of available data and knowledge gaps in human and environmental risk assessment. *Nanotoxicology,* 3**,** 109-U78.

WILEY, B., SUN, Y., MAYERS, B. & XIA, Y. 2005. Shape-controlled synthesis of metal nanostructures: the case of silver. *Chemistry,* 11**,** 454-63.

WIN-SHWE, T. T. & FUJIMAKI, H. 2011. Nanoparticles and Neurotoxicity. *International Journal of Molecular Sciences,* 12**,** 6267-6280.

WOEHRLE, G. H. & HUTCHISON, J. E. 2005. Thiol-functionalized undecagold clusters by ligand exchange: synthesis, mechanism, and properties. *Inorg Chem,* 44**,** 6149-58.

WU, J., WANG, C., SUN, J. & XUE, Y. 2011. Neurotoxicity of silica nanoparticles: brain localization and dopaminergic neurons damage pathways. *ACS Nano,* 5**,** 4476-89.

XIA, T., KOVOCHICH, M., BRANT, J., HOTZE, M., SEMPF, J., OBERLEY, T., SIOUTAS, C., YEH, J. I., WIESNER, M. R. & NEL, A. E. 2006. Comparison of the abilities of ambient and manufactured nanoparticles to induce cellular toxicity according to an oxidative stress paradigm. *Nano Lett,* 6**,** 1794-807.

XIA, T., KOVOCHICH, M., LIONG, M., ZINK, J. I. & NEL, A. E. 2008. Cationic polystyrene nanosphere toxicity depends on cell-specific endocytic and mitochondrial injury pathways. *ACS Nano,* 2**,** 85-96.

XU, L., SHI, C., SHAO, A., LI, X., CHENG, X., DING, R., WU, G. & CHOU, L. L. 2014. Toxic responses in rat embryonic cells to silver nanoparticles and released silver ions as analyzed via gene expression profiles and transmission electron microscopy. *Nanotoxicology***,** 1-10.

YAMASHITA, K., YOSHIOKA, Y., HIGASHISAKA, K., MIMURA, K., MORISHITA, Y., NOZAKI, M., YOSHIDA, T., OGURA, T., NABESHI, H., NAGANO, K., ABE, Y., KAMADA, H., MONOBE, Y., IMAZAWA, T., AOSHIMA, H., SHISHIDO, K., KAWAI, Y., MAYUMI, T., TSUNODA, S., ITOH, N., YOSHIKAWA, T., YANAGIHARA, I., SAITO, S. & TSUTSUMI, Y. 2011. Silica and titanium dioxide nanoparticles cause pregnancy complications in mice. *Nat Nanotechnol,* 6**,** 321-8.

YU, Y., LI, Y., WANG, W., JIN, M. H., DU, Z. J., LI, Y. B., DUAN, J. C., YU, Y. B. & SUN, Z. W. 2013. Acute Toxicity of Amorphous Silica Nanoparticles in Intravenously Exposed ICR Mice. *PLoS One,* 8.

ZAYATS, M., KATZ, E., BARON, R. & WILLNER, I. 2005. Reconstitution of apo-glucose dehydrogenase on pyrroloquinoline quinone-functionalized au nanoparticles yields an electrically contacted biocatalyst. *J Am Chem Soc,* 127**,** 12400-6.

ZHANG, L., GU, F. X., CHAN, J. M., WANG, A. Z., LANGER, R. S. & FAROKHZAD, O. C. 2008. Nanoparticles in medicine: therapeutic applications and developments. *Clin Pharmacol Ther,* 83**,** 761-9.

ZHANG, Q., LI, N., GOEBL, J., LU, Z. & YIN, Y. 2011. A Systematic Study of the Synthesis of Silver Nanoplates: Is Citrate a "Magic" Reagent? *Journal of the American Chemical Society,* 133**,** 18931-18939.

ZHANG, Q., LI, W., WEN, L.-P., CHEN, J. & XIA, Y. 2010. Facile Synthesis of Ag Nanocubes of 30 to 70 nm in Edge Length with CF3COOAg as a Precursor. *Chemistry – A European Journal,* 16**,** 10234-10239.

ZLOKOVIC, B. V. 2008. The blood-brain barrier in health and chronic neurodegenerative disorders. *Neuron,* 57**,** 178-201.

DOI:10.14753/SE.2015.1789

8. The publications related to the PhD thesis

- Kumarasamy Murali, Kata Kenesei, Yang Li, K. Demeter, Zs. Környei, Madarasz Emilia, Uptake and bio-reactivity of polystyrene nanoparticles is affected by surface modifications, ageing and LPS adsorption: in vitro studies on neural tissue cells, Nanoscale, 2015, 7, 4199 – 4210. Impact factor: 6.789.

- Izak-Nau E, Kenesei K, Murali K, Voetz M, Eiden S, Puntes VF, Duschl A, Madarász E. Interaction of differently functionalized fluorescent silica nanoparticles with neural stem- and tissue-type cells. Nanotoxicology. 2014, 8(1), 138-148. Impact factor: 7.336.

- Kata Kenesei, Kumarasamy Murali, Czéh Árpád, Jordi Piella, Victor Puntes, Emília Madarász, Effects of surface modifications on the distribution of polystyrene nanoparticles in mouse tissues, Nanomedicine (under review 2015).

The publications not related to the PhD thesis

- S. Bhattacharya, Subhas S. Karki, R. Suresh, L. Manikandan, G. P. Senthilkumar, M. Gupta, Upal K. Mazumder, R. Balaji and K. Murali, *In vitro* cytotoxicity and induction of apoptosis by ruthenium(II) complexes in HL-60 and K-562, Med. Chem. Res., 2012, 21(7), 1120-1126.

- K. Murali, R. Avinash, R. Kirthiga, Scott G. Franzblau Synthesis, antibacterial, and antitubercular studies of some novel isatin derivatives, Med. Chem. Res., 2012, 21(12), 4335-4340.

- V. Alagarsamy; M., Gopinath; P., Parthiban; B., Subba Rao; K., Murali, V. Raja Solomon"Synthesis and analgesic, anti-inflammatory activities of 3-(3-methoxyphenyl)-2-substituted amino-quinazolin- 4(3 H)-ones" Medicinal Chemistry Research, 2011, 20 (7), 946-954.

DOI:10.14753/SE.2015.1789

9. Acknowledgements

There are many people I would like to acknowledge for their help and support. First and foremost, it gives me immense pleasure to thank my mentor Prof. Dr. Madarasz Emilia for giving me the opportunity to carry out my research project as a Marie Curie fellow.

I would also like to thank Ms Kata Kenesei for helping me with microscopic studies and her suggestions and I could not forget to give huge thanks to all the past and present members of the Laboratory of Cellular and Developmental Neurobiology I have met along this “fantastic trip” for the great enthusiastic research and friendly atmosphere rendered, Especially I would like to thank Katalin Gaal, Lia Barabas and Piroska Nyamandi, for their excellent technical assistance.

I thank to my fellow ‘NanoTOES members’, especially Emilia Izak Nau and Yang li, for their research contributions.

My sincere thanks are also goes to Prof Albert Duschl (Coordinator, “EU FP7 Marie Curie Actions, and Network for Initial Training „NanoTOES” project) and Elisabeth Eppacher for their administrative support.

I would also give great thanks to my collaborative research labs at Bayer Technology Services GmbH (Leverkusen) at ICN (Barcelona), at Centre for BioNano Interactions (CBNI), University College Dublin, Belfield, Dublin, Ireland and at NILU (Oslo) for the great research environment.

Dr Diana Boraschi (Laboratory of Innate Immunity and Cytokines, Institute of Protein Biochemistry, National Research Council, 80131 Naples, Italy) for the critical reading and correcting the manuscript of my first authorship paper.

I sincerely thank the EU FP7 Marie Curie Actions, Network for Initial Training NanoTOES (PITN-GA-2010-264506) for the financial assistance. (www.nanotoes.eu)

I wish to thank the Nikon Microscopy Center of Nikon Austria GmbH, and Auro-Science Consulting Ltd operating at the Institute of Experimental Medicine of Hungarian Academy of Sciences, (Budapest, Hungary),

Dr. Jorge MEJIA, PMR-LARN, Faculty of Sciences, Université de Namur ASBL, Belgium for CPS measurements.

DOI:10.14753/SE.2015.1789

Sincere thanks are also to Széles Csilla, Radó Nikolett, Benko gabriella, and Seregély Sára for their administrative support througout my project and to the staff from Secreatry office of Doctoral School of Semmelweis University, Hungary.

Last but not the least I am also very thankful to the experimental animals for their sacrifices without which the study would not have been possible, may god keep their soul in peace.

A warm thanks to all my friends in Hungary who have enriched my life abroad.

I am grateful for the love and tolerance of my dearest Mritti.

Last, but certainly not least, I would express a deep sense of gratitude especially to my dearest mom, who has sacrificed her life for my growth and success and to whom I owe my life for her constant love, encouragement, moral support and blessings. Although, she is miles away from me, but her love and support were always with me.

Finally, I would like to dedicate this thesis to my grandpa and all my uncles, personally they have shown me unconditional love and support during my school days and they have played an important role in the development of my identity and shaping the individual that I am today.

I would like to finish with a quote that has helped me through the tough times over the last few years;

“Nothing is permanent in this wicked world, not even our troubles”.

-Charlie Chaplin.